UNIVERSITY OF
KWAZULU-NATAL

INYUVESI
YAKWAZULU-NATALI

Characterisation of Fumonisin B_1 toxicity in a cancerous liver cell line- Induction of Tissue Transglutaminase and the Endoplasmic Reticulum Stress Pathway

By

SAMANTHA MARY ANDERSON

B.Sc. B.Med.Sc. (Hons) (UKZN)

Submitted in fulfilment of the requirements for the degree of Masters in Medical Science

in the

Discipline of Medical Biochemistry and Chemical Pathology

School of Laboratory Medicine and Medical Sciences

College of Health Sciences

University of KwaZulu-Natal

Durban

2013

ABSTRACT

Fumonisin B_1 (FB_1) is a mycotoxin which is well characterised as a contaminant of maize and maize-based products worldwide, especially in South Africa. Its toxic effects have been associated with hepatotoxicity, nephrotoxicity and carcinogenicity. Tissue transglutaminase (TG2) is a unique and ubiquitous enzyme that catalyses the post-translational modification of proteins and has GTPase activity. Tissue transglutaminase is an important enzyme in a number of biological processes such as cell differentiation and proliferation, extracellular matrix organisation, cell signalling and apoptosis. This study investigated the possible role of TG2 induction by FB_1 and the effect FB_1 toxicity has on the endoplasmic reticulum (ER) stress pathway in HepG2 cells. A SDS-PAGE adaption of the TG2 activity assay confirmed TG2 crosslinking activity by FB_1 incorporation into fibronectin in the presence of calcium and TG2. This interaction was validated using fluorescent microscopy where FB_1 incorporated into the HepG2 cell's cytoplasmic vesicles and plasma membrane. The up-regulation of TG2 in HepG2 cells treated with FB_1 was further investigated using western blotting and showed increased TG2 up-regulation. Fumonisin B_1 disrupts membrane-bound sphingolipids as a mechanism of toxicity; FB_1 was shown to cause cytoskeletal damage and disrupted the cell's membranes leading to cell stress. The protein kinase RNA-like endoplasmic reticulum kinase (PERK) ER stress pathway was induced as a result of FB_1 exposure and investigated using western blotting and quantitative polymerase chain reaction. After 72hours with 50µM and 100µM FB_1 total PERK decreased, phosphorylated eukaryotic initiating factor α remained activated with a significant increase in messenger RNA (mRNA) expression ($p<0.05$) and transcription factor CCAAT-enhancer-binding protein homologous protein mRNA was significantly induced ($p<0.05$). The involvement of nuclear factor kappa B (NFkB) and TG2 in ER stress induced apoptosis was investigated through western blotting and quantitative polymerase chain reaction. After 72hours, an up-regulation of both nuclear NFkB and nuclear TG2 was observed; with a corresponding significant increase in nuclear TG2 mRNA expression ($p<0.05$). A significant

increase in transcription factor, Sp1 mRNA expression ($p<0.05$) was observed after 72hours. Data suggests PERK activation leads to NFkB induction and nuclear translocation; which promoted nuclear TG2 transcription. The activation of TG2 resulted in Sp1 crosslinks that could act as potential inducers of FB_1 induced apoptosis. Flow cytometry was used to measure apoptosis and mitochondrial depolarisation. Caspase activity was measured using the Caspase-Glo® assays and ATP concentration was measured using CellTitre-Glo^{TM} assay. After 72hours caspases 3/7 and 8 showed a significant decrease in activity at 100µM FB_1 ($p<0.05$) and a decrease in caspase 9. After 72hours with 10µM FB_1 treatment a significant increase in phosphatidylserine externalisation ($p<0.05$), a significant decrease in healthy/live cells ($p<0.05$) and a significant increase in depolarised mitochondria ($p<0.05$) were observed. There was also a significant increase in Sp1 mRNA expression ($p<0.05$). However, at 50µM FB_1 treatment there was a decrease in phosphatidylserine externalisation, a significant increase in live cells ($p<0.05$) and a significant decrease in depolarised mitochondria ($p<0.05$). Data suggests that ER stress persisted in HepG2 cells with no apoptosis or cell recovery occurring at high chronic doses of FB_1 whilst ER stress induced apoptosis at low chronic doses of FB_1 in HepG2 cells. Fumonisin B_1 may be a possible substrate for TG2 crosslinking activity due to its primary amine group, since this mycotoxin has the potential to induce TG2 expression and activation. Further studies are required to determine the role of FB_1 in the inositol-requiring protein 1α and activating transcription factor 6 arms of the ER stress pathway.

DECLARATION

This dissertation represents the original work by the author and has not been submitted in any form to another university. The use of work by others has been duly acknowledged in the text.

The research described in this study was carried out in the Discipline of Medical Biochemistry, School of Laboratory Medicine and Medical Sciences, Faculty of Health Sciences, University of KwaZulu-Natal, Durban, under the supervision of Prof A. A. Chuturgoon and Dr. A. Phulukdaree

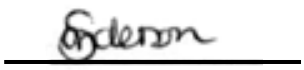

Miss S.M. Anderson

ACKNOWLEDGEMENTS

My Parents and Siblings

Thank you for your guidance, support and allowing me every opportunity to further my education and knowledge. I appreciate everything that you have done for me, your continuous encouragement and unwavering faith in my abilities as a student, scientist and person.

Prof A. A. Chuturgoon

Thank you for your guidance, support and motivation throughout these past two years. Your passion for science has kept me motivated and continuously inspires me as a scientist.

Dr. A. Phulukdaree

Thank you for all your guidance and support throughout the year.

Junior PhD Students in the discipline of Medical Biochemistry

Thank you so much for all your support, assistance in the laboratory and making everyday a pleasure to attend university. It really has been an exciting year.

Friends and Loved ones

Thank you for all your support, encouragement and unwavering faith in me.

LIST OF ABBREVIATIONS

µORF	Upstream open reading frames
AMP	Adenosine monophosphate
ANOVA	Analysis of variance
APAF	Apoptotic protease activating factor
APS	Ammonium persulfate
ASK	Apoptosis signal-regulating kinase
ATF	Activating transcription factor
ATP	Adenosine triphosphate
BCA	Bicinchoninic acid
BiP	Binding protein
BSA	Bovine serum albumin
BTC	Biotin-x-cadaverine
c	Complementary
C	Carbon
$CaCl_2$	Calcium chloride
CCM	Serum containing media
CD95	Cluster of differentiation 95

CHOP	CCAAT-enhancer-binding protein homologous protein
Co	Coenzyme
CS	Ceramide synthase
Ct	Threshold cycle
Cu^{+}	Cuprous ions
Cu^{2+}	Cupric ions
$CuSO_4$	Copper sulfate
d	Deionized
DEVD	Aspartate-glutamate-valine-aspartate
DMSO	Dimethyl sulfoxide
DNA	Deoxyribonucleic acid
dNTPs	Deoxynucleotide
DR	Death Receptor
ds	Double stranded
DTT	Dithiothreitol
EDTA	Ethylenediaminetetraacetic acid
eIF	Eukaryotic initiating factor
ER	Endoplasmic reticulum

ERAD	Endoplasmic reticulum associated degradation
F.	Fusarium
FB_1	Fumonisin B_1
FITC	Fluorescein isothiocyanate
FL	Fluorescent channels
FLOUS	Fluorescent
g	Gravitational force
G	Guanosine
GADD34	Deoxyribonucleic acid -damage protein
GAPDH	Glyceraldehyde 3-phosphate dehydrogenase
GDP	Guanosine diphosphate
GEF	Guanine nucleotide exchange factor
gpl	Guinea pig liver
GTP	Guanosine-5'-triphosphate
H	Histone
H_2O	Water
H_2SO_4	Sulfuric acid
HCl	Hydrochloric acid

HEPES	Hydroxyethyl piperazineethanesulfonic acid
HepG2	Human hepatocellular liver carcinoma cell line
HRP	Horseradish peroxidase
Hrs	Hours
htt	Huntingtin
IARC	International Agency for Research on Cancer
IgG	Immunoglobulin G
IkB	Inhibitor kappa B
IKK	Protein Inhibitor kappa B kinase
IL	Interleukin
IRE	Inositol-requiring protein
JC-1	5,5',6,6'-tetrachloro-1,1',3,3'-tetraethylbenzimidazolocarbocyanine I- /Cl- salt
JNK	c-jun N-terminal kinase
KCl	Potassium chloride
mAb	Monoclonal antibody
Mg^{2+}	Magnesium
$MgCl_2$	Magnesium chloride
MMP	Mitochondrial membrane potential

mRNA	Messenger ribonucleic acid
Mt	Mitochondria
N	Amino
n	Nuclear
NFkB	Nuclear factor kappa B
P	Phosphate
p-	Phosphorylated
PAGE	Polyacrylamide gel electrophoresis
PBS	Phosphate buffer saline
PCR	Polymerase Chain Reaction
PERK	Protein kinase RNA-like endoplasmic reticulum kinase
PI	Propidium Iodide
PP1	Protein phosphatase 1
PS	Phosphatidylserine
qPCR	Quantitative Polymerase Chain Reaction
RLU	Relative light units
RNA	Ribonucleic acid
rRNA	Ribosomal ribonucleic acid

RSA	Republic of South Africa
RT	Room temperature
S1P	Serine protease 1
S2P	Metalloprotease site-2 protease
SA	South Africa
Sa	Sphinganine
SDS	Sodium dodecyl sulfate
So	Sphingosine
sp.	Species
Sp1	Specificity Protein 1
Taq	Thermus *aquaticus*
TBS	Tris Buffered Saline
TCA	Propane-1,2,3-tricarboxylic acid
T-cell	Lymphocytes
TEMED	Tetramethylethylenediamine
TG	Transglutaminase
TG2	Tissue transglutaminase
TGF	Transforming growth factor

TGM2	Tissue transglutaminase promoter gene
TMB	3,3',5,5' – Tetramethylbenzidine
TNF	Tumor necrosis factor
TRAF	Tumor necrosis factor receptor-associated factor
Tris	Tris(hydroxymethyl)aminomethane
TRITC	Tetramethylrhodamine-5-(and 6)-isothiocyanate
tRNA	Transfer ribonucleic acid
TTBS	Tris Buffered Saline with Tween 20
µORF	upstream open reading frame
UP	Unfolded proteins
UPR	Unfolded protein response
USA	United States of America
UTR	Untranslated region
WHO	World Health Organisation

LIST OF FIGURES

Chapter two:

Chapter four:

Chapter five:

LIST OF TABLES

Chapter two:

Chapter three:

TABLE OF CONTENTS

CHAPTER ONE

1 INTRODUCTION

In southern Africa, maize is a staple food source for a large number of the population, with an average consumption of 100kg/capita/year. This maize consumption represents more than 31% of total calories in SA (Smale et al. 2013). A fungi, *Fusarium verticilliodes,* is a common contaminant of maize and maize-based products both locally and worldwide (Grenier et al. 2012) and is known to produce secondary metabolites. These secondary metabolites are known as fumonisins with fumonisin B_1 (FB_1) being the most prevalent and toxic mycotoxin produced (Voss et al. 2007). It has been reported that South Africans are continuously exposed to low doses of FB_1 with a daily dietary intake of 200µg/kg body weight (Domijan & Abramov 2011). This mycotoxin is an analogue of sphingoid bases and exerts its toxic effect through the competitive inhibition of ceramide synthase, which is important in the formation of complex sphingolipids (Voss et al. 2007). Sphingolipids play an important role in plasma membrane structure, cell growth regulation and in the transduction pathway where ceramide acts as a second messenger for a range of factors such as tumour necrosis factor (TNF)-α (Heidtmann-Bemvenuti et al. 2011; Soriano et al. 2005). A wide range of toxic effects have been associated with FB_1 exposure, including hepatotoxicity and nephrotoxicity (Domijan & Abramov 2011), neural tube defects in foetus (Voss et al. 2007) and is most commonly associated with oesophageal cancers, where an increase in the incidence rate has been observed in Transkei and China (Nour et al. 2007).

Tissue transglutaminase (TG2) is a ubiquitous enzyme located within the cytosol, nucleus and on the outer plasma membrane (Elli et al. 2009). These enzymes are responsible for the post-translational modification of proteins through the insertion of an isopeptide bond between or within polypeptide chains. This transamidation reaction results from the acyl transfer between a γ-carboxyamide glutamine residue (acyl donor) and a lysine Ɛ-amino residue of a primary amine (acyl

acceptor) which forms a proteinase-resistant covalent N-γ-glutamyl-Ɛ-lysyl-isopeptide bond (crosslink) (Griffin et al. 2002; Elli et al. 2009); with the crosslinked protein product being of higher molecular mass (Park et al. 2010). This reaction is calcium dependent because calcium binding is crucial for the induction of a conformation change within TG2 to expose the active site. Calcium activation however, can only occur at supraphysiological concentrations of calcium. The transcription of TG2 is regulated by retinoids, steroid hormones, cytokines and through methylation of its promoter region. This transcriptional regulation is time-dependent (Griffin et al. 2002). Cytokines such as TNF-α and stress molecule nuclear factor kappa B (NFkB) have been suggested to stimulate TG2 expression (Ientile et al. 2007). Where NFkB binds the tissue transglutaminase promoter gene (TGM2) directly and induces TG2 transcription (Ientile et al. 2007). The induction and activation of TG2 has been linked to increased apoptosis in rat hepatocytes (Fesus & Szondy 2005); with widespread evidence for TG2 gene up-regulation during apoptosis (Griffin et al. 2002). According to Kuo et al. (2012), TG2 has been shown to be induced and activated as a result of endoplasmic reticulum (ER) stress via the protein kinase ribonucleic acid-like endoplasmic reticulum kinase (PERK) pathway and NFkB activation. After activation TG2 translocates to the nucleus via importin α3 (Kuo et al. 2011) where it crosslinks and inactivates specificity protein 1 (Sp1), a general transcription factor that is responsible for the induction and expression of a proto-oncogene for the hepatocyte growth factor receptor (c-Met). Increased TG2 activity therefore, leads to silencing of Sp1 and a decrease in expression of survival factors leading to apoptosis (Kuo et al. 2011).

The ER is a vast membranous organelle (Hotamisligil 2010), that is the site of synthesis, modification and trafficking of secreted and transmembrane proteins (Rutkowski & Kaufman 2004; Saito et al. 2011). Due to this central regulatory role of the ER, it is paramount for it to possess the ability to adapt its capacity to manage metabolic, synthetic and other adverse conditions

(Hotamisligil 2010). This adaptive capacity of the ER, is achieved by the quality control machinery in the ER which operates in concurrence with the protein folding pathways (Rutkowski & Kaufman 2004). The increase in the accumulation of misfolded or unfolded proteins (UP) within the ER lumen, irrespective of endoplasmic-reticulum-associated protein degradation (ERAD) function, is sensed by resident molecules of the ER (Rutkowski & Kaufman 2004) and initiates the adaptive response known as the unfolded protein response (UPR) (Hotamisligil 2010). These resident molecules include three ER membrane-bound proteins: inositol-requiring protein 1α (IRE1α), PERK and activating transcription factor (ATF) 6; which act as UPR sensors that monitor the ER lumen for UP and transduce signals to the cytosol and nucleus. These three arms of UPR mitigate ER stress by suppressing protein synthesis, facilitate protein degradation and increase protein folding capacity of ER by increasing the production of protein chaperones (Hotamisligil 2010; Saito et al. 2011; Tam et al. 2012). Upon ER stress the PERK pathway is first activated, where PERK activation leads to the phosphorylation of serine 51 on eukaryotic initiating factor (eIF) 2α, which stimulates the translation of ATF4 messenger ribonucleic acid (mRNA) (Lasfargues et al. 2013). Activating transcription factor 4 controls selective pro-survival genes related to amino acid metabolism, redox balance, protein folding and autophagy as well as several micro ribonucleic acids (RNAs) that contribute to the inhibition of protein synthesis (Hetz 2012). A transcription factor CCAAT-enhancer-binding protein homologous protein (CHOP) is upregulated by ATF4 and is involved in ER stress-induced apoptosis (Lasfargues et al. 2013). The PERK- mediated eIF2α phosphorylation has also been linked to increased NFkB activation; where the attenuation of translation leads to a rapid decrease in inhibitor kappa (Ik) Bα, an inhibitor of NFkB, due to its relatively short half-life and the inhibition of its translation. This consequently leads to an accumulation of free and activate NFkB present within the cytosol. It was shown that the extent of translational attenuation is directly proportional to the level of active NFkB (Tam et al. 2012). Nuclear factor kappa B is an important regulator of inflammatory mediators such as TNF-α and

interleukin (IL) -6 (Hotamisligil 2010) as well as being a transcriptional inducer of TG2 (Ientile et al. 2007).

Fumonisin B_1 disrupts sphingolipid biosynthesis and therefore the plasma membrane, which could lead to the disruption of the cell and potentially cause ER stress and apoptosis. This study thus investigated the effect of FB_1 on ER stress, apoptosis and the involvement of TG2 within these processes.

1.1 Aims

This study was conducted to determine:

a) The effect of FB_1 toxicity in the induction and catalytic activation of a calcium-dependent crosslinking enzyme TG2 in HepG2 cells.

b) Whether FB_1 exposure to HepG2 cells induces the PERK ER stress pathway as a mechanism of toxicity; with respect to TG2 activation.

1.2 Hypotheses

The following statements were hypothesised:

a) Fumonisin B_1 exposure would induce TG2 up-regulation and activation in HepG2 cells.

b) Fumonisin B_1 toxicity would induce the PERK ER stress pathway as a result of TG2 activation.

CHAPTER TWO

2 LITERATURE REVIEW

2.1 Fumonisin B_1

Fumonisin B_1, is the most toxic and prevalent secondary metabolite produced by fungi in the *Fusarium* sp., but most commonly by *Fusarium verticilliodes* (Gelderblom et al. 1988). South Africans are continuously exposed to low doses of FB_1, with a daily dietary intake of 200µg/kg body weight (IPCS 2001) according to the world health organisation (WHO). This mycotoxin is well characterised as a contaminant of maize and maize-based products both locally and worldwide (cited in Grenier et al. 2012). There have also been reports of FB_1 found in other grains such as rice (Park et al. 2005), wheat and oats in Southern Brazil (Mallmann et al. 2001), including animal feeds. Poor storage conditions is the leading cause of contamination, where fungi favour moist, humid and dark conditions to grow (Hussein & Brasel 2001). This natural toxin has a wide range of toxic effects in both humans and animals. It has also been classified as a possible class 2B carcinogen by the International Agency for Research on Cancer (IARC) (IARC 1993).

2.1.1 Chemical Structure

Fumonisins' chemical structure was first reported by Gelderblom et al. (1988), which was followed by the discovery of more than 28 homologues (cited by Voss et al. 2007). The structure is based on a hydroxylated hydrocarbon chain, rather than a cyclic structure most commonly associated with mycotoxins (Heidtmann-Bemvenuti et al. 2011). Fumonisin B_1 is the most common and thoroughly studied of the fumonisin homologues (Voss et al. 2007) and is the most prevalent mycotoxin in Africa due to maize being the staple diet of most rural inhabitants (Domijan & Abramov 2011). Fumonisin B_1 is a diester of propane-1,2,3-tricarboxylic acid (TCA) and 2-amino-12,16-dimethyl-

3,5,10,14,15-pentahydroxyeicosane, in which the carbon in position 14 (C_{14}) and C_{15} hydroxyl groups are esterfied with a terminal carboxyl group of TCA (Figure 2.1A) (Soriano et al. 2005). The chemical structure of FB_1 is similar to sphingoid bases: sphinganine (Sa) and sphingosine (So) (Figure 2.1B and C) which are important molecules in the biosynthesis of sphingolipids. The sphingoid bases consist of an amine and two alcohol groups attached to a 3C chain which is connected to a long hydrocarbon chain (Figure 2.1B and C). This structural similarity is critical for FB_1 toxicity, where it disrupts the sphingolipid metabolism (Wang et al. 1991). The free amino group in FB_1 (Figure 2.1A) creates an amino pentol backbone, that is important in FB_1 toxic activity, where it competes with the sphingoid bases in the biosynthesis of sphingolipids (Soriano et al. 2005).

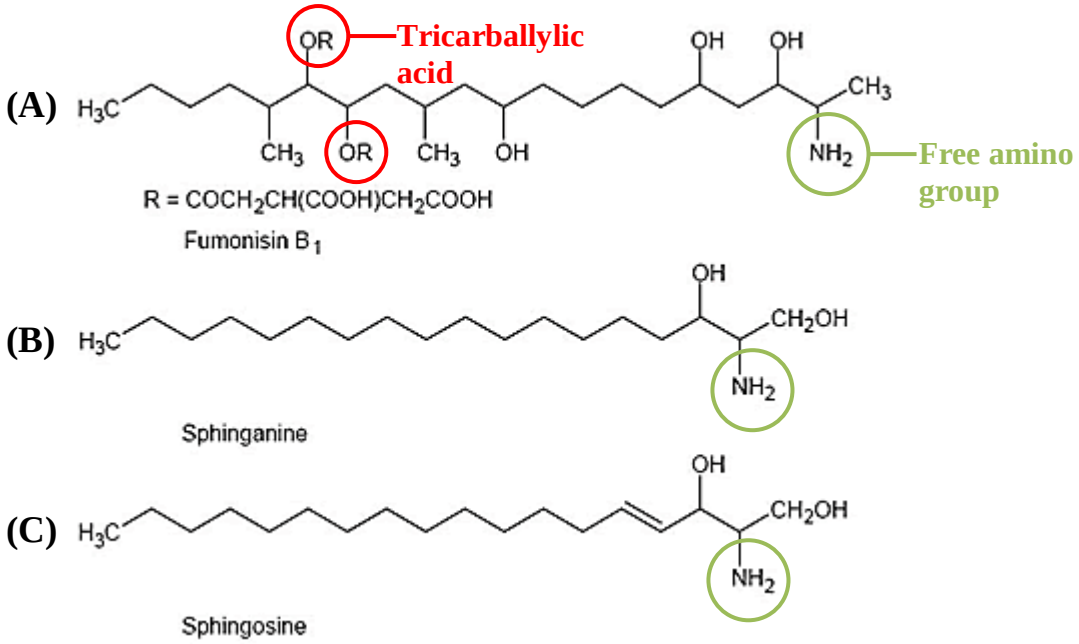

Figure 2.1: Chemical structure of (A) Fumonisin B_1 and its similarities to sphingoid bases (B) Sphinganine and (C) Sphingosine (Griessler 2008).

2.1.2 Mechanism of Toxicity

Fumonisin B_1 exerts its toxic effect through the disruption of sphingolipid metabolism (Wang et al. 1991). The structural similarity between FB_1 and the sphingoid bases: Sa and So, allow for the competitive inhibition of the rate limiting enzyme, ceramide synthase, in the *de novo* biosynthesis of sphingolipids (Figure 2.2) (cited in Voss et al. 2007).

2.1.2.1 De novo Sphingolipid biosynthesis

Sphingolipids play an important role in plasma membrane structure, cell growth regulation and in the transduction pathway, where ceramide acts as a second messenger for a range of factors such as TNF (Soriano et al. 2005). The *de novo* biosynthesis of sphingolipids (Figure 2.2) occurs at the cytosolic face of the ER. The first step is catalysed by serine palmitoyl-transferase, where serine and palmitoyl-CoA are condensed to form 3'-keto-Sa, which is then reduced to form Sa or dihydroSo. Sphinganine can either by phosphorylated to form Sa-1-phosphate or N-acylated to dihydroceramide by ceramide synthase (CS). The dihydroceramide undergoes desaturation to produce ceramide. Ceramide can either be transformed to form sphingomyelin or glycolipids, through the addition of phosphocholine or oligosaccharides, respectively. Sphingosine is generated through the catalytic conversion of ceramide by ceramidase. Sphingosine is phosphorylated by So kinase to produce So-1-phosphate. Sphingosine-1-phosphate and Sa-1-phosphate have the potential to produce ethanolamine phosphate and fatty aldehyde. When the last products are converted to serine and palmitoyl-CoA the cycle is closed (Soriano et al. 2005).

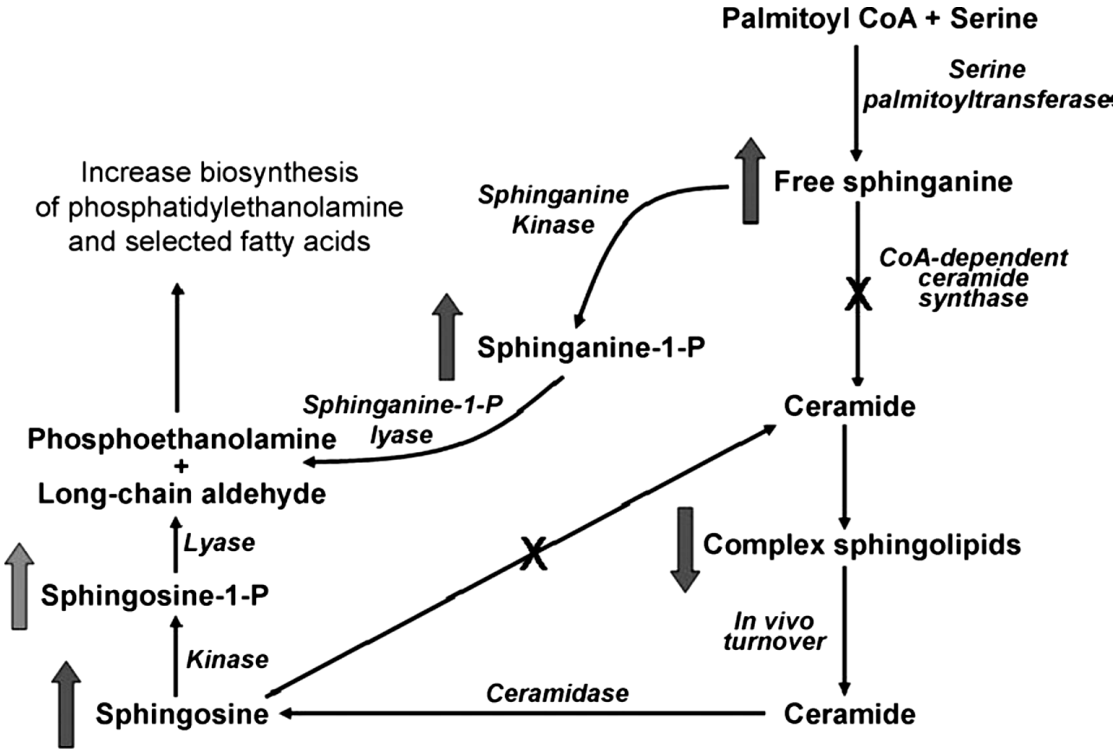

Figure 2.2: Schematic summary of sphingolipid metabolism and the disruption of the *de novo* synthesis of ceramide due to the inhibition (X) of ceramide synthase by FB_1 (Voss et al. 2007).

2.1.2.2 Competitive Inhibition of ceramide biosynthesis

Ceramide synthase is an important enzyme in sphingolipid metabolism; it is responsible for the acylation of Sa to form ceramide and the reacylation of So to ceramide. The amino-pentol backbone of FB_1 competes for the same binding site on ceramide synthase as the sphingoid base substrates and FB_1's anionic TCA interferes with the binding site for the fatty acyl-CoA, therefore effectively inhibiting ceramide synthase (Merrill et al. 2001). The inhibition of ceramide synthase leads to a cascade of events; which include the inhibition of ceramide biosynthesis, increased free Sa and So, decreased reacylation of So derived from complex sphingolipid turnover and increased sphingoid base degradation of dietary sphingolipids (Riley et al. 2001). The accumulation of free Sa and few So and their metabolites in tissue has been correlated with apoptosis in the liver and kidneys of rats (reviewed by Voss et al. 2007), thus suggesting that Sa and So exert a pro-apoptotic effect as a mechanism of FB_1 toxicity. The inhibition of ceramide formation results in fewer complex sphingolipids such as sphingomyelin, which is a major component of the plasma membrane. This

compromises the integrity of the plasma membrane thus suggesting a further mechanism of FB_1 toxicity (Nour et al. 2007).

2.1.3 Toxicity

2.1.3.1 In Animals

Fumonisin B_1 is associated with several animal diseases as a result of consumption of mouldy maize and feeds. It has been reported that F. *verticillioides'* FB_1 is the main cause of equine leukoencephalomalacia (Kellerman et al. 1990) and has been shown to be cardiotoxic to pigs and also causes porcine pulmonary oedema (Harrison et al. 1990; Voss et al. 2007). In rats, FB_1 has been shown to be hepatotoxic and nephrotoxic (Gelderblom et al. 1991).

2.1.3.2 In Humans

In humans, it has been linked with higher incidences of oesophageal cancers in the Transkei Region (Marasas et al. 1988). In populations consuming large amounts of contaminated maize, there has been higher incidences of neural tube defects in foetuses and cardiovascular problems (Gelineau-van Waes et al. 2005; Fincham et al. 1992). There is also a higher incidence in hepatotoxicity and nephrotoxicity observed where maize is the staple diet of the population (IPCS 2001; cited in Domijan & Abramov 2011).

2.2 Tissue Transglutaminase

Transglutaminases (E.C 2.3.2.13) are enzymes that catalyse post-translational modifications of proteins. There are 9 different TGs identified within the human body all having different

biochemical functions (Table 2.1). Tissue transglutaminase is a unique member of this family, due to it also being able to act as a G-protein when bound to guanosine-5'-triphosphate (GTP). Tissue transglutaminase is a ubiquitous protein that is predominately found in the cytosol (80%) but is also localised in plasma (10-15%) and in the nuclear membrane. Tissue transglutaminase is an important enzyme in a number of biological processes such as cell differentiation and proliferation, extracellular matrix organisation, cell signalling and apoptosis (cited in Martin et al. 2012).

Table 2.1: Transglutaminases found within the human body and their important features (Mehta 2005).

Protein	Main functions	Distribution	Disease	Alternate names
TG1	Cell envelope formation during keratinocyte differentiation	Membrane-bound in keratinocytes	Lamellar ichthyosis	TG1, TG_K, keratinocyte TG, particulate TG
TG2	Apoptosis, cell adhesion, matrix stabilization, cell-survival signaling	Widely distributed in many tissues; cytosolic, nuclear, membrane, extracellular	Autoantigen in celiac disease	Tissue TG, TG_C, liver TG, endothelial TG, erythrocyte TG, Gh_a
TG3	Cell envelope formation during keratinocyte differentiation	Hair follicle, epidermis, brain	Expression downregulated in head and neck squamous cell carcinoma and in laryngeal carcinoma	TG_E, callus TG, hair follicle TG, bovine snout TG
TG4	Reproduction especially in rodents as a result of semen coagulation	Prostate	Not known	Prostate TG, TG_p androgen regulated major secretory protein, vesiculase, dorsal prostate protein 1 (DP1)
TG5	Cornified cell envelope formation during keratinocytes differentiation	Foreskin keratinocytes, epithelial barrier lining and skeletal muscular striatum	Secondary effect to the hyperkeratotic phenotype in ichthyosis and in psoriasis	TG_X
TG6	Not known	Testis and lung	Not known	TG_Y
TG7	Not known	Ubiquitous but predominantly in testis and lung	Not known	TG_Z
FXIIIa	Blood clotting, wound healing, bone growth	Platelets, placenta, synovial fluid, chondrocytes, astrocytes, macrophages	Factor XIIIa deficiency	Fibrin-stabilizing factor, fibrinoligase, plasma TG, Laki-Lorand factor
Band 4.2	Major component in erythrocyte skeletal network	Erythrocyte membranes, bone marrow, spleen	Spherocytic elliptocytosis	B4.2, ATP-binding erythrocyte membrane protein band 4.2

2.2.1 Structure

The TG2 gene is located on chromosome 20q11-12, it is 32.5kb in size and consists of 13 exons and 12 introns (Gentile et al. 1994). Regulatory sequences are found on the 5' terminal region of the TGM2 (Figure 2.3), where transcription factors bind and activate transcription of TG2 (Elli et al. 2009). There are several transcriptional inducers of TG2 which include retinoic acid, cyclic adenosine monophosphate (AMP), hydrogen peroxide, vitamin D, steroid hormones, cytokines and growth factors including: TNFα, IL-6, transforming growth factor (TGF)-β and interferon- y and β (cited in Elli et al. 2009). Nuclear factor kappa B has also been found to induce TG2 transcription (Mirza et al. 1997).

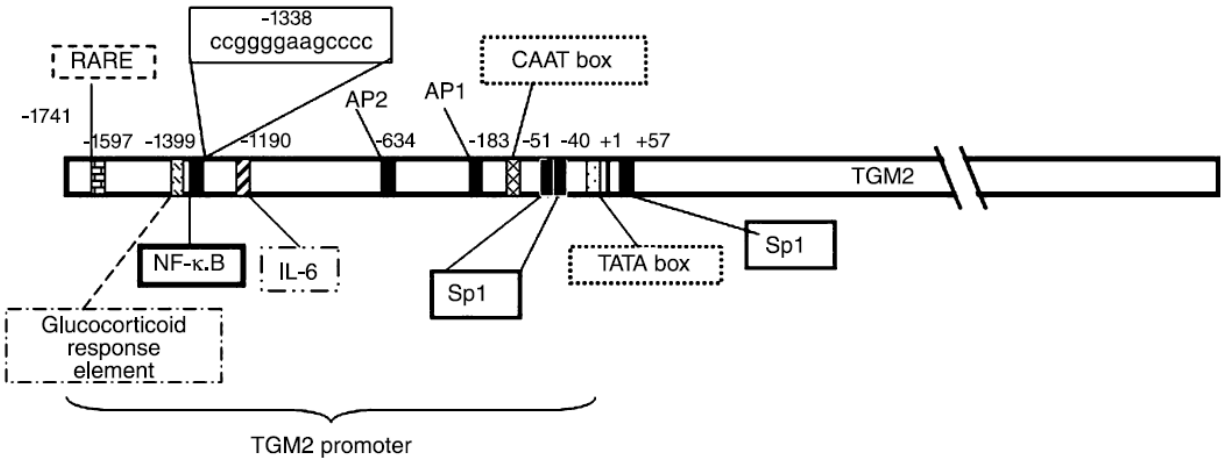

Figure 2.3: Tissue transglutaminase promoter gene. Illustrating the proximal binding sites of transcriptional inducers of TGM2 (Ientile et al. 2007).

The full length TG2 protein consists of 687 amino acids and is approximately 77kDa in size. Tissue transglutaminase has four distinct domains (Figure 2.4A): an N-terminal β-sandwich with fibronectin and integrin binding sites, a central catalytic core that contains a catalytic triad (cysteine 277, histidine 335 and aspartic acid 358) for the acyl transfer reaction and a conserved tryptophan (Trp) which is vital for catalytic activity. There are also two C-terminal β-barrel domains where the

second domain contains a phospholipase C binding sequence (reviewed by: Fesus & Piacentini 2002; Lesort et al. 2000).

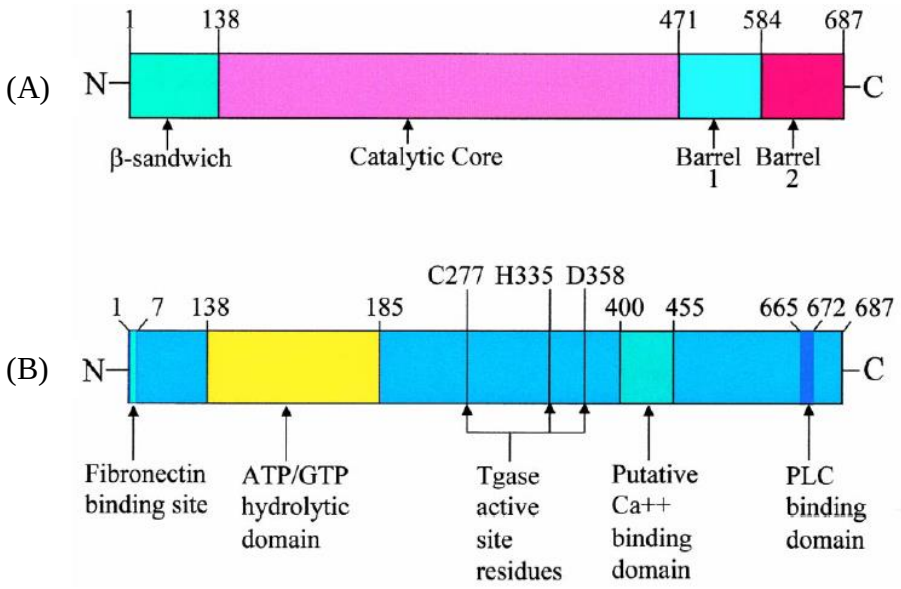

Figure 2.4: Structural (A) and functional (B) domains suggested for the human TG2 gene (Lesort et al. 2000).

The catalytic core contains domains for adenosine triphosphate (ATP)/GTP and calcium binding sites as well as the active site which consists of the catalytic triad (Figure 2.4B). When TG2 is bound to guanosine diphosphate (GDP), the catalytic triad is blocked by two loops and the active site cysteine is hydrogen-bonded to a tyrosine residue thus rendering TG2 transamidation activity latent (Figure 2.5B) (Liu et al. 2002). Upon calcium binding, TG2 undergoes a conformational change which induces the transamidation activity of TG2 by exposing the active site. The conformational change occurs through an increase in the interdomain distance between the catalytic domain and the two C-terminal barrel domains which exposes the catalytic triad to substrates (Figure 2.5C) (Pinkas et al. 2007). When TG2 is bound to ATP, it does not inhibit TG2 transamidation activity but instead inhibits GTP hydrolysis (Lai et al. 1998).

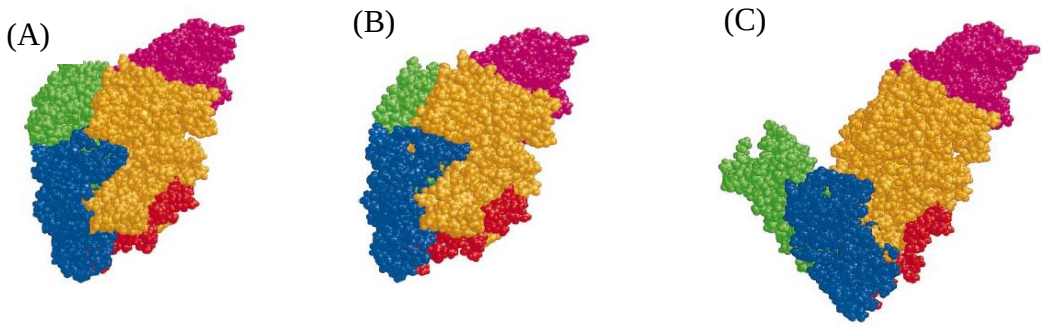

Figure 2.5: Structure of TG2 under normal conditions (A) TG2 bound to GTP (B) and TG2 activated in the presence of calcium (C) (Griffin et al. 2002). The blue section indicates the catalytic core, green indicates the β-barrel and pink indicates the barrel domain.

2.2.2 Biochemical Function

Tissue transglutaminase is unique because it not only catalyses the post-translational modification of proteins but also has GTPase activity where it participates in transmembrane signalling (Figure 2.6). Under normal physiological conditions, TG2 activity is latent due to low intracellular calcium concentrations (10-20nM) and high GTP concentrations (Fesus & Piacentini 2002; Kuo et al. 2011). Under pathophysiological conditions however, when the intracellular calcium concentration (>700-800nM) is high; TG2 crosslinking ability is activated (Kuo et al. 2011). This binding of GTP and calcium is regulated in a reciprocal manner, where GTP binding inhibits calcium binding and vice versa (Martin et al. 2012).

2.2.2.1 Post-translation modification of proteins

This reaction occurs via a two-step mechanism:

The transamidation activity of TG2 is activated by calcium binding resulting in the exposure of the active site cysteine residue. The γ-carboamide group of the glutamine substrate reacts with the

cysteine residue to produce a thioacyl-enzyme intermediate and ammonia. The nucleophilic primary amine substrate reacts with the thioacyl-enzyme intermediate, resulting in a covalent bond between the amine donor and the glutaminyl acceptor. The cysteine residue within the active site is regenerated once the covalent bond is formed.

When the primary amine is donated by a polyamine then a γ-glutamylamine bond is produced (Figure 2.6A1). A polyamine can also act as a N,N-*bis* (γ-L-glutamyl) polyamine bridge between two glutamine donors, whether on the same protein or between different proteins. If the primary amine is donated by the Ɛ-amino group of the lysine residue of the substrate a protease-resistant covalent N-γ-glutamyl-Ɛ-lysyl-isopeptide bond is generated (Figure 2.6A2). In the absence of a primary amine donor, water may act as the attacking nucleophile resulting in the deamidation of the donor glutamine to glutamate (Figure 2.6A3) (cited in Martin et al. 2012; Elli et al. 2009).

Tissue transglutaminase has isopeptidase activity (Figure 2.6A4). It can also be externalised from the cell to the extracellular space where it promotes cell-matrix interactions, especially between fibronectin and integrin, and it crosslinks proteins within the extracellular matrix (Figure 2.6B5) (Fesus & Piacentini 2002).

2.2.2.2 Guanine Triphosphatase activity

The binding and hydrolysing of GTP by TG2, is with an affinity and catalytic rate similar to heterotrimetric G protein α subunits and small Ras-type G proteins. This TG2 bound to GDP (Figure 2.6B) couples α-adrenoreceptors, oxytocin and thromboxane receptors to phospholipase C thus initiating inositol phosphate production. This stimulates a transmembrane signalling cascade (Figure 2.6B6) (Reviewed by Fesus & Piacentini 2002).

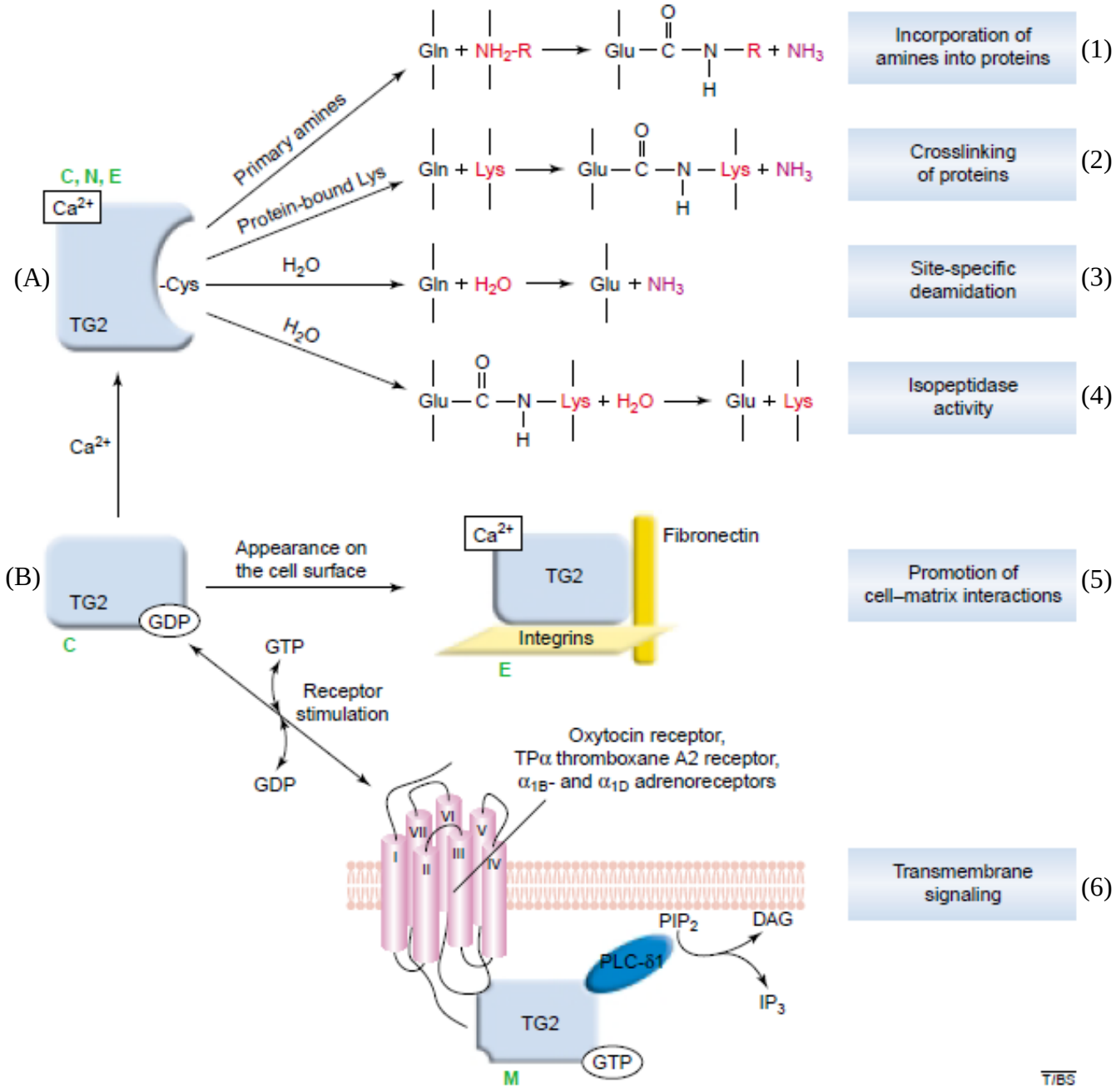

Figure 2.6: Tissue transglutaminase's Biochemical Activities. Catalytic calcium-dependent acyl transfer (A) between: γ-carboxamide group of glutamine substrates and either primary amines (1) or the Ɛ-amine group of protein bound lysine residue to form an irreversible crosslink (2), water can replace the amine donor substrate which results in deamination of glutamine to glutamate (3) and isopeptidase activity of TG2 (4). Guanosine triphosphate-bound TG2 promotes cell-matrix interactions (5) and has GTPase activity where it binds and activates phospholipase C thereby initiating transmembrane signaling (6) pathways. Tissue transglutaminase functions within the nucleus (N), cytosol (C), extracellular matrix (E) and the plasma membrane (M) (Fesus & Piacentini 2002).

2.2.3 Role in apoptosis

Apoptosis is an important pathway that controls normal growth and tissue homeostasis. The induction and activation of TG2 has been linked to increased apoptosis in rat hepatocytes (Fesus et al. 1987); with widespread evidence for TG2 gene up-regulation during apoptosis (cited in Griffin et al. 2002). An important feature of TG2 calcium-dependent crosslinking activity is the stabilisation of apoptotic cells prior to phagocytic clearance during the final events of apoptosis (Knight et al. 1991). This stabilisation is a result of detergent-insoluble protein scaffolds that form to prevent the release of harmful intracellular components into the extracellular space, which limits inflammation and auto-immune responses (Piredda et al. 1997; Fesus & Piacentini 2002).

During increased intracellular calcium levels, TG2 is translocated into the nucleus via importin α3, a nuclear transporter (Peng et al. 1999). Nuclear TG2 (nTG2) regulates gene expression through post-translational modifications and interactions with transcription factor and related proteins such as Sp1 and histones. This feature of nTG2 allows it to control cell growth and apoptosis. Nuclear TG2 crosslinks core histone proteins: H2A, H2B, H3 and H4, which are glutamine substrates of nTG2 (Ballestar et al. 1996). These crosslinked histones are suggested to contribute to chromatin condensation which is a morphological hallmark of apoptosis (Park et al. 2010).

A general transcription factor, Sp1 that is rich in lysine and glutamine residues is a good substrate for TG2 transamidation. Nuclear TG2 crosslinks Sp1 resulting in dimers and trimers of Sp1, which has been suggested to have higher transcription factor activation activity compared to a single Sp1 molecule. It has also been reported however, that highly crosslinked and oligomerised Sp1 leads to inactivation and silencing of Sp1 transcriptional activity in hepatocytes, leading to decrease expression of c-Met. Increased TG2 activity therefore, leads to silencing of Sp1 and a decrease in expression of survival factors, leading to apoptosis (reviewed in Kuo et al. 2011).

2.2.4 Role in inflammation

An increase in TG2 activity has been observed in inflammation and fibrotic conditions (Martin et al. 2012). The inappropriate protein associations that form due to TG2 crosslinking activity could become cytotoxic and induce inflammatory responses (Ientile et al. 2007). A central downstream mediator of inflammation, NFkB is activated by TG2. The inhibitor of NFkB; inhibitor kappa B (IkB) is polymerised by TG2, where it crosslinks its C-terminal glutamine cluster which renders IkBα inactive (Figure 2.7). Upon inactivation of IkB, NFkB is activated and able to enter the nucleus and act as a transcription factor (Lee et al. 2004; Ientile et al. 2007). Interestingly, NFkB is also a transcriptional inducer of TG2, where NFkB binds the TGM2 promoter gene directly and induces TG2 transcription (Figure 2.7) (Mirza et al. 1997). This could lead to further NFkB activation.

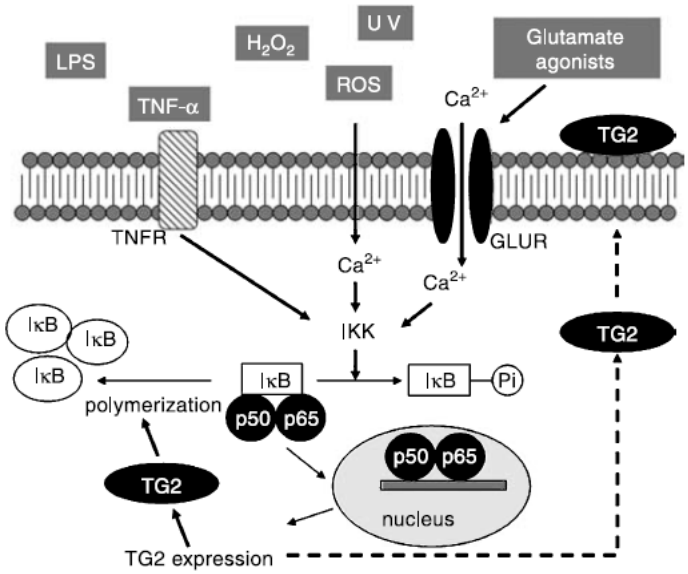

Figure 2.7: Proposed mechanism of TG2 induction and activation of NFkB (p50p65 molecule) (Ientile et al. 2007)

2.2.5 Disease associated with Tissue transglutaminase

Tissue transglutaminase has been reported in several inflammatory, neurodegenerative and liver diseases such as Coeliac disease, Huntington's Disease and Alzheimer's Disease. Coeliac disease is

a malabsorption syndrome, characterised by atrophy of villi in the jejunum on exposure to dietary glutens. Tissue transglutaminase deamidates specific glutamines that stimulate T-cell stimulatory gluten peptides. This leads to an immune response that destroys jejunum epithelium. Huntington's disease is characterised by progressive loss of neuronal cells due to the accumulation of ubiquitinated huntintin (htt) aggregates within the nucleus. There is an expansion of cytosine adenine guanine (CAG) trinucleotide repeats in the gene encoding for htt which results in a large number of contiguous glutamine residues in the htt protein. These htt aggregates, could be due to TG2 activity, as the expanded polyglutamine repeats are excellent glutamine donors for TG2 (reviewed in Fesus & Piacentini 2002).

2.3 Endoplasmic Reticulum Stress Pathway

2.3.1 The Endoplasmic Reticulum

The ER is a vast membranous organelle (Figure 2.8) (Hotamisligil 2010), that is the site of synthesis, folding, maturation and modification and trafficking of secreted and transmembrane proteins (Rutkowski & Kaufman 2004; Saito et al. 2011). The ER also acts as a major reservoir of intracellular calcium and therefore also plays a critical role in calcium homeostasis (Hetz 2012; Hotamisligil 2010). Due to this central regulatory role of the ER, it is paramount for the ER to possess the ability to adapt its capacity to manage metabolic, synthetic and other adverse conditions (Hotamisligil 2010). This adaptive capacity of the ER, is achieved by the quality control machinery in the ER, which operates in concurrence with the protein folding pathways (Rutkowski & Kaufman 2004). This machinery is highly selective, so that minor perturbations in the efficiency of protein folding would lead to the rejection of nascent proteins as misfolded, consequently causing the accumulation and degradation of these misfolded proteins (Rutkowski & Kaufman 2004). The presence of ERAD machinery, ensures that unfolded or misfolded proteins are retrotranslated to the

cytosol for targeted proteasomal degradation (Pagliassotti 2012). The increase in the accumulation of misfolded or UP within the ER lumen, irrespective of ERAD function, is sensed by resident molecules of the ER (Rutkowski & Kaufman 2004) and initiates the adaptive response known as the UPR (Hotamisligil 2010).

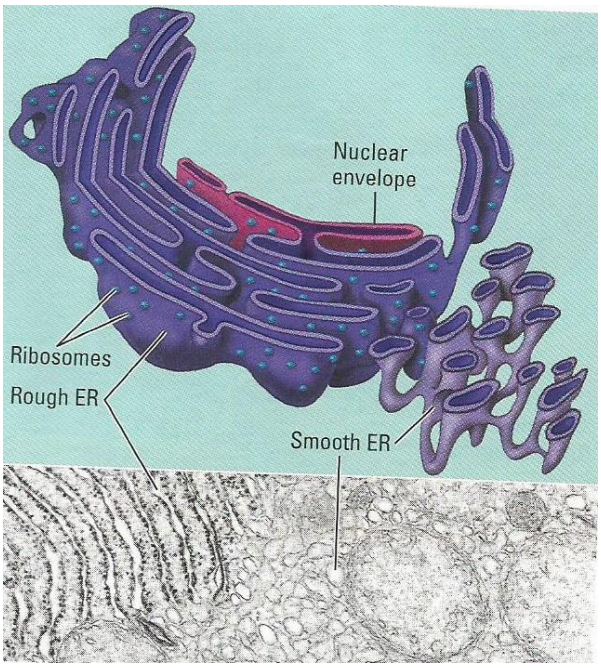

Figure 2.8: The Endoplasmic Reticulum (ER). Diagram of Rough ER with ribosomes and smooth ER without ribosomes (Above). Micrograph of both smooth and rough ER within the cell (Below) (Campbell et al. 2007).

2.3.2 Unfolded Protein Response Signaling

The UPR is initiated within the ER when protein folding becomes compromised. This could be a result of mutations in genes coding for transmembrane and secretory proteins, pathogen infections or metabolic conditions such as ischemia (Rutkowski & Kaufman 2004). Three ER membrane-bound proteins: IRE1α, PERK and ATF6 act as UPR sensors that monitor the ER lumen for UP and transduce signals to the cytosol and nucleus. In stress free conditions, luminal protein chaperone binding immunoglobulin protein (BiP) binds to the intraluminal domain of these UPR sensors, rendering them inactive (Bertolotti et al. 2000). The accumulation of UP and increased protein

cargo within the ER, leads to the dissociation of BiP from the UPR sensors, and sequester on UP due to its higher affinity for UP (Bertolotti et al. 2000). The dissociation of BiP from IRE1α (Figure 2.9A) and PERK (Figure 2.9C) causes the oligomerisation, auto-phosphorylation and activation of these sensors and downstream signalling pathways (Hotamisligil 2010; Pagliassotti 2012). Whilst the dissociation of BiP from ATF6 allows the translocation of ATF6 to the Golgi apparatus, where it is processed by serine protease 1 (S1P) and metalloprotease site-2 protease (S2P) to yield an active transcription factor which enters the nucleus (Figure 2.9B) (Shen et al. 2002). The UP sequestered on BiP are translocated to the cytosol for proteasomal degradation by ERAD (Kaufman 2004). These three arms of UPR mitigate ER stress by suppressing protein synthesis, facilitate protein degradation and increase protein folding capacity of ER by increasing the production of protein chaperones (reviewed by: Hotamisligil 2010; Saito et al. 2011; Tam et al. 2012).

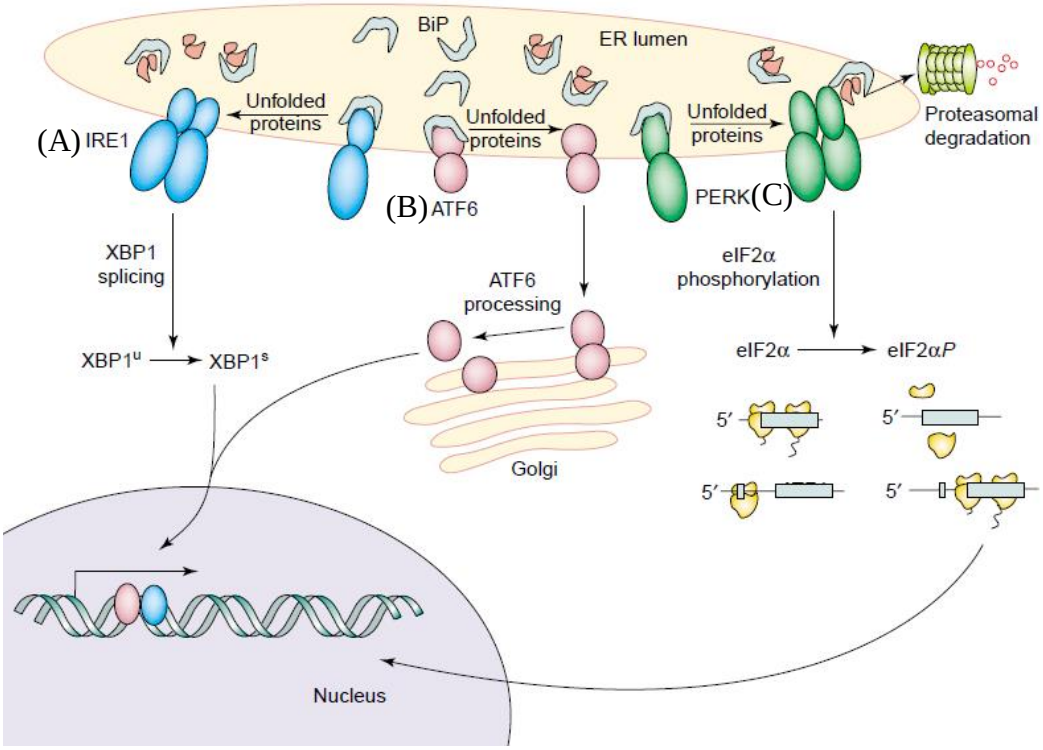

Figure 2.9: The Unfolded Protein Response (UPR). The UPR stress sensors are activated when there is an accumulation of misfolded proteins within the ER lumen. This causes BiP dissociation from the UPR sensors and sequester on unfolded proteins. The unfolded proteins undergo proteasomal degradation. The active UPR sensors initiate downstream signalling mechanisms to restore ER folding capacity via: (A) inositol-requiring protein 1α (IRE1α) pathway, (B) activating

transcription factor 6 (ATF6) pathway and (C) protein kinase RNA-like endoplasmic reticulum kinase (PERK) pathway (Kaufman 2004).

2.3.3 Protein kinase ribonucleic-like endoplasmic reticulum kinase Attenuation of Protein Translation

The first step in protein synthesis is the transcription of the genetic code into mRNA. The mRNA is then translated into polypeptides or proteins. The translation initiation step is controlled by eIFs. The binding of the 40S ribosomal RNA (rRNA) and transfer RNA (tRNA), is dependent on group 2 eIF proteins (eIF2α and eIF2β), to form the 43S pre-initiation complex. After the 43S pre-initiation complex is assembled it binds to mRNA to generate the 48S pre-initiation complex. This step is regulated by eIF group 3 and 4F. During ER stress, these eIFs are targeted and inactivated which results in the attenuation of protein translation (reviewed in Lasfargues et al. 2013).

The reversible, transient attenuation of translation initiation is the immediate response to ER stress which reduces the demand on protein folding machinery (Kaufman 2004; Malhotra & Kaufman 2007). This inhibition of protein translation is a downstream effect of PERK activation. The N-terminal domain of PERK, an ER type 1 transmembrane protein kinase, is exposed to the ER lumen and is sensitive to ER stress signals (Ron 2002). Its C-terminal cytoplasmic serine/threonine kinase domain directly phosphorylates eIF2α (Rutkowski & Kaufman 2004).

The heterotrimetric complex, eIF2, is composed of eIF2α, β and γ. In order for tRNA to interact with the eIF2 complex, the eIF2γ subunit needs to be bound to a GTP molecule. This interaction is controlled by eIF2β, as it possesses a guanine nucleotide exchange factor (GEF) where it converts GDP to GTP (Lasfargues et al. 2013). This ternary complex of eIF2-GTP-$tRNA^{Met}$ delivers the initiator methionyl tRNA to the 40S ribosomal subunit which is essential for adenine uracil guanine (AUG) start codon selection during translation (Kaufman 2004). During ER stress however, PERK

activation leads to the phosphorylation of serine 51 on eIF2α which causes GEF to have a higher affinity for GDP and is sequestered by the eIF2γ subunit. This inhibition of tRNA and eIF2 complex interaction due to eIF2α phosphorylation, prevents the assembly of the 43S pre-initiation complex which leads to the attenuation of protein synthesis (Figure 2.10) (Kaufman 2004; Lasfargues et al. 2013).

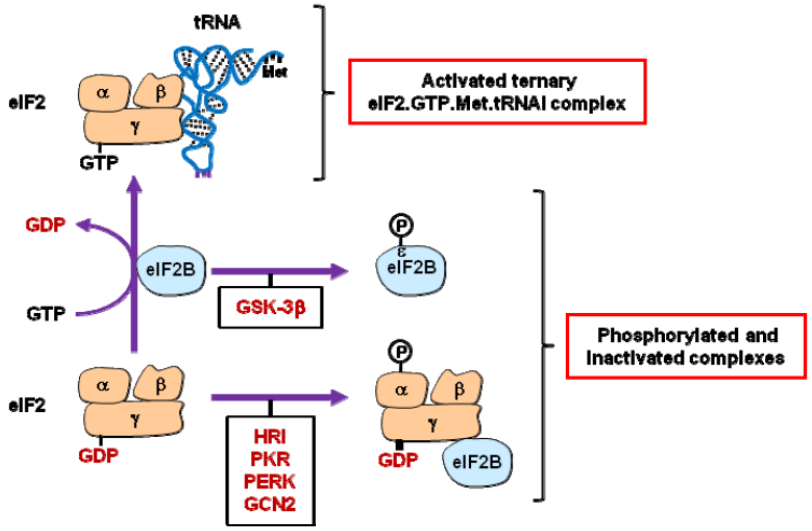

Figure 2.10: The regulation of eIF2 activity. The association between eIF2γ subunit with GTP occurs as a result of guanine nucleotide exchange activity of eIF2β. This results in the formation of the ternary eIF2.GTP.Met.tRNA initiation complex. The phosphorylation of eIF2α by PERK inhibit eIF2β exchange activity which inhibits the formation of the initiation complex (Lasfargues et al. 2013).

Stressed cells require the activity of pro-survival and pro-apoptotic proteins and therefore require protein synthesis of specific proteins. Eukaryotic initiating factor 2α phosphorylation, can therefore paradoxically stimulate the selective translation of specific mRNAs (Kaufman 2004). The synthesis of these proteins is permitted despite general protein synthesis attenuation, due to their mRNAs containing specific *cis*-acting elements that allow for ribosomal recruitment (Lasfargues et al. 2013). The activation of PERK leads to the phosphorylation of eIF2α which stimulates the translation of ATF4 mRNA. In non-stressed cells, ATF4 mRNA translation is silenced due to the

presence of 2 short upstream open reading frames (µORF), located within the 5' untranslated region (UTR). After ribosomes translate the first µORF, they can efficiently re-initiate at the second µORF which prevents translational initiation at the downstream ATF4 start codon therefore silencing the ATF4 mRNA. Upon ER stress, eIF2 becomes phosphorylated which impairs the initiation at the second µORF due to decreased ternary complex activity. The second µORF is therefore bypassed and the ribosomes are able to scan the downstream ATF4 start codon, allowing for the translation of ATF4 mRNA (Lasfargues et al. 2013). Activating transcription factor 4 controls selective pro-survival genes related to amino acid metabolism, redox balance, protein folding and autophagy as well as several microRNAs that contribute to the inhibition of protein synthesis (Hetz 2012).

The transcription factor CHOP is also translated paradoxically during translation attenuation activated by PERK. The phosphorylation of eIF2α allows the ribosome to bypass an inhibitory µORF which allows the mRNA translation of CHOP (Lasfargues et al. 2013). This transcription factor is upregulated by ATF4 and is involved in ER stress mediated apoptosis (Fawcett et al. 1999).

2.3.4 Protein kinase ribonucleic-like endoplasmic reticulum kinase Activation of Nuclear factor kappa B

It has been reported that ER stress activates NFkB (cited in Tam et al. 2012). Nuclear factor kappa B is found within the cytosol bound to IkB which renders NFkB inactive. A protein IkB kinase (IKK) is composed of IKKα, β and γ subunits. The IKKβ subunit phosphorylates IkBα serines at position 32 and 36 which then undergoes proteasome-mediated degradation. This phosphorylation and degradation of IkBα, allows the release and activation of NFkB. The active NFkB translocates to the nucleus and binds to its consensus sequence, leading to the transcriptional activation of target genes (DiDonato et al. 1996). The activation of NFkB has been linked to PERK-mediated eIF2α

phosphorylation; where the attenuation of translation leads to a rapid decrease in IkBα due to its relatively short-half life and the inhibition of translation. This consequently, leads to an accumulation of free and active NFkB present within the cytosol. It was shown that the extent of translational attenuation is directly proportional to the level of active NFkB (cited in Tam et al. 2012). Nuclear factor kappa B is an important regulator of inflammatory mediators such as TNF-α and IL-6 (Li et al. 2005).

2.3.5 Endoplasmic Reticulum Stress Feedback Mechanisms

The UPR requires a feedback mechanism that prevents a hyper-activated response or prematurely turned off response. This negative feedback loop is done through the repression of the PERK pathway, mediated by $p58^{IPK}$ a co-chaperone and growth arrest and deoxyribonucleic acid (DNA) damage-inducible protein (GADD34). The activation of the PERK pathway leads to the transcription of ATF4 which up-regulates GADD34 expression. This gene associates with protein phosphatase1 (PP1) which contains an ER localised motif. This motif dephosphorylates eIF2α which leads to increased protein synthesis and restoration of ER folding capacity. The $p58^{IPK}$ gene down-regulates and dephosphorylates PERK which leads to the termination of the UPR when the ER folding capacity returns to normal and ER stress is overcome (Yan et al. 2002; Rutkowski & Kaufman 2004).

2.3.6 Endoplasmic Reticulum Stress Induced Apoptosis

In circumstances where the translational adaptive responses are insufficient and fail to resolve protein folding defects to restore the protein folding capacity of the ER due to prolonged or severe stress; the apoptotic pathway is activated (Lasfargues et al. 2013; Malhotra & Kaufman 2007). The initiation of apoptosis occurs via two signalling pathways: the intrinsic mitochondrial-dependent

pathway and the extrinsic mitochondrial-independent pathway. The extrinsic pathway, involves Fas (member of TNF family) death receptor-induced activation of initiator caspase 8 which activates downstream effector caspase 3. The intrinsic pathway, involves mitochondrial induction by B-cell lymphoma 2 (Bcl-2) family of proteins, such as Bax, to release cytochrome *c* into the cytosol. The cytochrome c then binds apoptotic protease activating factor 1 (Apaf-1) resulting in initiator caspase 9 activation which forms an apoptosome that activates caspase 3. The activated effector caspases induce the cleavage of cellular components, especially the cytoskeleton causing apoptosis (Ghobrial et al. 2009; Rutkowski & Kaufman 2004).

Apoptosis induced by ER stress is described more often as an intrinsic pathway however, it has elements of both extrinsic and intrinsic pathways. Apoptosis is induced by the following signals (Figure 2.11):

Caspase 12 localised within the ER membrane is dissociated from TNF receptor-associated factor (TRAF2) which allows its dimerization and activation which leads to the activation of caspase 9 independent of cytochrome *c* and Apaf-1. The active caspase 9 then activates downstream effectors of apoptosis (Rutkowski & Kaufman 2004).

The apoptosis signal-regulating kinase 1 (ASK1)/ c-jun N-terminal kinase (JNK) pathway is activated by IRE1α. Endoplasmic reticulum stress causes the interaction between IRE1 and TRAF2, which results in the activation of ASK1 and JNK leading to the initiation of the proapoptotic phosphorylation cascade (Rutkowski & Kaufman 2004).

The calcium concentration regulation within the ER might also act as a trigger for apoptosis. Endoplasmic reticulum stress triggers conformational changes and oligomerisation of Bcl-2 homology (BH) 3-only proteins such as Bax and Bak, at the ER membrane. The ER localised Bak causes the depletion of calcium within the ER which activates caspase 12. The rapid release of calcium from the ER into the cytosol, leads to calcium uptake within the mitochondria which causes

the collapse of mitochondrial inner-membrane potential most commonly associated with apoptosis (Rutkowski & Kaufman 2004).

The transcriptional suppression of anti-apoptotic Bcl-2 protein by CHOP induces apoptosis. The pro-apoptotic transcription factor, CHOP is induced and activated by the PERK/eIF2α-dependent ER stress pathway (Rutkowski & Kaufman 2004). The transcription factor, CHOP is known to activate the transcription of several genes that have the potential to initiate apoptosis; these include GADD34 and death receptor (DR) 5. The gene GADD34 encodes for protein phosphatase 2C subunits that dephosphorylates eIF2α and promotes protein synthesis. Increased protein synthesis during ER stress, leads to the chronic activation of the UPR therefore inducing apoptosis as the ER cannot resolve proper protein folding capacity. The DR5 gene encodes death receptors on the cell surface that potentially activate the caspase cascade leading to apoptosis (reviewed in Malhotra & Kaufman 2007).

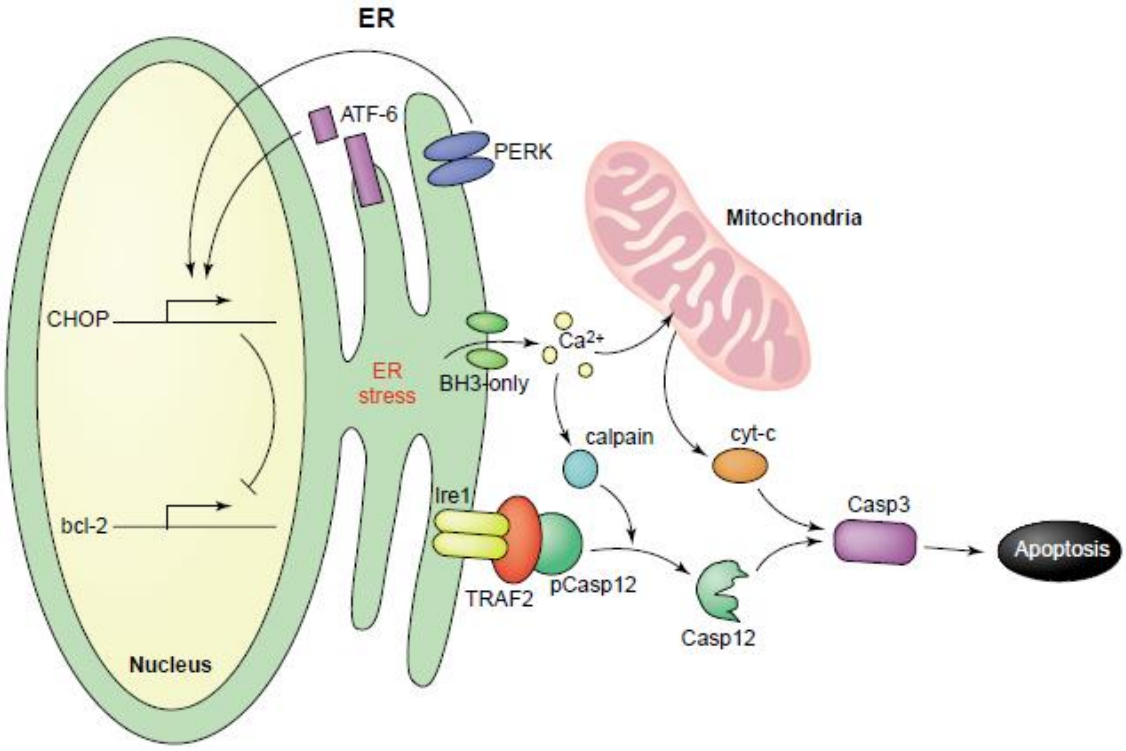

Figure 2.11: The ER stress induced Apoptosis via: PERK/eIF2α mediated CHOP transcription, Bak/Bax regulation of calcium release from ER, IRE1 mediated activation of ASK1 and JNK and the cleavage and activation of caspase 12 (Rutkowski & Kaufman 2004).

CHAPTER THREE

3 MATERIALS AND METHODS

3.1 Cell Culture

HepG2 cells are a human liver hepatocellular carcinoma cell line and were purchased from Highveld Biological Association (Johannesburg, RSA). Fumonisin B_1 is highly cytotoxic especially to the liver, where it has been reported in studies that FB_1 causes hepatocarcinogenity in mice and liver injury (He et al. 2005). The liver, as a result of its regenerative properties and the first site of detoxification of harmful substances including FB_1, is an important organ within the body. It is therefore, important to determine the effects of FB_1 on the liver and to specifically look at mechanisms by which liver damage occurs.

HepG2 cells were cultured in Eagle's minimal essential medium buffer (Lonza) supplemented with 10% Foetal Calf serum (GIP Co), 1% penicillin/streptomycin (GIP Co), 1% Gentamycin (Sigma, lot 95K2411) and 1% L-glutamate (GIP Co).

HepG2 cells were first reconstituted; vials containing $1x10^6$ cells/ml were removed from liquid nitrogen and thawed at 37°C. Once the cells were thawed, they were placed into a medium flask and 10ml cell medium was added to the flask and incubated for 24hours to allow the cells to attach to the flask. After 24hours, the cell medium was removed, the cells washed with 5ml 0.1M PBS (pH7.4) twice and 10ml of fresh cell media was added to the flask. The flask was incubated at 37°C for 3days to allow the cells to increase in number. When the flask was 90% confluent, the flask was trypsinised and half the cells were cryopreserved and the other half used to continue making a cell stock. To trypsinise cells, the cell medium was removed from the confluent flask, the cells washed with 5ml 0.1M PBS (pH7.4) twice to remove media, as the foetal calf serum deactivates the trypsin. To the flask, 1ml of Trypsin-Versene (EDTA) (GIP Co) was added and the flask incubated for

5minutes at 37°C, to allow the Trypsin to break the adherent proteins between cells and the flask. After the proteolytic activity of the Trypsin the cells appeared round. The trypsin was removed from the flask and 2ml of cell media was added to the flask. The flask was then gently agitated repeatedly, against the palm of the hand, to detach the cells from the flask surface. The cells were then collected within a 15ml sterlin tube and the cells were counted. To count the number of cells within the flask after trypsinisation, the Trypan Blue method was used. In an eppendorf 150µl of cell media, 50µl 3.4% Trypan blue and 50µl cell suspension was added to make the Trypan blue solution. A cover slip was placed over the hemocytometer chamber and 10µl of the above Trypan blue solution was added to both chambers of the hemacytometer, using capillary action. The hemocytometer was observed under a microscope with a 10x ocular and 10x objective and the cells counted within each of the 5 squares (Figure 3.1A). The hemocytometer is divided into nine 1mm squares and the cover glass is supported 0.1mm from the surface of the chamber which allows for a total volume over each square is 0.0001 cm^3. Since $1cm^3$ is approximately equivalent to 1ml, the cell concentration per ml will be the average count per square times 10 000. As the cells were diluted, the dilution factor must also be taken into account therefore, to determine the number of cells per ml the average count per square was multiplied by $1x10^4$ and multiplied by the dilution factor which was 5 (Figure 3.1B).

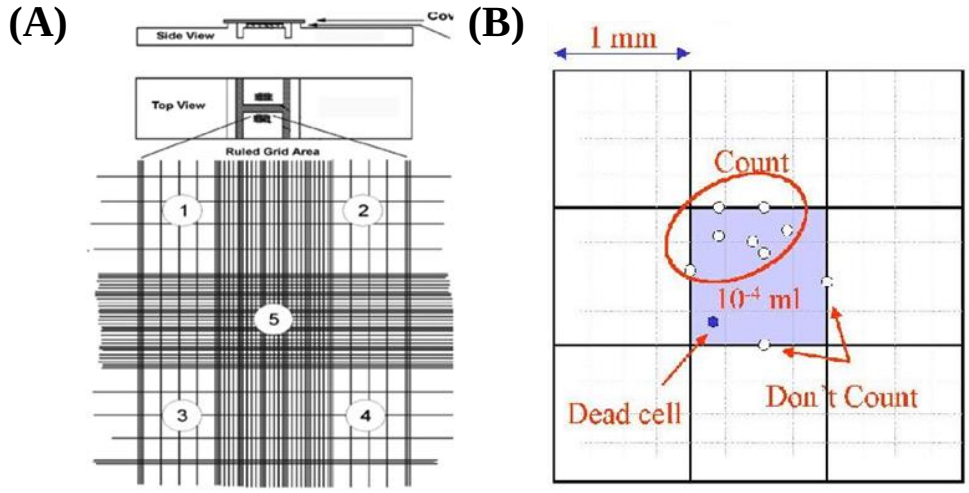

Figure 3.1: (A) Image of the hemocytometer and the 5 squares the cells are counted within (Harisha S 2007). (B) Image showing which cells are counted and which are not counted (ScienceGateway.org 2013).

Once the cells were counted, half the cells were cryopreserved and the other half were placed in a flask with 10ml cell media and incubated at 37°C to further replicate and then used for experiments once the cells were confluent. The cells undergoing cryopreservation, were placed in cell media containing 20% foetal calf serum. Equal volume cell suspension and dimethyl sulfoxide (DMSO) (1ml of each) were added to the cryopreservation vial, mixed well and placed within an isopropanol tube overnight which allowed the cells to freeze at a rate of 0.5-2°C per minute throughout the range of 4 and -30°C. After the incubation period, the vials were removed from the isopropanol tube and stored at -80°C.

3.2 Fumonisin B_1 Preparation

Fumonisin B_1 (FB_1) was obtained from the PROMEC Unit, Batch A/11 at a mass of 5.01mg. A stock of 6.93mM (5mg/ml) was prepared by dissolving the 5.01mg FB_1 in 1ml 0.1M PBS (pH7.4). From this stock a 1mM working concentration in 1ml was prepared (use 144µl 6.93mM stock) and used for treatments. The cell viability assay was performed to determine the treatment concentrations (Appendix A; figure A1 and A2).

3.3 Protein Expression Analysis

To determine the protein expression in HepG2 cells after treatment with FB_1, the sodium dodecyl sulfate (SDS) polyacrylamide gel electrophoresis (PAGE) and western blotting was performed. The SDS-PAGE is a relatively simple technique used to separate proteins based on their molecular size which involves the migration and sieving of protein complexes through the polyacrylamide gel matrix. This technique has a higher resolution compared to other separation methods, due to the combination of its sieving and SDS properties within the gel matrix and the gels relative pore sizes. Initially the proteins react with SDS, an anionic detergent, which denatures the protein therefore

destroying its tertiary structure. The SDS binds to both the hydrophilic and hydrophobic areas, within the polypeptide chain for each protein subunit therefore, producing negatively charged rod shaped molecules that have negatively charged sulfonate ions attached through the polypeptide surface. The intrinsic charge of the SDS-protein complex as a result of the individual amino acids is buried therefore, this complex has a net negative charge (Banga 1998; Pagano 1999).

After the formation of these SDS-protein complexes, the proteins need to be separated according to the different polypeptide components, i.e. molecular size. These complexes are separated by applying an electric current through a polyacrylamide gel which allows for SDS-protein complex migration. A synthetic polymer, polyacrylamide, is formed from the catalytic polymerisation of bi-functional cross-linking agents with acrylamide monomers. This polyacrylamide polymer consists of a three-dimensional network of pores, whose size is determined by the concentration ratio of acrylamide monomer and crosslinking agents. The molecular size of the pores within the polyacrylamide gel is therefore, comparable to protein molecular size. During electrophoresis, the application of an electrical current allows for the migration of the SDS-protein complexes through the polyacrylamide matrix towards the anode, thus allowing the separation of these protein complexes according to size. The proteins are sieved though the gel pores, so that the large proteins migrate at a slower rate, compared to smaller proteins that migrate at a faster rate through the gel matrix (Banga 1998; Pagano 1999).

The concentration of acrylamide within the gel is important for the good separation of proteins. Usually proteins needed to be separated fall between the molecular weights 10-200kDa therefore an 8-12% acrylamide gel concentration is sufficient for protein separation. The resolution of protein separation is increased by the incorporation of a concentration gradient of acrylamide within the gel. A gel with a single concentration of acrylamide however, is sufficient for separation of proteins. The presence of a 5-15% acrylamide concentration gradient within the gel, results in the

gradual reduction of pore size which leads to the gel having a greater sieving effect during electrophoresis which forms sharper protein bands (Banga 1998; Pagano 1999) .

Western Blotting involves the transfer of the proteins from the SDS-polyacrylamide gel onto a nitrocellulose membrane, as a result of an electrical current passing through the membrane and gel. The membrane that has been blotted with the proteins is an exact replica of the SDS-polyacrylamide gel. Following this transfer, the membrane is exposed to various antibody probes to characterise desired proteins as a result of specific treatments (Kurien & Scofield 2006).

3.3.1 Protein Isolation:

3.3.1.1 Sample preparation for each isolation method:

Eight small flasks were seeded with $5x10^4$ HepG2 cells/ml each and incubated at 37°C for 48hours, until the cells were 95% confluent. The flasks were then treated with a negative control, 10µM, 50µM and 100µM FB_1 (in duplicate) in CCM. The one set of flasks were incubated for 24hours and the other set for 72hours, both at 37°C. After the relevant time intervals, each flask underwent protein isolation.

3.3.1.2 Crude Protein Extract:

To obtain crude protein extract, each flask underwent the following procedure: The CCM was removed and the flask washed three times with 0.1M PBS (pH7.4). The cells were then homogenised using Cytobuster [500µl/flask (Novagen: #71009); containing protease inhibitor Cocktail (III) (Roche: #04693124001)] and the cell monolayer was removed using a cell scraper; whilst on ice. The sample was collected, stored in an eppendorf and incubated on ice for 10minutes. The samples where then centrifuged at 10 000 x *g* for 5minutes at 4°C, the supernatant containing

proteins was then standardised using the bicinchoninic acid (BCA) assay below. The protein homogenate was kept on ice at all times.

3.3.1.3 Subcellular Fractionation was preformed according to the abcam® protocol:

The CCM was removed and the flask washed three times with 0.1M PBS (pH7.4). The cells were then homogenised on ice using subcellular fractionation buffer (250mM sucrose, 20mM HEPES (pH 7.4), 10mM KCl, 1.5mM $MgCl_2$, 1mM Ethylenediaminetetraacetic acid (EDTA); in 10ml buffer add 1mM dithiothreitol (DTT), Pl Cocktail (lll) (Roche: #04693124001)). The cell monolayer was removed using a cell scraper and placed in an eppendorf. The lysate was then passed through a 25Ga needle ten times, using a 1ml syringe and left on ice for 20minutes. Following incubation, the lysate was centrifuged at 720 x *g* for 5minutes to separate out the nuclear pellet. The supernatant was removed and placed in a fresh labelled eppendorf tube and centrifuged at 10 000 x *g* for 10minutes. The supernatant was removed again and placed in a fresh eppendorf; this was the cytosolic fraction. The nuclear pellet (from the first centrifugation) was washed once through the addition of fractionation buffer and passed through a 25Ga needle ten times and centrifuged again for 10minutes at 720 x *g*. The buffer was then removed and the pellet re-suspended in nuclear buffer. Sample buffer (1:1) was added to the re-suspended nuclear fraction and the cytosolic fraction heated for 5minutes at 100°C and then stored at -20°C until use in SDS-PAGE and western blotting.

3.3.2 The Bicinchoninic acid Assay

The BCA assay is based on the biuret reaction where cupric ions (Cu^{2+}) from copper sulfate is oxidised to cuprous ions (Cu^{+}) in the presence of peptide bonds. The Cu^{+} then reacts with 2BCA to form a stable BCA-Cu^{+} complex, which changes the colour of the reaction to purple detected at

562nm (Figure 3.2). This reaction occurs under alkaline conditions. In the BCA assay the Cu^{2+} ions are reduced by cysteine, tyrosine, cystine, tryptophan and the peptide bond to form cuprous ions (Sapan et al. 1999). The more intense the purple colour the higher the protein concentration in the sample.

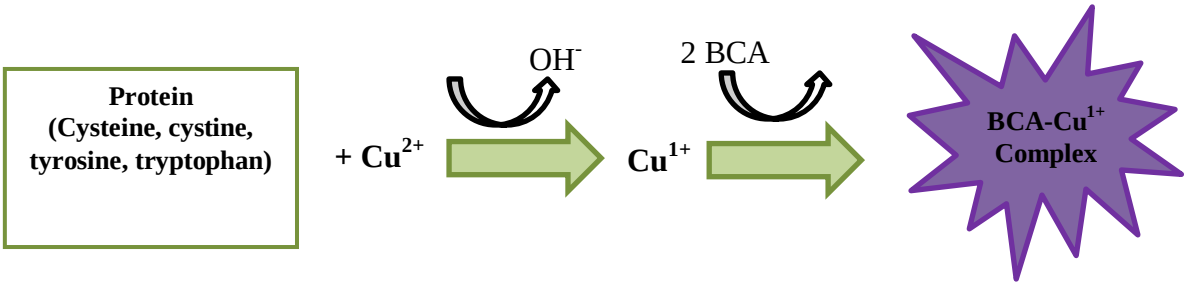

Figure 3.2: The BCA assay reaction where the copper ions bind to proteins changing the reaction colour to purple with a wavelength of 562nm (prepared by author).

The BCA assay is used to quantify and standardise proteins after protein isolation. A 1mg/ml stock of bovine serum albumin (BSA) was serially diluted to 0mg/ml, 0.2mg/ml, 0.4mg/ml, 0.6mg/ml and 0.8mg/ml. To a 96-well plate, 25µl of each sample and the relevant standards (BSA: 0, 0.2, 0.4, 0.6, 0.8, 1mg/ml) where added to appropriately labelled wells. To each well, 200µl BCA working solution (4µl 4% $CuSO_4$ and 198µl BCA) was added. The 96-well plate was then incubated at 37°C for 30minutes. Following incubation, the plate was read at 562nm using a spectrometer. The absorbance values of the BSA standards were then used to construct a standard curve which was used to calculate the protein concentrations of each sample (Appendix B; figures B1 and B2). The samples were then standardised, using Cytobuster, to the lowest protein concentration in the sample. The crude protein samples from above were standardised to 1mg/ml (Appendix B; table B1). The subcellular fractionation protein isolates were not standardised.

After standardisation and under the laminar flow hood, sample buffer (dH_20, 0.5M Tris(hydroxymethyl)aminomethane (Tris)-HCl (pH 6.8), glycerol, 10% SDS, β-mercaptoethanol,

1% bromophenol blue) was prepared, where the β-mercaptoethanol was added to the sample buffer at a 1:19 ratio before use. The 1x sample buffer was then added to each sample (50µl:50µl) and boiled for 5minutes at 100°C, in order to activate the β-mercaptoethanol and SDS to allow for reduction and unfolding of proteins. The samples where then stored at -20°C until use in SDS-PAGE and western Blotting.

3.3.3 Sodium Dodecyl Sulfate – Polyacrylamide Gel Electrophoresis

The Bio Rad mini-PROTEAN 3 SDS-PAGE apparatus was assembled and the samples were run on a SDS-polyacrylamide gel, containing a 7.5% resolving gel (deionised water, 1.5M Tris (pH 8.8), 10% SDS, 25% acrylamide, 10% ammonium persulfate (APS) and 0.05% tetramethylethylenediamine (TEMED)) and 4% stacking gel (deionised water, 0.5M Tris (pH 6.8), 10% SDS, 10% acrylamide, 10% APS and 0.1% TEMED). A molecular weight marker, precision plus protein standard (Bio-Rad: #161-0373), was run alongside the samples. After sample loading, the gels were electrophoresed in 1L running buffer (30.3g Tris, 144g Glycine, 10g SDS and deionised water) for 1hour at 150V using the Bio-Rad compact power supplier and apparatus; whilst on ice. The run was monitored until the tracker dye reached the bottom of the gel. The gels then underwent western blotting.

3.3.4 Western Blotting

For western blotting, the electrophoresed gels and fibre pads were placed in transfer buffer to equilibrate (25mM Tris, 191.8mM glycine and 20% methanol). The gel sandwich was assembled: fibre pad, nitrocellulose membrane, gel and fibre pad within the Bio-Rad cassette (Figure 3.3) which was placed within the Bio-Rad semi-dry Western Blot machine and run for 45minutes at 25V. After the transfer, the membranes were blocked for 1hour at 25°C, with 5% non-fat milk

protein in Tris-Buffered Saline with Tween 20 (TTBS). After blocking, the primary antibody (Table 3.1) was added overnight at 4°C. The membranes were then washed three times for 15minutes with TTBS followed by incubation with secondary antibody (Table 3.1) for 2hours at 25°C. After 2hours, the membranes underwent three 15 minute washes. The horseradish peroxidase (HRP) component of the secondary antibody was exposed for 90 seconds to enhanced Kirkegaard and Perry Laboratories LumiGlo® (Lot#: 111142) chemiluminescence substrate (equal parts reagent A and B).

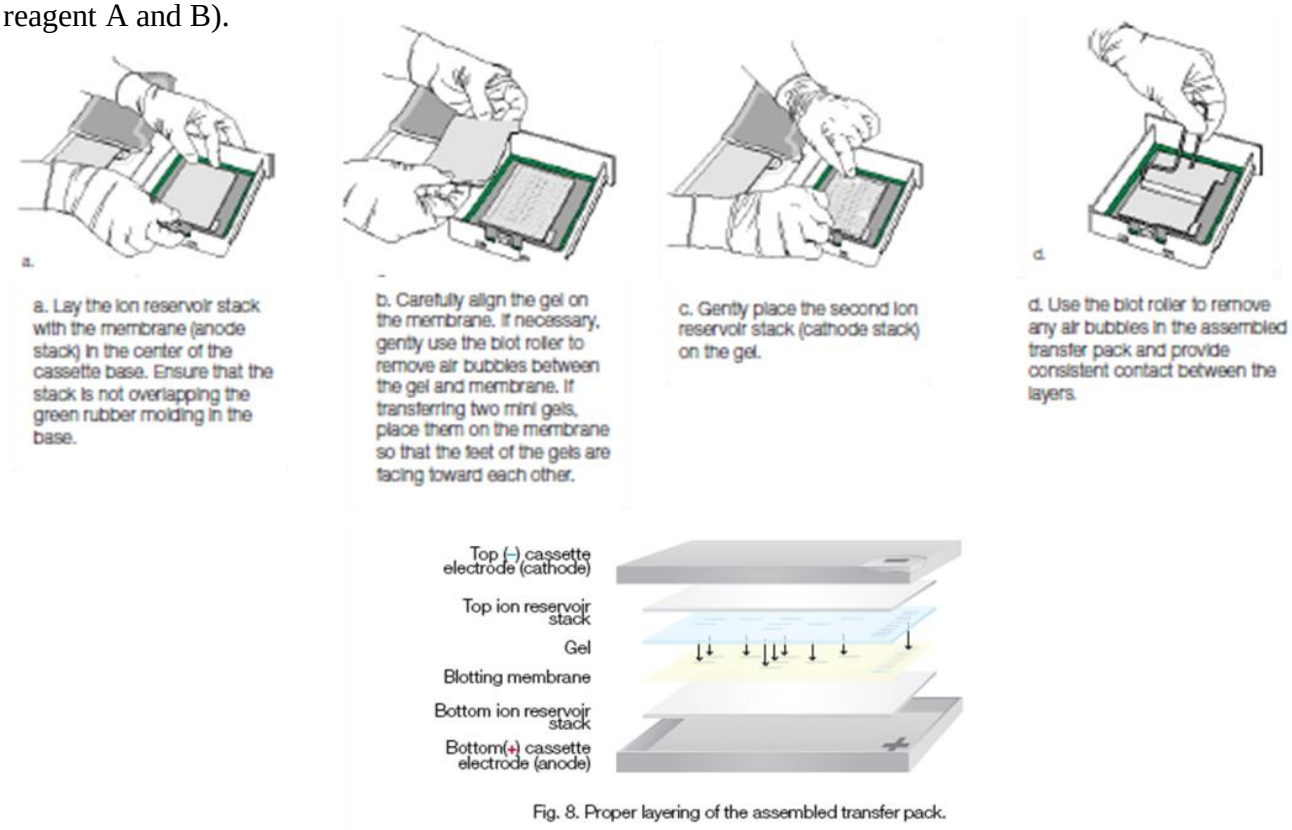

Figure 3.3: Method for assembling the gel sandwich within the Bio-Rad cassette (Bio-Rad Trans Blot Turbo Blotting System Instruction manual).

The membrane was viewed after chemiluminescence exposure and the image captured using the GelDoc XRS apparatus (Bio-Rad).

The membranes were stripped and re-probed with β-actin, to ensure equal loading of proteins: this was done by adding hydrogen peroxide and TTBS (1:1 ratio) to the membranes for 30minutes at 37°C, followed by a wash with TTBS, blocking step and then the steps as described above. The

western blots were analysed with Image J software and Microsoft Excel and the bands were normalised against β-actin.

Table 3.1: Western Blotting Primary and Secondary Antibodies used to probe for protein expression; diluted in 5% non-fat milk protein in TTBS * except p-eIF2α which was diluted in 5% BSA in TTBS.

Protein	**Primary Antibody**		**Secondary Antibody**	
TG2	Rabbit mAb anti-TG2 (Sigma: Lot310350)	1:1000	Goat anti-rabbit IgG- HRP (Santa Cruz Biotechnologies: Lot# B2213)	1:2000
p-NFkB	Rabbit mAb anti-p-NFkB p65 (Ser538) (Cell Signaling: #3031)	1:1000	Goat anti-rabbit IgG- HRP (Santa Cruz Biotechnologies: Lot# B2213)	1:2000
PERK	Rabbit mAb anti-PERK (Cell Signaling: #5683)	1:250	Goat anti-rabbit IgG- HRP (Santa Cruz Biotechnologies: Lot# B2213)	1:2000
p-elF2	Rabbit mAb anti-p eIF2α (Ser51) (Cell Signaling: #3597)	1:1000*	Goat anti-rabbit IgG- HRP (Santa Cruz Biotechnologies: Lot# B2213)	1:2000
B-actin	Mouse mAb anti- β actin peroxidase (Sigma-Aldrich: #A3854)	1:5000		

3.4 Tissue Transglutaminase Activity Assay

The TG2 activity in HepG2 cell homogenates was measured through the incorporation of biotin-x-cadaverine (BTC) into fibronectin. In the presence of excess calcium (above 0.5mM), TG2 undergoes a conformational change which exposes its active site rendering the enzyme active. The enzyme catalyses an acyl transfer reaction; where fibronectin acts as the acyl donor and BTC acts as the acyl acceptor. This reaction results in the insertion of an isopeptide bond between the two

proteins resulting in a proteinase resistant covalent N-γ-glutamyl-Ɛ-lysyl-isopeptide bond or crosslink (Figure 3.4). The crosslink produces a higher molecular mass protein aggregate (Griffin et al. 2002). A 3,3',5,5' – Tetramethylbenzidine (TMB) tablet (Sigma-Aldrich: # T5525) was used as a chromogenic substrate that reacts with the extravidin peroxidase conjugates to produce a blue soluble end product that is detectable spectrophotometrically at 370 or 655nm. The reaction is stopped using 2M sulfuric acid (H_2SO_4) which produces a yellow solution read at 450nm (Protocol; Sigma-Alderich Inc.).

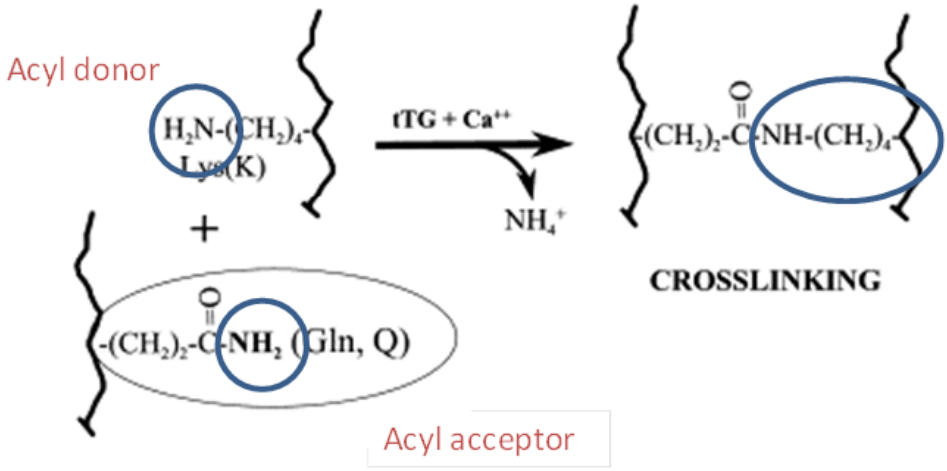

Figure 3.4: Tissue transglutaminase transamidation reaction. Tissue transglutaminase catalyses an acyl-transfer between an acyl donor and acyl acceptor with the insertion of an isopeptide bond to generate a proteinase-resistant covalent N-γ-glutamyl-Ɛ-lysyl-isopeptide bond (Lesort et al. 2000).

HepG2 cells seeded at a density of $1x10^5$ cells/ml in a 6-well plate, were treated with a negative control and 50µM FB_1 for 24hours at 37°C. The negative control and 50µl FB_1 treatments were only used because this experiment was being optimised therefore, to prevent wastage of FB_1 reagent. This experiment also never worked and instead was adapted in section 3.4.1. After incubation, the cells were rinsed with 0.1M PBS (pH7.4) twice and 200µl homogenising buffer (0.32M sucrose, 5mM Tris-HCl (pH 7.4), 2mM EDTA, broad range of protease inhibitor cocktail (Roche: #04693124001)) was added to each well. The cell monolayer was removed, using a cell scraper and passed through a thin gauge needle ten times to lyse the cells; whilst on ice. The

homogenate was then standardised, using the BCA protein assay, to protein levels of 1mg/ml BSA. The human plasma fibronectin (5µg/ml; Sigma- Aldrich: #F085) pre-coated 96-well plate (50µl/well) was blocked for 1hour at 37°C, after which it was rinsed twice with 50mM Tris-HCl (pH 7.4) and then incubated with the reaction mix (100µl/well) for 1 hour at 37°C (Table 3.2). The BTC substrate (Sigma-Aldrich: #B7306) was added last to the 1ml total reaction mix. After incubation, the wells were rinsed with 50mM Tris-HCl (pH 7.4) containing 5mM EDTA to stop the enzyme reaction (100µl/well) and then blocked with 3% BSA in 50mM Tris-HCl (pH 7.4) for 30minutes at 37°C (100µl/well). The wells were then incubated with 100µl/well extravidin peroxidase conjugate (1:5000 in 3% BSA in 50mM Tris-HCl, pH 7.4; Sigma-Aldrich: #E2886)) at 37°C for 2hours. After incubation, the wells were rinsed with 50mM Tris-HCl (pH 7.4) twice and then equilibrated with phosphate citrate buffer (pH 5.0) for 5minutes at 25°C (100µl/well). The colour development was timed for each well (between 1-5minute intervals to achieve a blue colour). A tablet of TMB was dissolved in 0.05 M phosphate citrate buffer (pH 5.0) containing 4µl 0.014% urea-hydrogen peroxide and added at 100µl/well. After the blue colour was detected the reaction was stopped, using 2.5M H_2SO_4. The plate was then analysed colorimetrically in a SpectrFluor ELISA plate reader at 450nm.

Table 3.2: Reaction Mix for Colorimetric TG2 Activity Assay (Purified guinea pig liver (*gpl*) TG2 (Sigma-Aldrich: #T5398): 0, 10 and 20ng to set up a standard curve, this was repeated with concentrations of 0, 10, 20, 50, 100, 1000ng/ml).

Positive Reaction Mix	**Negative Reaction Mix**
10mM $CaCl_2$	10mM EDTA
10mM DTT	10mM BTC
0.125mM BTC	
Cell homogenate/ *gpl* TG2	

The purified *gpl* TG2 (1mg/ml) was used to set up the standard curve (Appendix C; figure C1) because it was of known concentration therefore, can be used to determine the concentration of TG2 in the cell homogenates. The gpl TG2 was used as it has a molecular weight of 75kDa whilst human TG2 has a molecular weight of about 80kDa; therefore would have similar absorbance values. A FB_1 inhibition curve was also down to determine whether FB_1 could act as a possible substrate for TG2 (Appendix C; figure C2)

3.4.1 Tissue transglutaminase Activity Assay (Sodium Dodecyl Sulfate – Polyacrylamide Gel Electrophoresis Adaptation)

A SDS-PAGE/western blot was done to verify TG2 enzyme activity, which was adapted from the colorimetric TG2 assay principle described above (Jones et al. 1997). The TG2 activity, whether from *gpl* TG2 (Sigma-Aldrich: #T5398) or HepG2 homogenates, is tested here through the incorporation of FB_1 into fibronectin. In this assay, the reaction mix is done in 1.5ml eppendorfs and heated in a waterbath at 37°C for a specific reaction time period. The samples were electrophoresed, using SDS-PAGE and stained with Coomassie Blue to verify equal protein loading of the purified human fibronectin. A duplicate SDS-PAGE gel was then processed for western blot transfer to detect specific proteins (FB_1 and TG2).

3.4.1.1 Incorporation of Fumonisin B_1 into fibronectin:

Sample Preparation: The TG2 crosslinking of FB_1 into fibronectin was carried out in an eppendorf containing the reaction mix (Table 3.3). The concentrations of FB_1 used show a negative control, a treatment of 100µM and 1000µM. The 1000µM FB_1 treatment was done to compensate for the concentration of fibronectin used. In the colorimetric assay, 5µg/ml of fibronectin was used

however, within the adapted TG2 activity 0.5µg/ml of fibronectin was used due to dilution within the reaction mix. Therefore, 10 times more FB_1 would need to be used to ensure the reaction between fibronectin and FB_1 occurred, as seen in the colorimetric assay. In this reaction mix therefore, 1000µM FB_1 and 0.5µg/ml of fibronectin is used instead of 100µM FB_1 and 5µg/ml of fibronectin as seen in the colorimetric assay. The *gpl* TG2 reaction mix was incubated at 37°C for 15minutes or 1hour, while the HepG2 homogenate reaction was incubated at 37°C for 1hour. The HepG2 homogenate reaction was incubated for an hour only, as it was the optimal time for the reaction to occur. The reactions were stopped by adding 10µl 5mM EDTA/Tris (pH 8.0). Sample buffer (1X) was added to each reaction mix, heated for 5minutes at 90°C then stored at -20°C until needed for SDS-PAGE and western blot.

Table 3.3: Positive and negative reaction mix for the incorporation of FB_1 into fibronectin; incubated in a waterbath at 37°C for reaction times of 15minutes and 1hour.

Positive Reaction Mix	**Negative Reaction Mix**
5µl Fibronectin (5µg/ml)	5µl Fibronectin (5µg/ml)
5µl *gpl* TG2 (100ng/ml) or 5µl HepG2 Cell homogenate	-
10mM $CaCl_2$	20mM EDTA
10mM DTT	-
FB_1 (0, 100, 1000µM)	FB_1 (0, 100, 1000µM)
50mM Tris-HCl (pH 7.4) (top up to 50µl)	50mM Tris-HCl (pH 7.4) (top up to 50µl)

The SDS-PAGE and western blots were carried as previously described (Section 3.3.3 and 3.3.4). The antibodies used and probed for are listed in table 3.4 below:

Table 3.4: Western Blotting Primary and Secondary Antibodies used to probe for TG2 activity; diluted in 5% non-fat milk protein in TTBS.

Protein	Primary Antibody		Secondary Antibody	
FB_1	Mouse mAb anti-FB_1 (Abcam: #ab42124)	1:1000	Goat anti-mouse IgG- HRP (Abcam: #ab97046)	1:2000

3.5 Immunocytochemistry

Indirect immunocytochemistry (Figure 3.5) is used to detect and localise any constituent or inclusion of a biological system in which an antibody can be raised and marked by a visible label. The indirect method has higher sensitivity compared to the direct method because primary antibodies are unlabelled. These retain their specificity and strong signal. There are also an increased number of labels per antigen because at least two labelled secondary antibodies can bind one primary antibody therefore increasing the intensity which allows the detection of smaller amounts of antigen (Ramos-Vara 2005). The technique of indirect immunocytochemistry is as follows:

The cells are first fixed, using paraformaldehyde which is a crosslinking fixative. Fixation is important to preserve the cellular structure, to prevent the migration and loss of antigens and to stabilise the cell against damaging effects from the subsequent procedure. Paraformaldehyde is a good lipid preservative and preserves peptides, general cell structure and interacts with nucleic acids with little effect on carbohydrates. This fixative crosslinks proteins by the addition of reactive hydroxyl methyl compound between the formalin and uncharged reactive amino groups (-NH and NH_2). These compounds when in close proximity to other proteins undergo condensation, to produce chemically stable methylene bridges that crosslink the proteins (Ramos-Vara 2005). The next step is cellular membrane permeabilisation, to allow antibodies entry into the cell through the plasma membrane in order to bind to its specific antigen. There are several types of permeabilising

agents such as solvents, saponins, lysolecithin and non-ionic detergents. A polyoxyethylene non-ionic detergent, Triton X-100 was used as it does not denature proteins. This permeabilising agent acts through its intercalation within the phospholipid bilayer, where it solubilises lipids and transmembrane proteins which disrupt the plasma membrane, creating pores through which antibodies can enter the cell. Triton X-100 is particularly useful to detect antigens localised within mitochondria and the nucleus (Melan 1999). After permeabilisation, the cells are first exposed to blocking buffer that prevents non-specific binding on the secondary antibody. After blocking, the cells are exposed to a mouse monoclonal primary antibody which binds with high specificity to only one epitope of the antigen it was raised against. The next step is the incubation of the cells with a polyclonal secondary antibody labelled with a fluorescent probe. This polyclonal antibody is raised in goat, rat, rabbit, horse or monkey, against the animal the primary antibody was raised in ie. Anti-mouse IgG. Polyclonal antibodies have higher affinity, wide reactivity but lower specificity for epitopes compared to monoclonal antibodies (Ramos-Vara 2005). After this step the chamber slide is removed, mounting gel is added to the slide and a coverslip is placed over the cells. The slides are then viewed, using the fluorescent microscope to detect the fluorescent probe.

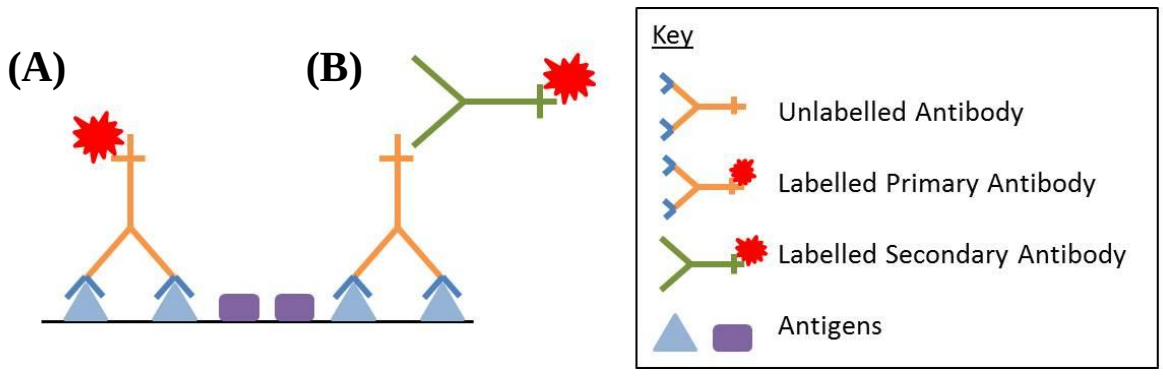

Figure 3.5: Diagram of (A) Direct vs (B) Indirect Immunocytochemistry (as prepared by author).

Fluorescent microscopy is used to visualise objects of interest through fluorescence. A specific antigen of interest is labelled with a fluorophore, through immunocytochemistry technique mentioned above. A light source will excite the fluorophore, where the molecule absorbs light photons inducing its electrons to move from a ground state to an excited state. The absorbed energy

eventually is shed through the emission of fluorescence from the molecule, allowing the electrons to move back to ground state (Figure 3.6A). The excitation wavelength is shorter than the emission wavelength known as Stoke's Shift, allowing for the complete filtering out of the excitation light without blocking the emitted fluorescence which is then used to visualise the object of interest. The fluorescent emission is detected by the fluorescence microscope eye piece and camera, allowing the quantification of intensity of fluorescence by using computer software.

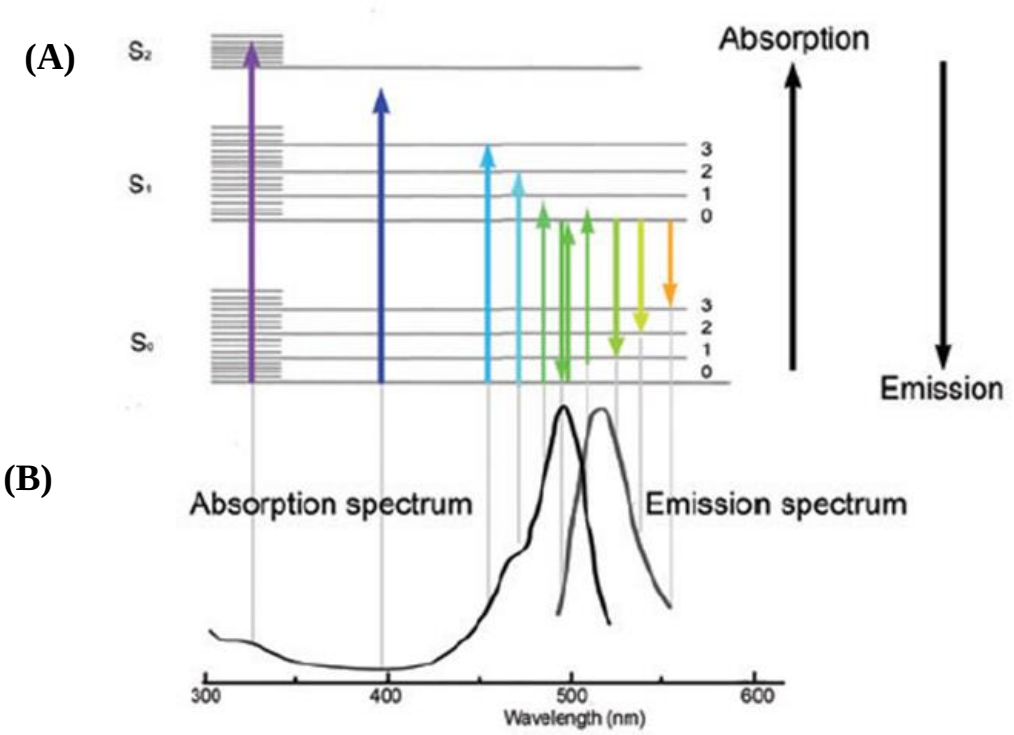

Figure 3.6: Fluorescence Principles. (A) Jablonski Diagram showing energy states of a fluorophore. Molecule absorbs light photons and moves to an excited state from ground state. The fluorophore emits fluorescence and transitions back to ground state. (B) The absorption and emission spectra of the fluorophore fluorescein isothiocyanate (FITC) (Lichtman & Conchello 2005).

To validate the expression of FB_1 and TG2 and further characterise apoptotic proteins, immunocytochemistry and fluorescent microscopy was performed. An indirect immunocytochemistry was performed using chamber slides as seen in Figure 3.7.

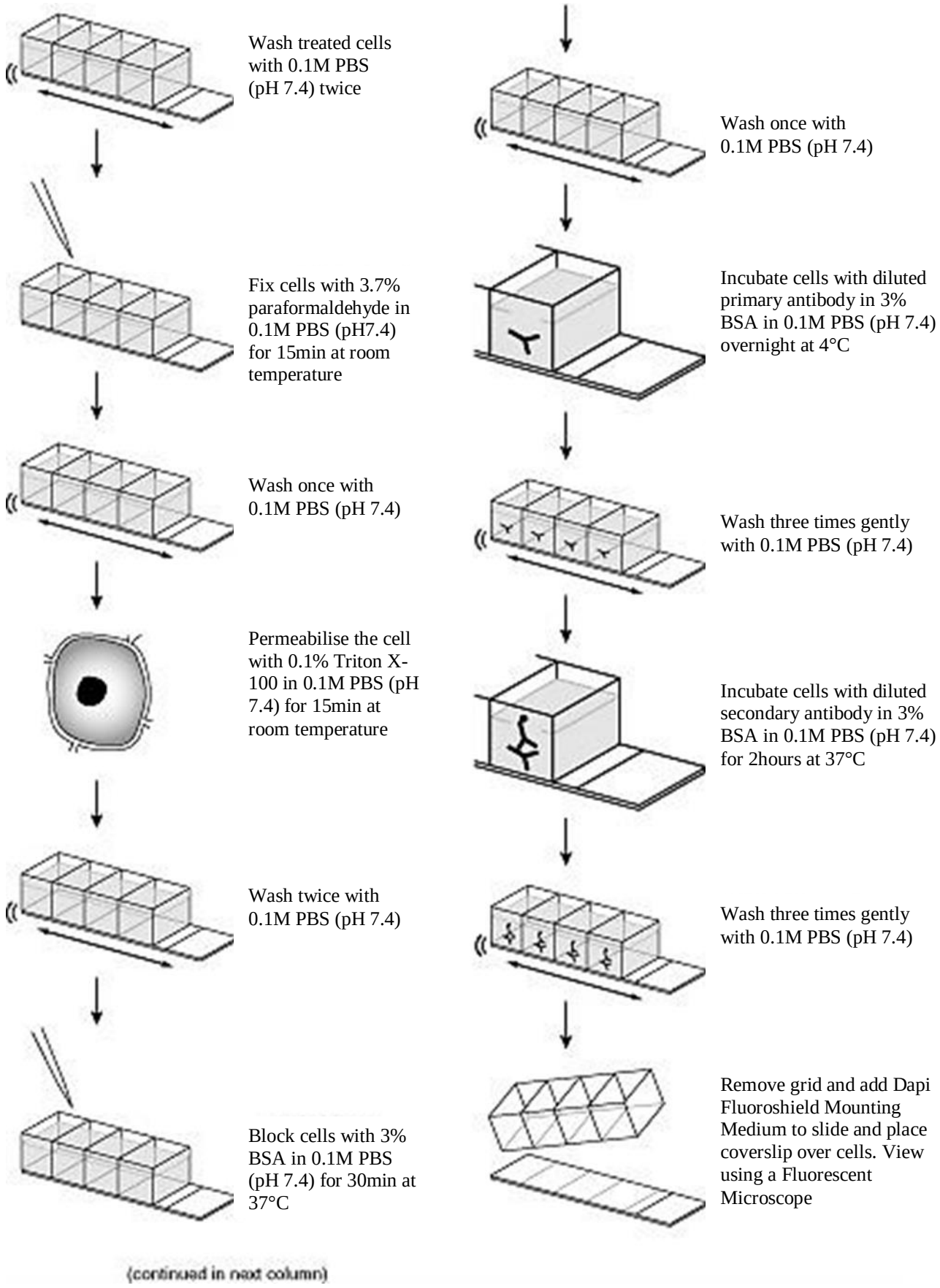

Figure 3.7: Schematic Diagram of Immunocytochemistry using a chamber slide. Fluorescent microscopy was used to detect specific probes (Cell Signaling Protocol 2013).

The cells were seeded at a density of $12.5x10^4$ cells/ml in six 8-well glass chamber slides (housed in a petri dish) and then treated with the negative control in the top four wells and 50µM FB_1 in the bottom four wells for 24 and 72hours at 37°C. After each treatment period, the wells were rinsed with 0.1M PBS (pH7.4) twice and then fixed in of 3.7% paraformaldehyde in 0.1M PBS (pH 7.4) for 15minutes at 25°C. This was followed by a 0.1M PBS (pH7.4) rinse then permeabilised in 0.1% Triton X-100 in 0.1M PBS (pH 7.4) for 15minutes at 25°C. The wells were then rinsed twice with 0.1M PBS (pH7.4) and blocked in 3% BSA in 0.1M PBS (pH 7.4) for 30minutes at 37°C. After blocking, the wells were incubated overnight with primary antibody in 3% BSA at 4°C. After incubation, the wells were then rinsed with 0.1M PBS (pH7.4), treated with secondary antibody, and incubated for 2hours at 37°C (Table 3.5). After which the wells were rinsed three times with 0.1M PBS (pH7.4) and the chamber and rubber gasket were removed. The Dapi Flouroshield Mounting medium (100µl) was added onto the slide and a coverslip was gently placed over the cells and stored at 4°C. The slides were viewed using a Zeiss Fluorescent Microscope and images were taken on the Axiovision imaging system (2010) software.

Table 3.5: Proteins probed for immunofluorescence microscopy. Slide 1 was incubated for 24 hours and slide 2 for 72 hours. Each slide has a negative control and 50µM FB_1 treatment well per immunofluorescent probe.

	Protein	**Primary Antibody**		**Secondary Antibody**	
Slide 1 (24hours) and Slide 2 (72hours)	Co-localised TG2 and FB_1	Mouse mAb anti-FB_1 (Abcam: #ab42124) Rabbit mAb anti-TG2 (Sigma: Lot310350)	1:120	Goat anti-mouse IgG FITC (Sigma-Aldrich: #F0257) Goat anti-rabbit IgG Tetramethylrhodamine-5-(and 6)-isothiocyanate (TRITC) (Santa Cruz Biotechnologies: Lot# B2213)	1:500
	Actin	Mouse mAb anti-β-actin conjugated FITC (Abcam: #ab6277)	1:500		

3.6 Quantitative Polymerase Chain Reaction

Quantitative Polymerase Chain Reaction (qPCR) allows for the reliable detection and measurement of the PCR product generated during each cycle which is directly proportional to the amount of template present prior to the PCR reaction. This relationship can be used to determine the amount of mRNA present within an experimental sample. The reaction requires a complementary DNA (cDNA) template that is synthesised from isolated RNA (described below), Thermus aquaticus (Taq) polymerase, deoxyribonucleotide triphosphates (dNTPs), antisense and sense primers. The double stranded (ds) cDNA undergoes denaturation to form single-stranded DNA at 95°C. The temperature is then cooled to between 55-60°C, which is primer dependent, allowing the primers to anneal to the 5'-end of the two single-stranded DNA templates. After annealing, the Taq polymerase adds dNTPs to the primers and extends the new DNA strand to create a new dsDNA strand. This generates two dsDNA strands from one initial DNA template. This reaction occurs for 35-40 more cycles to create an exponential amount of PCR product (Bridge 1998). In qPCR a SYBR® Green dye is also included within the reaction mix. This dye is a nonsequence specific fluorogenic minor groove DNA-binding dye that intercalates into dsDNA. The SYBR Green dye exhibits little fluorescence unbound within solution but emits a strong fluorescent signal when it intercalates into dsDNA (Figure 3.8). The intensity of the fluorescence is therefore proportional to the amount of dsDNA present within the reaction. The fluorescence is measured at the end of the elongation step during each PCR cycle, to monitor the increase in the amount of amplified DNA. A melt curve (fluorescence as a function of temperature) is also generated, using a LightCycler™ which increases the specificity of the reaction; this is because each amplicon, at its melting temperature, has a characteristic melting peak, which can be used to distinguish it from amplification artefacts that melt at a lower temperature and have broader peaks (Arya et al. 2005).

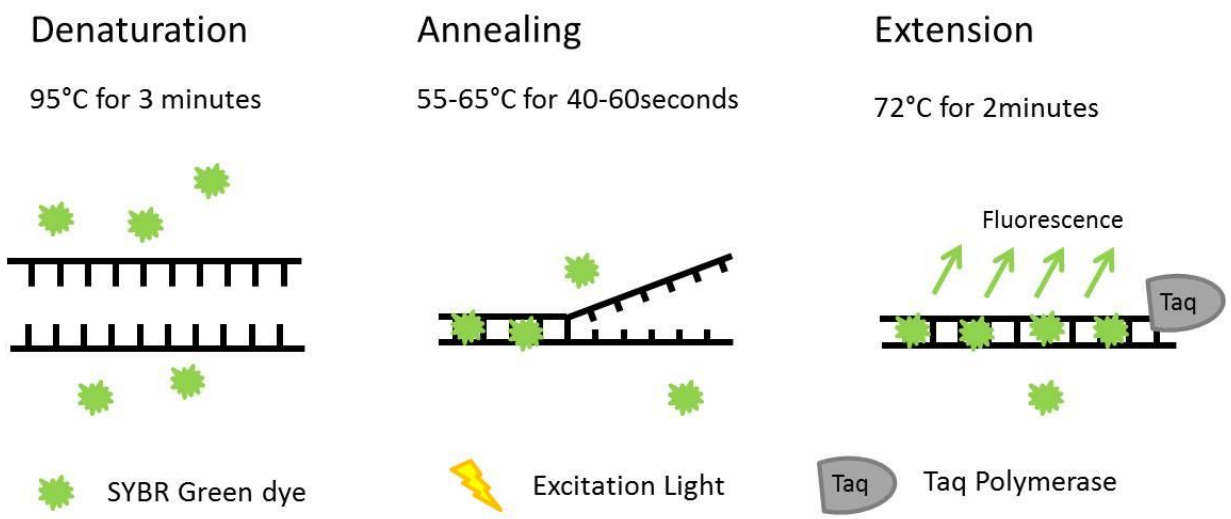

Figure 3.8: Diagram showing the polymerase chain reaction with the intercalation of SYBR Green into dsDNA (prepared by author).

During the PCR reaction, the increase in fluorescent emissions could be detected in real time by the thermocycler. This emission data collected during PCR was used by the computer software (Bio Rad CFX Manager) to construct amplification plots (Figure 3.9). The software first sets up a baseline between cycles 3-15 which refers to the PCR cycle, where the reporter fluorescent signal accumulated is beneath the detection limit of the instruments. It also calculates ΔRn which is the difference between the fluorescent emission of product at each time point and the fluorescent emission at baseline. The ΔRn are plotted against the cycle number and do not exceed the baseline during each amplification cycle. The software then arbitrarily determined the threshold which was calculated as ten times the standard deviation of the baseline signal between cycles 3-15. Fluorescent signal detected above this threshold was identified as a real signal and could be used to determine the threshold cycle for a sample. The PCR cycle number where the reporter fluorescent signal was detected above the minimal detection level i.e. baseline is referred to as the threshold cycle (Ct). This Ct value was used to determine the amount of starting template present before the reaction. If there was a greater amount of templates prior to the reaction then there would be fewer cycles needed in order for the fluorescent signal to be detected above threshold that is statistically

significant. This Ct value occurs during the early cycles of PCR exponential phase of the target amplification. After many cycles the reaction components are limited therefore the rate of amplification decreases until the PCR components are depleted at which time the exponential rate of amplification ceases and a plateau is formed (Arya et al. 2005).

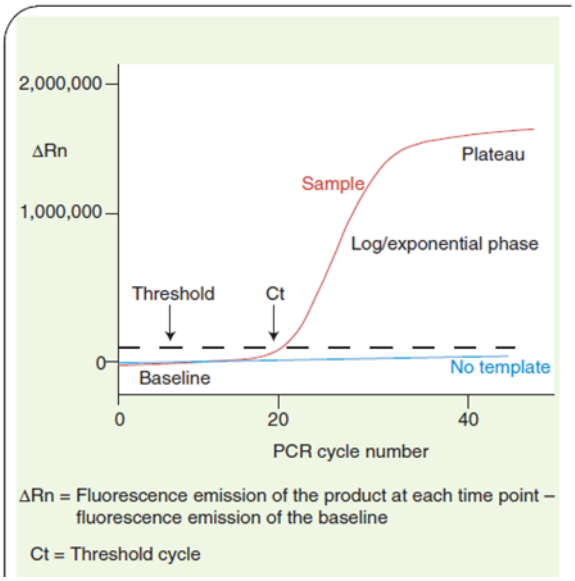

Figure 3.9: Model showing a single amplification plot including nomenclature commonly used in qPCR (Arya et al. 2005).

Specific errors could be introduced into qPCR experiments as a result of human error such as; minor differences in the amount or quality of the RNA starting material or due to different efficiencies of cDNA synthesis or PCR amplification. These errors are minimised and sample to sample variation are corrected by the simultaneous amplification of a housekeeping gene such as Glyceraldehyde 3-phosphate dehydrogenase (GAPDH). The GAPDH could be used as an internal reference that RNA sample values are normalised against (Arya et al. 2005).

The Ct value was used in the comparative threshold method ($2^{-\Delta\Delta Ct}$ method) to calculate the relative expression level of the target gene against the reference control. This method first normalises the target gene against the housekeeping gene ([GAPDH) where ΔCt is the difference between the Ct value of target gene and the Ct value of the housekeeping gene (GAPDH). The method then

calculates the ΔΔCt which is the difference between the ΔCt value of the sample and the ΔCt value of the control. The sample ΔΔCt values are then compared against the control ΔΔCt value of 1 to determine the relative expression level of the target gene (Livak & Schmittgen 2001).

3.6.1 Sample Preparation

Six-well plates were seeded with $5x10^4$ HepG2 cells/ml each and incubated at 37°C for 48hours, until the cells were 95% confluent. The flasks were then treated with a negative control, 10µM, 50µM and 100µM FB_1 (in duplicate) in CCM. The one set of plates were incubated for 24hours and the other set for 72hours (with 1ml of treatment added after 24hours), both at 37°C. After the relevant time intervals each treatment underwent RNA isolation.

3.6.2 Ribonucleic acid Isolation:

After treatment the CCM was removed from each well and the cells washed with 500µl 0.1M PBS (pH7.4) and removed. To each well, 200µl 0.1M PBS (pH7.4) and 500µl Trizol was added, mixed gently and incubated for 5minutes at room temperature (RT). Trizol is a monoplastic solution comprising of phenol and guanidine isothiocyanate. It disrupts the cell membrane and solubilises cell components whilst maintaining RNA integrity (Simms et al. 1993). The 700µl mixture was collected in an eppendorf and stored at -80°C for at least an hour {recommended to increase RNA yield}. The Trizol samples after incubation at -80°C was thawed at RT. To each sample, 700µl Chloroform was added, the eppendorf was shaken vigorously, for approximately 15 seconds and then incubated for 2-3minutes at RT. Following incubation, the samples were centrifuged at 12 000 x *g* for 5minutes at 4°C. Chloroform was added to allow for the separation of solutions into an aqueous phase containing RNA and an organic phase containing DNA and proteins after centrifugation (Simms et al. 1993). Whilst working on ice; 350µl aqueous phase was carefully

transferred to a new eppendorf. To each sample; 350µl isopropanol, which precipitates out RNA, was added and incubated at -80°C for at least one hour {potential indefinite stopping point @ -80°C}. The samples were then thawed at RT, after incubation and centrifuged at 12 000 x *g* for 20minutes at 4°C. The supernatant was removed and discarded. The pellet (flicked to loosen) was washed with 525µl 75% cold ethanol and then centrifuged at 7 400 x *g* for 15minutes at 4°C. The ethanol was removed and the pellet left to air dry for 5-10minutes. The RNA pellet was then resuspended in 15µl Nuclease-free water and incubated for 2-3minutes at RT. After incubation, the sample was placed on ice and the RNA was quantified, using a Nanodrop. The total RNA was stored at -80°C until further use.

3.6.3 Ribonucleic acid verification and standardisation:

The quality of the RNA was checked by running the total RNA samples (5µl RNA with 20µl 5x Glotaq) on a 2% Agarose gel with 1x GR green in 1x Tris/Borate/Ethylenediaminetetraacetic acid (pH 8.3) buffer at 120V for 30minutes. The gel was visualised by exposing the gel to ultraviolet light for 3seconds and the image captured on the GelDoc XRS apparatus (Bio-Rad). Two separate bands at 18s and 28s and the A26/A280 ratio was greater than 1.8 therefore verifying the RNA was pure. The RNA samples were then standardised to 1µg/µl.

3.6.4 Complementary Deoxyribonucleic synthesis*:*

The Bio-Rad iScript^{TM} cDNA Synthesis Kit (#170-8891) was used as per manufacturer's instructions to synthesise cDNA from mRNA. The kit contains an iScript RNase H+ Moloney Murine Leukemia Virus-derived reverse transcriptase and is pre-blended with RNase inhibitor. The kit also contains an iScript reaction mix which consists of oligo-deoxy-thymine nucleotides (dT) and random hexamer primers, dNTPS, buffers and stabilisers. To a PCR tube, 4µl

5x iScript reaction mix, 1µl iScript reverse transcriptase, 13µl Nuclease free water and 2µl RNA was added per reaction. The PCR tubes containing the complete reaction mix was then incubated within the Applied Biosystems' GeneAmp PCR system 9700 for 5minutes at 25°C and then 30minutes at 42°C for the random-primer cDNA reaction. This reaction occurs at the Poly-A tail 3' end of the mRNA where the DNA primer will bind to start transcription of cDNA. The reverse transcriptase binds at this poly-A tail sequence and adds complementary dNTPs to the DNA primer and elongates the cDNA (Figure 3.10). The complete reaction mix was then incubated for 5minutes at 85°C, to inactivate the reverse transcriptase and held at 4°C.

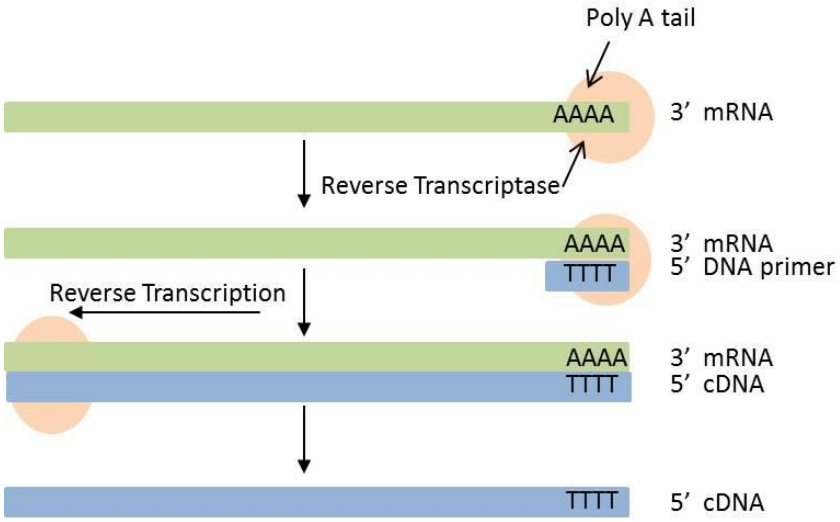

Figure 3.10: Diagram showing the synthesis of complementary DNA (cDNA) from mRNA template (prepared by author).

3.6.5 Primer optimisation:

Primers received from Inqaba Biotechnical Industries (Pty) Ltd were first optimised (Table: 3.6) for the Bio-Rad CFX96^{TM} Real Time System C1000 Touch Thermal Cycler.

Table 3.6: Optimised Concentrations and Annealing Temperature and Time for qPCR primers.

Primer	Sequence	Concentration	Annealing Temperature and Time
CHOP sense	ACCAAGGGAGAACCAGGAAACG	1.2µM	55° for 40sec
CHOP antisense	TCACCATTCGGTCAATCAGAGC		
elF2 sense	CCTCACCATTTGCCTAAGGA	1.4µM	55°C for 40sec
elF2 antisense	GGGGGACTTTCCTTCTTCTG		
ATF4 sense	GTTCTCCAGCGACAAGGCTA	1.5µM	65°C for 1min
ATF4 antisense	ATCCTCCTTGCTGTTGTTGG		
TG2 sense	ATGAGAAATACCGTGACTGCCTTAC	800nM	60°C for 1min
TG2 antisense	CAGCTTGCGTTTCTGCTTGG		
Sp1 sense	CTTGGTATCATCACAAGCCAGTT	800nM	60°C for 1min
Sp1 antisense	TCCCTGATGATCCACTGGTAGTA		

3.6.6 Reaction Mix Preparation and Thermal Cycling Protocol:

The iQ^{TM} SYBR® Green Supermix (Bio Rad) contained iTaq DNA polymerase, $MgCl_2$, dNTPs, SYBR® Green I dye, stabilisers, enhancers and fluorescein. The iQ^{TM} SYBR® Green Supermix and other components were thawed and stored on ice. The master mix was prepared for all reactions; this was done by adding all required components except the DNA template according to Table 3.7 below (as per manufacturer's instructions).

Table 3.7: Components of qPCR master mix

	Volume per 1x Reaction
iQ™ SYBR® Green Supermix	6.25µl
Antisense primer	0.5µl
Sense primer	0.5µl
Nuclease free water	3.25µl
Total	10.5µl

* add 10µl master mix per well with 2µl cDNA

The master mix was vortexed to ensure homogeneity and then 10µl master mix was aliquoted into each well of the qPCR plate. Good pipetting practice was followed to ensure assay precision and accuracy. To each well, 2µl cDNA sample was added and mixed, with a blank where 2µl nuclease free water was added to a well. Each sample cDNA was done in triplicate with a GAPDH done to normalise the RNA expression (appendix D; table D1-D5). The qPCR plate was then placed within the Bio-Rad CFX96™ Real Time System C1000 Touch Thermal Cycler and the following protocol was selected {with a variation in the annealing temperature and time according to table for the different primers}. The polymerase activation and DNA denaturation was set at 95°C for 3minutes. The amplification step of 35-40 cycles included: denaturation at 95°C for 10-15sec and annealing/extension according to Table 3.6. The Melt curve analysis occurred between 55-95°C in 0.5°C increments every 2-5sec/step (as per manufacturer's instructions).

The Ct value was calculated in Microsoft Excel using the $2^{-\Delta\Delta Ct}$ Method as described above to determine the expression level of specific target genes.

3.7 Sample Preparation for Flow Cytometry and Luminometry

Four small flasks were seeded with $5x10^4$ HepG2 cells/ml each and incubated at 37°C for 48hours, until the cells were 95% confluent. The flasks were then treated with 0µM (used as the negative control), 10µM, 50µM and 100µM FB_1 (in duplicate) in serum-containing media (CCM). The flasks were incubated for 72hours, both at 37°C. After the relevant treatment period, the CCM was removed and washed with 0.1M PBS (pH7.4) three times. The cells were then trypisinised by adding 2ml trypsin and incubating the cells for 5minutes at 37°C. After incubation, the trypsin was removed and 2ml CCM was added per flask, the flask was shaken to remove the cells attached to the flask into the CCM. The cell suspension was then collected and the cells counted using the Trypan Blue method. The cells were then centrifuged at 450 x *g* for 5minutes at RT, the supernatant discarded and resuspended in 0.1M PBS (pH7.4) where the cells were adjusted to $1x10^6$ cells/ml. These cells were then used in Flow cytometry and Luminometry and the results measured, using relative light units (RLU).

3.8 Flow Cytometry

This technique allows for the measurement of properties of individual particles. It does this through the use of a fluids system (Figure 3.11A) which organises the sample of randomly distributed particles into a single stream of particles. This is known as hydrodynamic focusing which occurs as a result of a massive drag effect on the narrow central chamber set up by the outer sheath fluid moving at a greater velocity than the sample within the central chamber. The particles in single file are then passed through one or more beams of light from either an argon or diode laser which produces light at 488nm and 635nm wavelengths respectively. This light excites the fluorochromes attached to the particle which causes a fluorescent emission to be produced which is detected in fluorescence channels (FL-). The Fluorescence-activated cell sorting (FACS) Calibur flow

cytometer has four fluorescent channels (Figure 3.11B): FL-1 Green which detect fluorescent emissions between wavelengths 515-545nm, FL-2 Yellow detects 564-606nm wavelengths, FL-3 Red detects fluorescent emissions with wavelengths greater than 670nm and FL-4 Orange which detects wavelengths between 653 and 669nm. Each fluorescent channel uses a separate optical detector which is controlled by optical filters that block through absorption specific wavelengths whilst transmitting others. For example the FL-1 channel filter will transmit wavelengths between 515-545nm whilst blocking all other wavelengths it comes into contact with. After the fluorochrome is excited and emits a fluorescent signal, this signal is transmitted to the relevant FL channel; at this detector the light generates a small current only a few microamperes in size. The currents associated voltage has amplitude directly proportional to the number of light photons received at the detector. The voltage received at the detector is then amplified by a number of linear or logarithmic amplifiers and by analogue to digital convertors that generate an electrical signal large enough to be plotted graphically. One measurement from a detector is known as a parameter, for example fluorescence. The data generated at each parameter is known as an event which refers to the number of cells displaying the specific characteristic. During flow cytometry 50 000 events are taken for each parameter to ensure accuracy of the result.

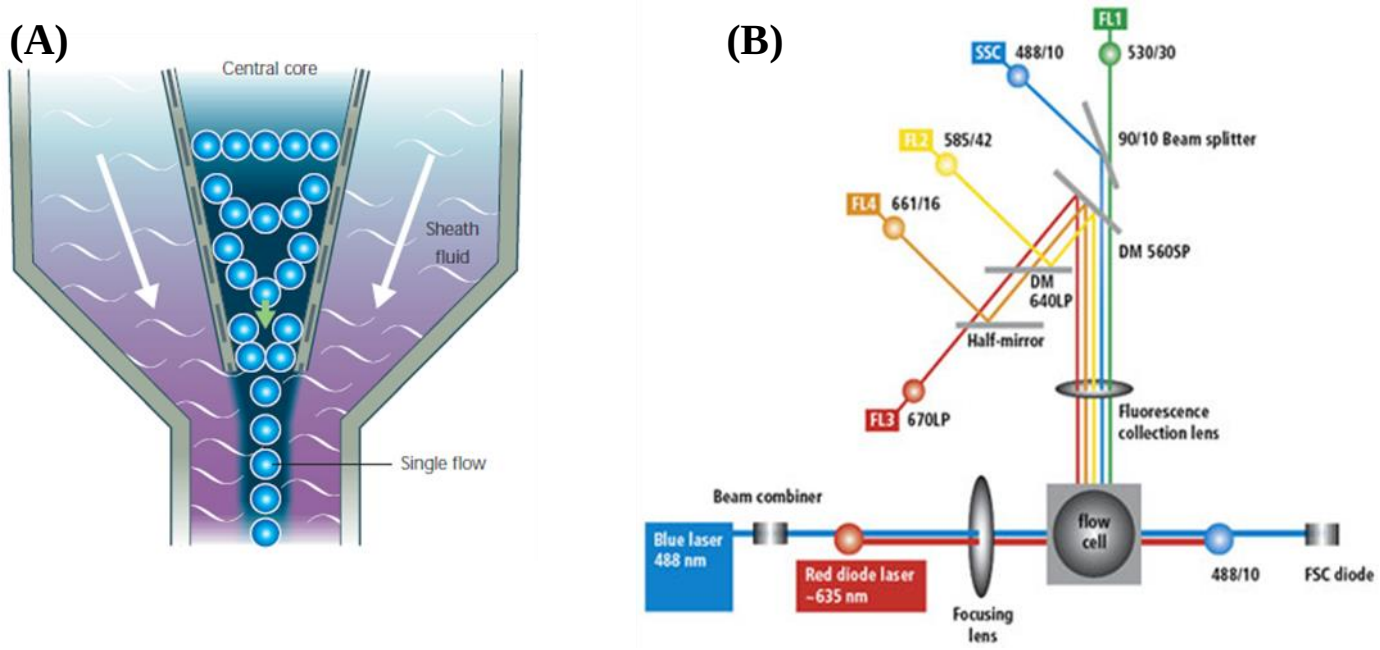

Figure 3.11: Diagram illustrating (A) Hydrodynamic Focusing (Rahman 2006) and (B) the setup of the FACS Calibur Flow Cytometer (BDbiosciences 2013a).

The data acquired during flow cytometry was the analysed using FlowJo 7.1 software (Tree Star Inc., Ashland, USA). It is important to first selectively visualise the cells of interest and eliminate other unwanted particles such as debris and dead cells. This is done through the process called gating. Once the cells of interest have been gated, the results call be visualised either as a one parameter histogram where the fluorescence is plotted against the number of cells. This is used in the cluster of differentiation 95 (CD95) analysis (Figure 3.12A). The data could also be visualised using a two parameter dot plot which displays two parameters against each other for example in the Annexin-V-FLOUS experiment: Annexin-V- FITC vs Propidium Iodide (Figure 3.12B) and in 1st J-aggregate-forming cationic dye (JC-1): FL-2 channel vs FL-1 channel (Figure 3.12C).

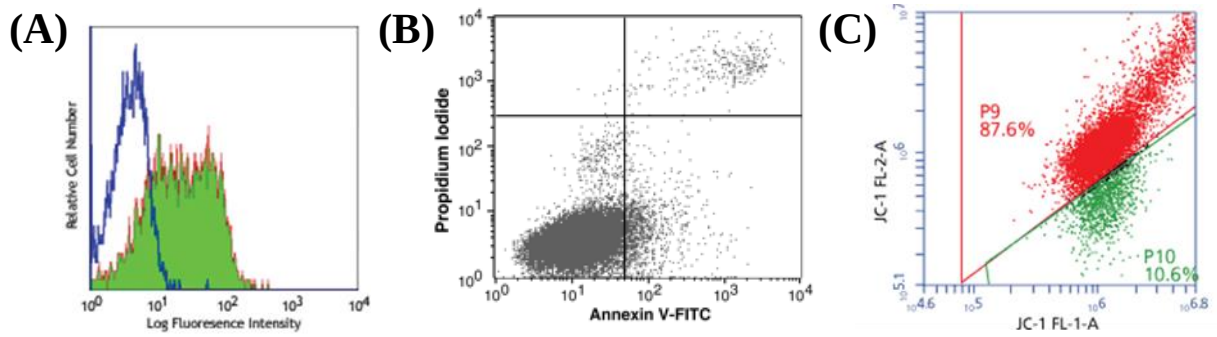

Figure 3.12: Graphs showing (A) a one parameter histogram (Biolegend 2013), (B) Annexin-V-FITC vs PI dual parameter dot plot (Chacko et al. 2010) and (C) JC-1 FL-1 vs JC-1 FL-2 dual parameter dot plot (BDBiosciences 2013).

3.8.1 Annexin-V-Fluorescent

The Annexin-V-Fluorescent (FLOUS) Staining Kit (Roche) was used to detect apoptotic cells and differentiate out necrotic cells due to FB_1 treatment. During the early stages of apoptosis there are plasma alterations which include the translocation of phosphatidylserine (PS) from the inner part of the membrane to the outer part of the membrane therefore exposing PS to the external cell environment. The PS on the outer surface of the cell is analysed using an Annexin-V-FLOUS probe which binds in a calcium-dependent manner to the negatively charged PS surface with high

specificity. To differentiate the necrotic cells, as these cells also expose PS on their outer surface due to their damaged plasma membrane, Propidium Iodide (PI) dye is used simultaneously to stain leaky DNA in necrotic cells only (Figure 3.13). Annexin-V-FLOUS has an excitation wavelength of 488nm and emission wavelength of 518nm. Propidium Iodide has an excitation wavelength of 488-540nm and an emission wavelength of 617nm (Roche Protocol).

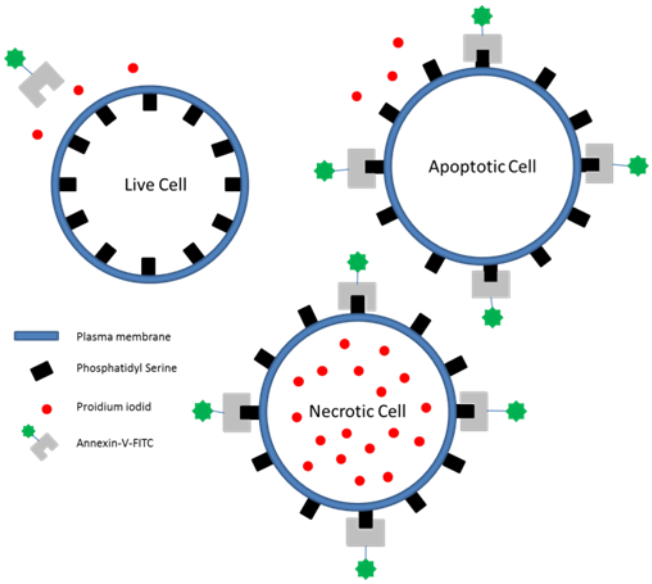

Figure 3.13: Annexin-V-FITC binding to phosphatidyl serine in apoptotic and necrotic cells with Propidium Iodide staining of leaky DNA in necrotic cells thereby differentiating apoptotic from necrotic cells (prepared by author).

The Annexin-V-FLOUS labelling reagent was pre-diluted in 1ml incubation buffer and added to 20µl PI solution. The cells (prepared above [section: 3.7]) were centrifuged at 200 x *g* for 5minutes and re-suspended in 100µl Annexin-V-FLOUS labelling solution and incubated at 15-25°C for 10-15minutes. To the cell suspension 0.5ml incubation buffer was added. A positive control with HepG2 cells treated with 5µM Campthothecin was done as well (Appendix E; table and figure E1). The cells were analysed using the flow cytometer (FACS Calibur, BD Biosciences, Johannesburg, South Africa) at 488nm excitation with a 515nm bandpass filter for fluorescence detection and a filter >600nm for PI detection. Data was collected for 50000 events per sample and analysed with FlowJo 7.1 software (Tree Star Inc., Ashland, USA).

3.8.2 Mitochondrial Membrane Potential Detection

The BD^{TM} MitoScreen Kit from BD Biosciences was used to detect the mitochondrial membrane potential after HepG2 cells were treated with varying concentrations of FB_1. This kit contains JC-1 fluorochromes that are used to detect mitochondrial membrane potential. JC-1 exists in two states, either as a monomer in cases of low dye concentrations or as aggregates when there is a high dye concentration; each having their own emission spectra. The JC-1 monomers and aggregates both emit fluorescence in the Green (FL-1) channel of the flow cytometer. When live cells are exposed to JC-1, this fluorochrome penetrates the plasma membrane of the cell and enters the cytoplasm. As healthy cells are known to have polarised mitochondrial membrane potentials, the JC-1 is rapidly taken up into the mitochondria thus increasing the concentration gradient within the mitochondria which causes the formation of JC-1 aggregates. These JC-1 aggregates show a red spectral shift therefore increasing red fluorescence emission which is measured on the Red (FL-2) Channel of the flow cytometer. In damaged or apoptotic cells the mitochondrial membrane potential becomes depolarised and as a result the JC-1 monomers are unable to enter the mitochondria; therefore JC-1 remains as monomers within the cytoplasm (Figure 3.14). As monomers do not show a red spectral shift there is decreased fluorescence in the FL-2 channel and increased green fluorescence in the FL-1 channel. As a result polarised cells will emit fluorescence in both FL-1 and FL-2 channels whilst depolarised cells will emit fluorescence in FL-1 channel with minimal to no fluorescence in FL-2 channel. The JC-1 fluorochrome is typically excited with a 488nm argon ion laser and the monomers emit maximally at 527nm whilst the aggregate emits maximally at 590nm.

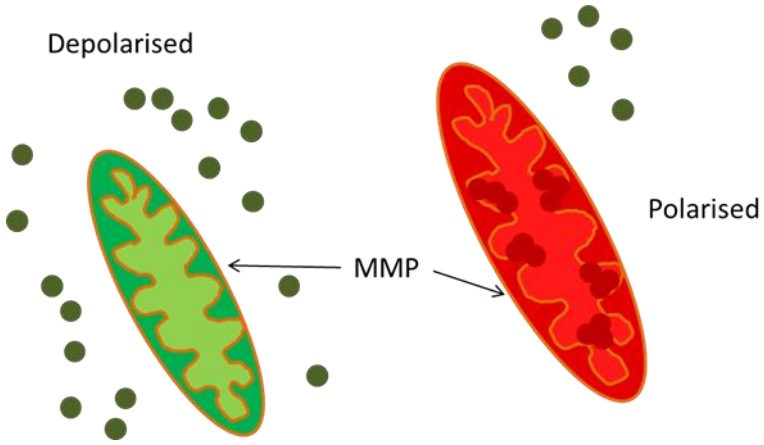

Figure 3.14: Mitochondrial membrane potential (MMP) and JC-1 fluorochrome reaction. Left: Depolarised MMP with JC-1 monomers. Right: Polarised MMP with JC-1 aggregates within mitochondria and JC-1 monomers in cytoplasm (prepared by author).

Initially the kit reagents were prepared: The 10x Assay Buffer was first diluted to 1x solution and warmed to 37°C prior to use. This is used as a reaction buffer and to wash cells. The JC-1 was reconstituted by adding 125µl DMSO to form a stock solution; which is either diluted into a working solution or stored at -20°C. The working solution was prepared by the dilution of JC-1 stock solution with the 1x Assay Buffer. The cells prepared as described above were centrifuged at 400 x *g* for 5minutes at RT and the supernatant removed. The freshly prepared JC-1 Working Solution was added to the cell pellet, re-suspended gently and vortexed to remove cell-to-cell clumping (Figure 3.15). The cells in JC-1 working solution were incubated at 37°C for 15minutes and washed twice. The first wash was done by adding 2ml 1x Assay Buffer to each tube, the cells were then vortexed and centrifuged at 400 x *g* for 5minutes and the supernatant was carefully removed. The second wash was done by the addition of 1ml 1x Assay Buffer, the cells were re-suspended gently, vortexed and centrifuged at 400 x *g* for 5minutes. The cells were resuspended in 0.5ml 1x Assay Buffer, vortexed and then analysed by flow cytometry (FACS Calibur, BD Biosciences, Johannesburg, South Africa). A positive control with HepG2 cells treated with 5µM

Campthothecin was done as well (Appendix E; table and figure E2). Data was collected for 50000 events per sample and analysed with FlowJo 7.1 software (Tree Star Inc., Ashland, USA).

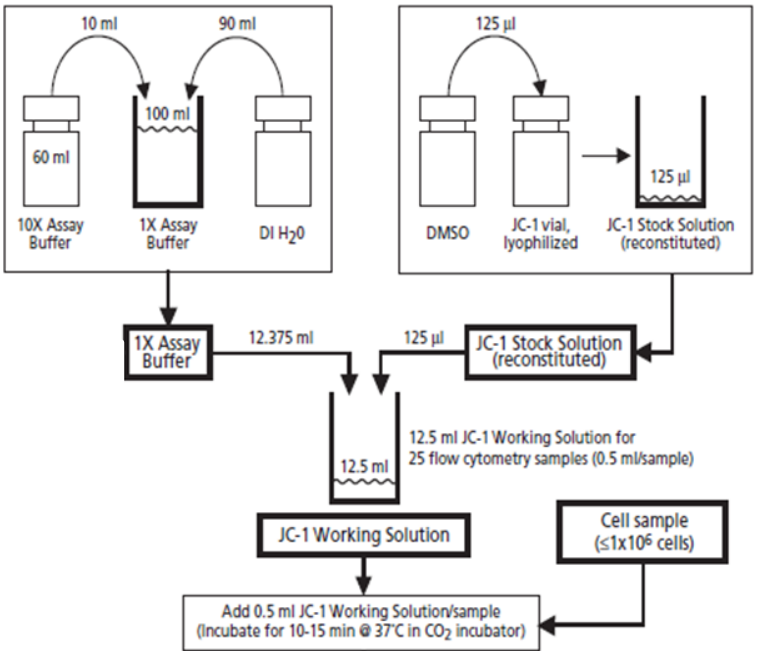

Figure 3.15: Overview of Reagent Preparation and JC-1 staining of cells used for Flow cytometry analysis of mitochondrial membrane potential (BDbiosciences 2013b).

3.9 Luminometry

3.9.1 The CellTiter-Glo® Luminescent Cell Viability Assay (Promega)

This luminescent assay is used to identify the number of viable, metabolically active cells through the quantitation of ATP present and its relation to metabolic functioning of the cells. The amount of ATP present is proportional to the number of viable cells. The assay is based on the luciferase reaction where luciferase in the presence of ATP, magnesium (Mg^{2+}) and molecular oxygen will generate luminescence (Figure 3.16). The greater the luminescence; the greater the amount of ATP; and the greater the number of viable cells present.

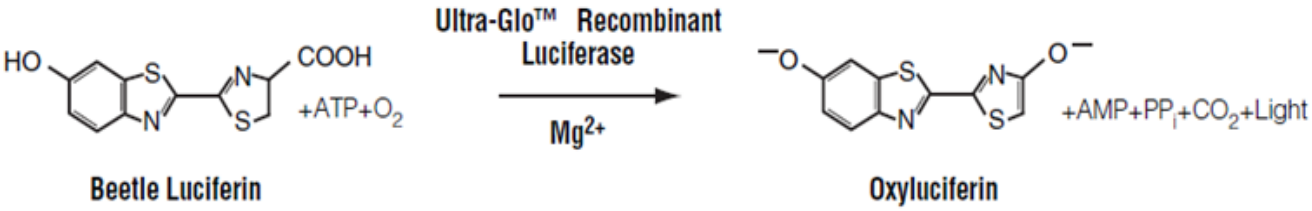

Figure 3.16: The luciferase reaction. The enzyme, luciferase catalyses the mono-oxygenation of luciferin; in the presence of Mg^{2+}, ATP and molecular oxygen (Promega Protocol).

3.9.2 Caspase -Glo® 3/7, 8 and 9 Assay (Promega)

This luminescent assay measures the activity of caspase 3/7, 8 and 9 which are members of the cysteine aspartic family that are important affecters and effectors in apoptosis in mammalian cells. This assay provides luminogenic caspase 3/7, 8 and 9 substrates conjugated with a tetrapeptide sequence aspartate-glutamate-valine-aspartate (DEVD). This DEVD sequence is cleaved by active caspases which allows for the luciferase reaction that produces a "glow-type' luminescent signal which is quantified by the luminometer (Figure 3.17). The amount of luminescence is proportional to the amount of caspase activity within the sample.

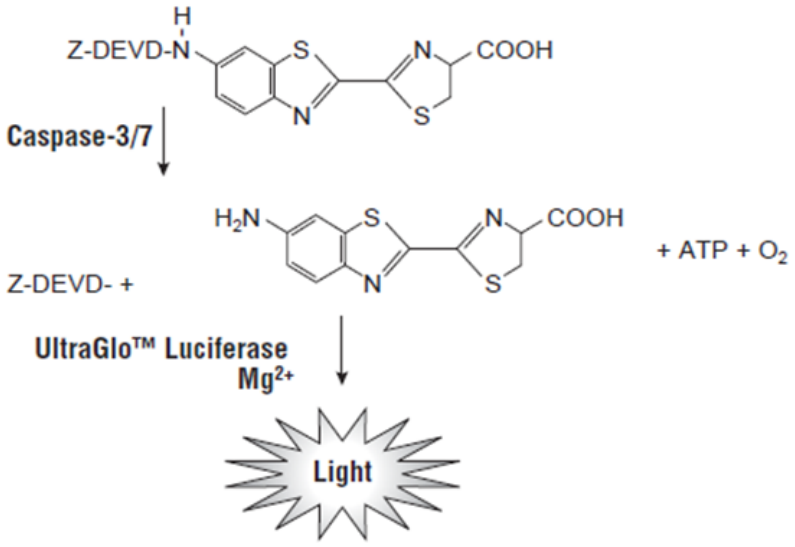

Figure 3.17: Caspase 3/7, 8 and 9 cleavage of the DEVD sequence to produce aminoluciferin that undergoes the luciferase reaction and produces light (Promega Protocol).

The method for the Caspase- Glo 3/7, 8, 9 and CellTiter-Glo Cell Viabilty assays were performed (Figure 3.18). The Caspase-Glo 3/7, 8, 9 and CellTiter-Glo buffer and lyophilised Caspase-Glo 3/7, 8, 9 and CellTiter-Glo substrate was equilibrated to RT. The Caspase-Glo 3/7, 8, 9 and CellTiter-Glo Reagent was prepared by the addition of equal amounts of Caspase-Glo 3/7, 8, 9 and CellTiter-Glo buffer and Caspase-Glo 3/7, 8, 9 and CellTiter-Glo lyophilised substrate. To each well of the white-walled 96-well plate, 100µl of treated cells (as prepared above [section 3.7]) was added and 100µl Caspase-Glo 3/7, 8, 9 and CellTiter-Glo reagent was added. The plate was then incubated at RT for 30minutes. The luminescence of each sample was then measured using a Turner Biosystems Modulus microplate luminometer.

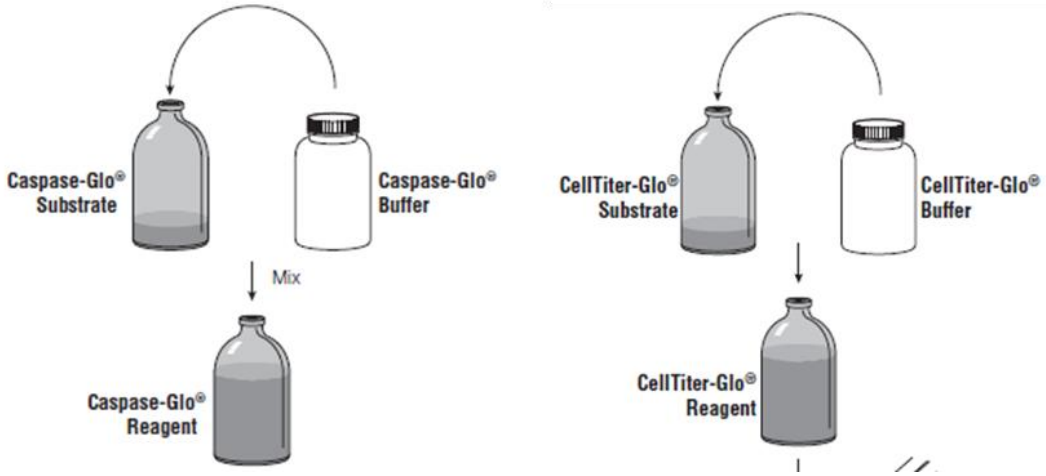

Figure 3.18: Flow Diagram showing the Promega Caspase-Glo® 3/7, 8, 9 (Left) and the Promega CellTiter-Glo® (Right) Reagent Preparation (Promega Protocol).

3.10 Statistical Analysis

The data was reported as mean ± standard deviation. The data was analysed by the GraphPad prism5 software, Image J software and Microsoft Excel 2010. The student unpaired *t* test and one-way analysis of variance (ANOVA) was done on all data to determine the significance ($p<0.05$) when the treatment was compared to the control value.

CHAPTER FOUR

4 RESULTS

4.1 Fumonisin B_1-Tissue transglutaminase interaction

4.1.1 Fumonisin B_1 incorporation into Fibronectin- Tissue transglutaminase Guinea pig liver Standard

The Coomassie Blue stain and western blotting was performed to determine whether FB_1 was incorporated in fibronectin as a result of *gpl* TG2 activation. This assay tests *gpl* TG2 activity. The Coomassie blue staining (Figure 4.1A and 4.2A) is to reveal equal loading of fibronectin in all the wells. Western blots were then probed for anti-FB_1 (Figure 4.1B and 4.2B). The no calcium reaction mix (Figure 4.1B) showed no bands present after 15minutes reaction time but slight bands present at about 270kDa following the 1hour reaction time. The high calcium reaction mix (Figure 4.2B) showed a dose and time-dependent increase in band densities where FB_1 bands are prominent for 1000µM FB_1 treatments after 1hour reaction time. These bands show that FB_1 has been covalently crosslinked into the fibronectin by TG2.

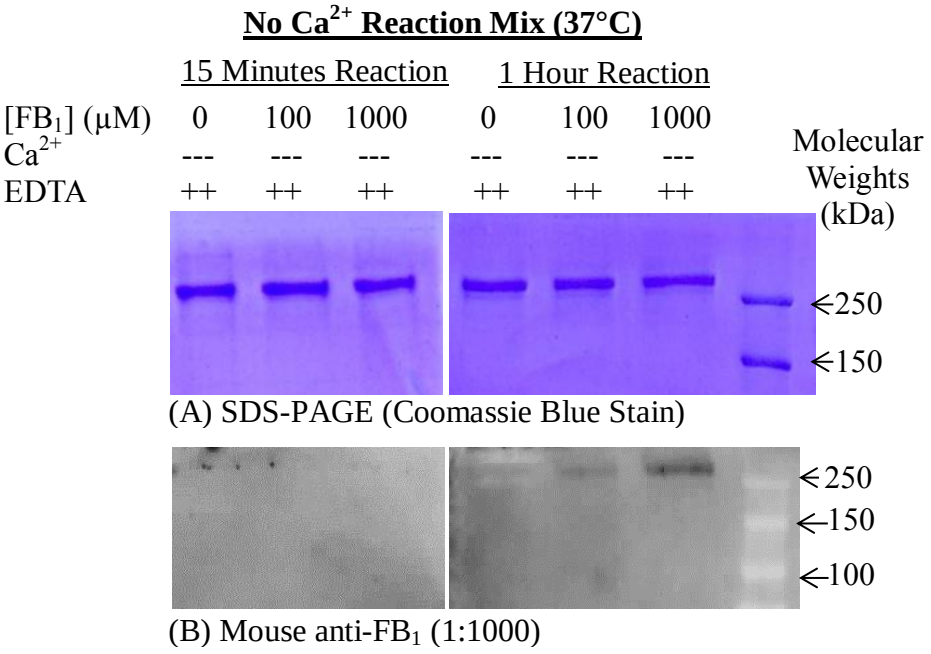

Figure 4.1: Fumonisin B_1 incorporation into fibronectin in No Calcium Reaction Mix (using *gpl* standard of TG2) – adaptation of TG2 activity assay using SDS-PAGE (Coomassie Blue staining to show equal loading, A) and Western Blotting to probe for FB_1 (B) proteins using a mouse anti-FB_1 (1:1000) primary antibody and anti-mouse (1:5000) secondary antibody. Precision plus protein standard (Bio-Rad: #161-0373) was used as the molecular weight marker.

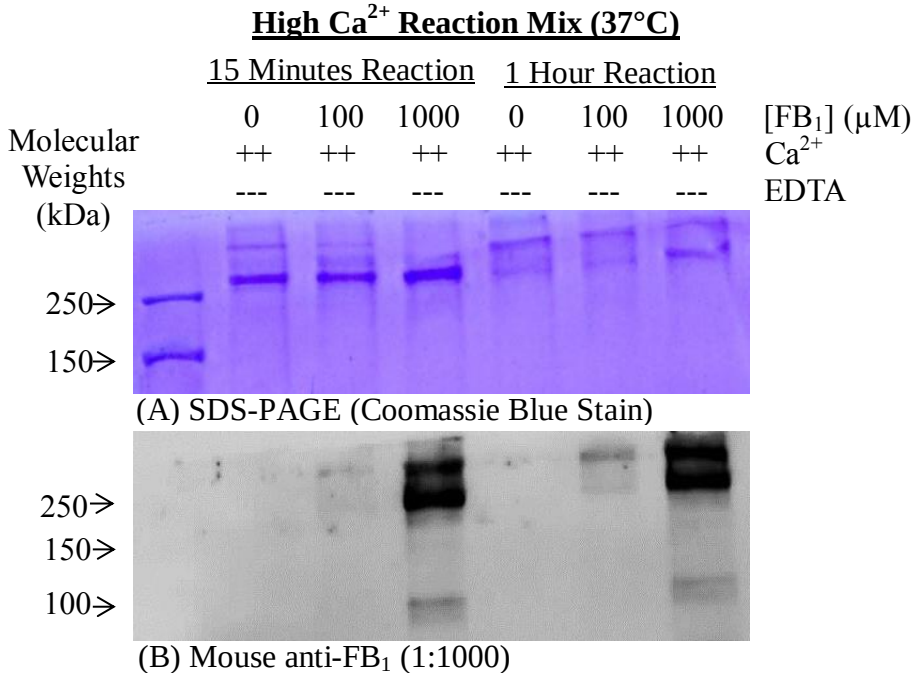

Figure 4.2: Fumonisin B_1 incorporation into fibronectin in High Calcium Reaction Mix (using *gpl* standard of TG2) – adaptation of TG2 activity assay using SDS-PAGE (Coomassie Blue staining to show equal loading, A) and Western Blotting to probe for FB_1 (B) proteins using a mouse anti-FB_1 (1:1000) primary antibody and anti-mouse (1:5000) secondary antibody. Precision plus protein standard (Bio-Rad: #161-0373) was used as the molecular weight marker.

4.1.2 Fumonisin B_1 incorporation into Fibronectin- HEPG2 Cell Homogenates

Western blotting was performed to investigate TG2 activity within HepG2 cells after exposure to FB_1. This method tests TG2 activity by investigating whether FB_1 was incorporated in fibronectin. The TG2 enzyme was catalytically activated in the high calcium reaction and crosslinked FB_1 into the fibronectin as seen by the bands in the western blot probed for anti-FB_1 (Figure 4.3B) where there is an increase in FB_1 crosslinking. The no calcium reaction mix (Figure 4.3A) had slight FB_1 crosslinking possibly due to the endogenous TG2 within the cell homogenates.

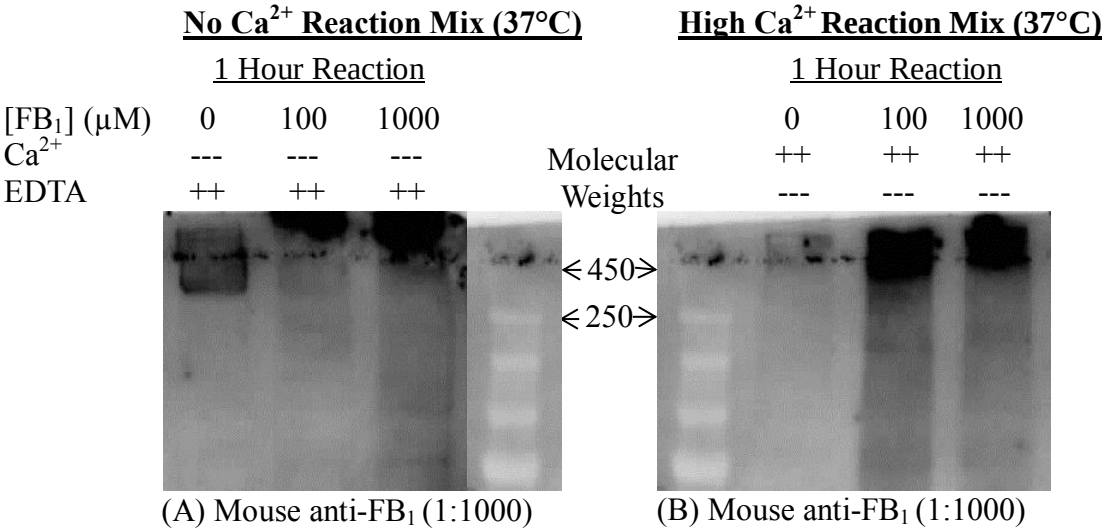

Figure 4.3: Fumonisin B_1 incorporation into fibronectin (using HepG2 cell homogenate) – adaptation of TG2 activity assay using SDS-PAGE and Western Blotting to probe for FB_1 (A and B) proteins using a mouse anti-FB_1 (1:1000) primary antibodies and anti-mouse (1:5000) secondary antibodies. Precision plus protein standard (Bio-Rad: #161-0373) was used as the molecular weight marker.

4.1.3 Tissue transglutaminase Expression – Western blotting

To determine whether TG2 activity was induced in HepG2 cells as a result of FB_1 exposure, western blotting was performed and the results validated using fluorescent microscopy. Tissue transglutaminase expression is increased after 24hours (Figure 4.4A). After 72hours, there is an increase of TG2 expression observed (Figure 4.4B). These results were validated in the immunofluorescent photographs (Figure 4.5 and 4.6) which show TG2 up-regulation after 24 and 72hours (Figure 4.5E and 4.6E) with co-localisation of TG2 and FB_1 being seen in the merged image (Figure 4.5F and 4.6F). The FB_1 is seen to be incorporated intracellularly (Figure 4.5D and 4.6D), with greater incorporation seen after 72hours (Figure 4.6D).

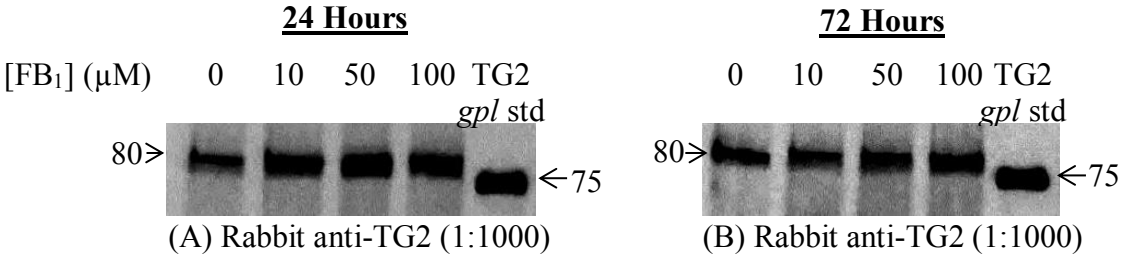

Figure 4.4: Tissue transglutaminase expression in HepG2 cells following treatment with 0μM, 10μM, 50μM and 100μM FB_1 incubated for 24 and 72 hours at 37°C. The concentration of the TG2 *gpl* standard is 10μg/ml. Western Blotting was used to probe for TG2 proteins using rabbit anti-TG2 (1:1000) primary antibody and goat anti-rabbit (1:2000) secondary antibody.

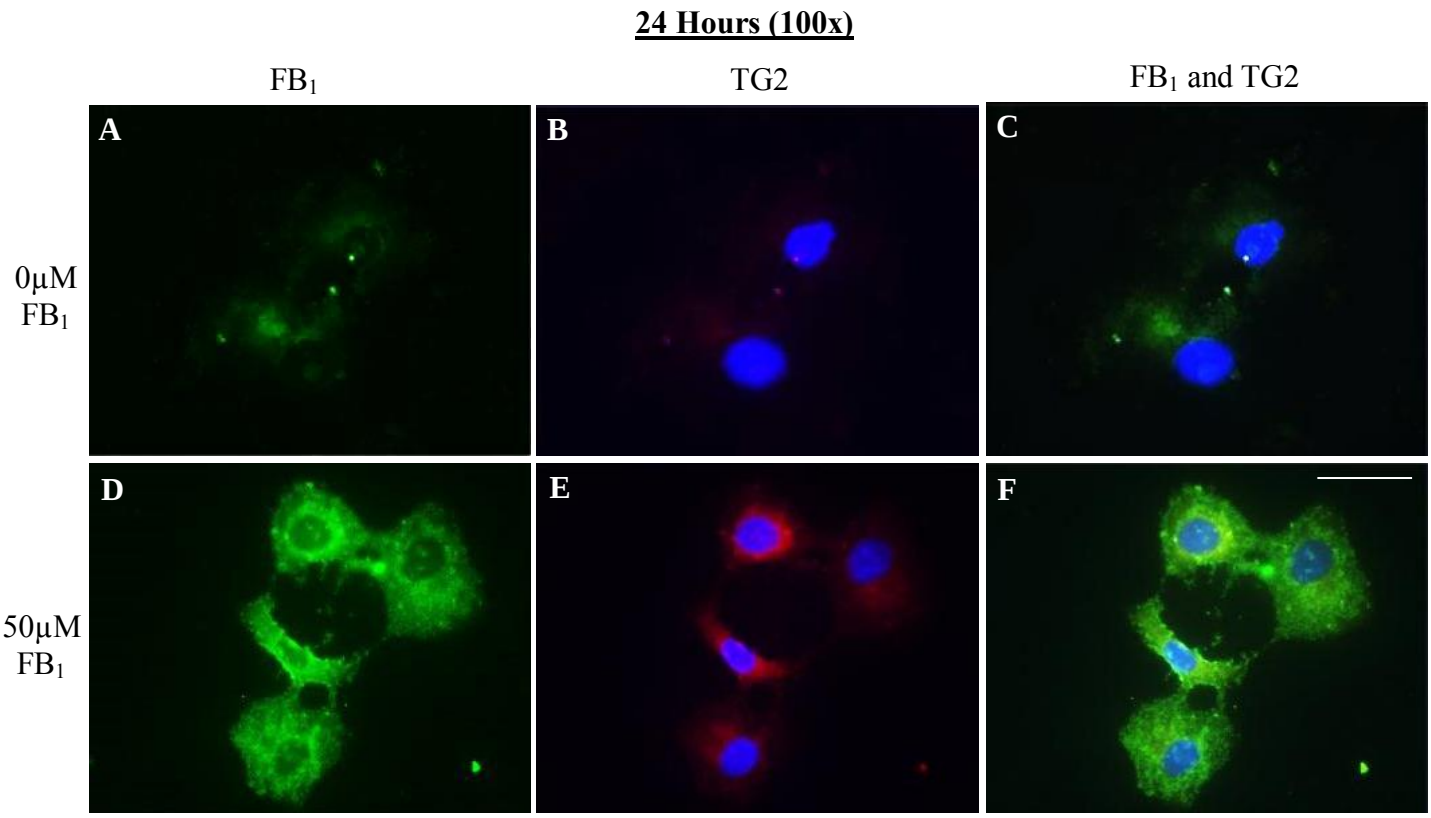

Figure 4.5: Fumonisin B_1 and Tissue transglutaminase co-localisation in HepG2 cells after treatment with FB_1 at concentrations of 0 and 50µM for 24 hours, fluorescent microscopy validation viewed at 100x oil immersion using Axiovision software. Images A and D represent FB_1 expression in green (FITC), images B and E represent TG2 expression in Red (TRITC) and images C and F represents the co-localised FB_1 and TG2 in yellow with Dapi showing the cell's nucleus. Bar equals 40µm.

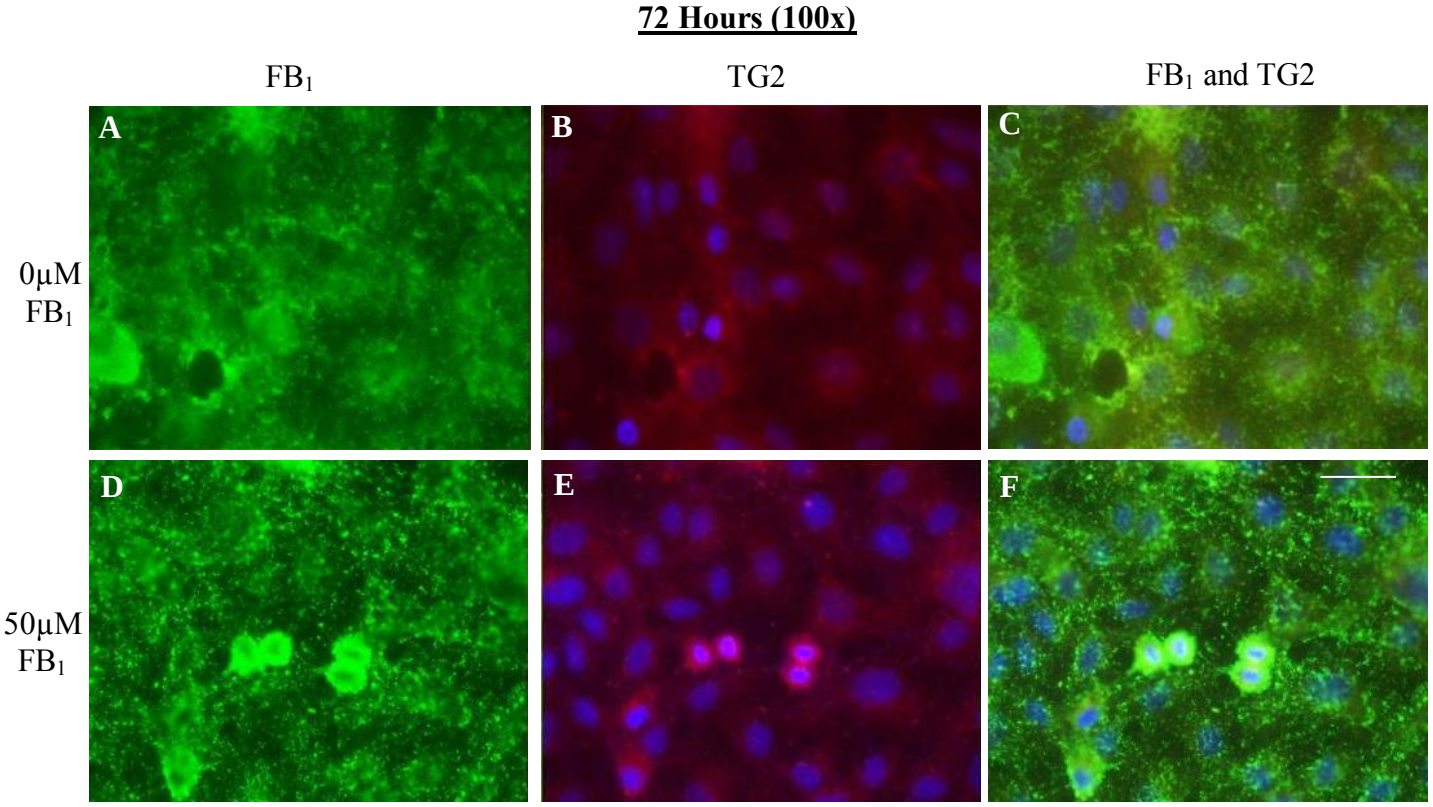

Figure 4.6: Fumonisin B_1 and Tissue transglutaminase co-localisation in HepG2 cells after treatment with FB_1 at concentrations of 0 and 50µM for 72hours, fluorescent microscopy validation viewed at 100x oil immersion using Axiovision software. Images A and D represent FB_1 expression in green (FITC), images B and E represent TG2 expression in Red (TRITC) and images C and F represents the co-localised FB_1 and TG2 in yellow with Dapi showing the cell's nucleus. Bar equals 40µm.

4.2 Fumonisin B_1 induces cytoskeletal damage

To determine whether the cytoskeleton is damaged when HepG2 cells are exposed to FB_1; a β-actin antibody was used. The actin (Figure 4.7A and C) is structurally intact in the controls with disruption being observed after 24 and 72hour 50µM FB_1 treatment (Figure 4.7B and D).

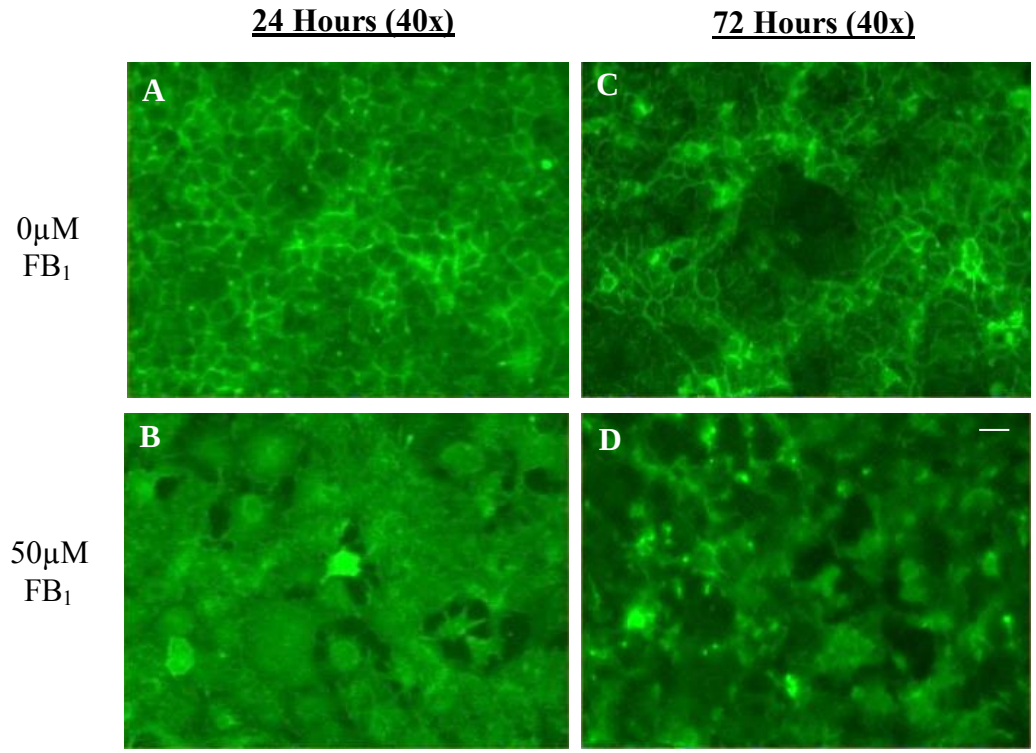

Figure 4.7: Actin expression in HepG2 cells after FB_1 treatment with 0 and 50µM concentrations for 24 and 72hours. Fluorescent microscopy images captured at 40x magnification using Axiovision software. Green FITC (A, B, C and D) represents actin. Bar equals 40µm.

4.3 Endoplasmic Reticulum Stress Pathway Induction

4.3.1 Fumonisin B_1 effect on Protein kinase ribonucleic-like endoplasmic reticulum kinase – Endoplasmic Reticulum Stress Pathway

The effect of FB_1 on the PERK ER stress pathway was investigated using western blotting and qPCR techniques. The expression of total PERK was increased after 24hours at 10µM and 50µM FB_1 concentrations with a decrease in total PERK observed at 100µM FB_1 compared to the control. However, after 72hours the total PERK expression was shown to decrease across all concentrations of FB_1 relative to the control (Figure 4.8). There was an overall increase in phosphorylated eIF2α (p-eIF2α) across both treatment periods and at all FB_1 concentrations (Figure 4.9); however the basal level of p-eIF2α expression at the 24hour treatment is higher than after 72hours. The mRNA

levels of eIF2α showed a corresponding significant increase in eIF2α mRNA expression at 50µM ($p<0.05$) and 100µM FB_1 ($p<0.05$) at the 72hours treatment period. However, a significant decrease in eIF2α mRNA levels was observed at 10µM ($p<0.05$) and 100µM FB_1 ($p<0.05$) after the 24hour treatment period (Figure 4.10). A marker of ER stress, CHOP showed a significant increase in mRNA expression at all concentrations of FB_1 ($p<0.05$) after 72hours (Figure 4.11). There was no change in CHOP mRNA expression levels observed after 24hours (Figure 4.11). A downstream marker of the PERK ER stress pathway ATF4 (Figure 4.12) showed a significant decrease in mRNA levels after treatment with FB_1 over 24hours and 72hours ($p<0.05$).

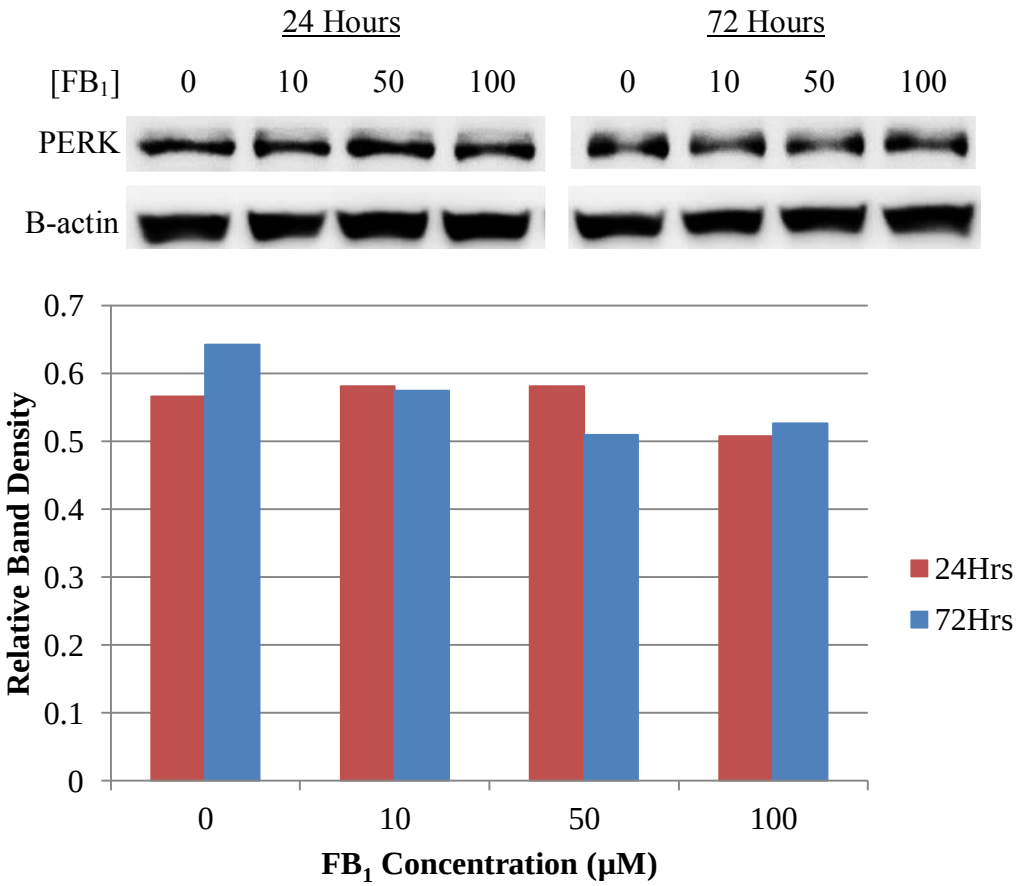

Figure 4.8: The protein expression of total PERK in HepG2 cells after treatment with concentrations 0µM, 10µM, 50µM and 100µM of FB_1 after 24hours (red bars) and 72hours (blue bars). Results were normalised against β-actin. The mean relative band densities are represented by the bars. Representative of two separate experiments.

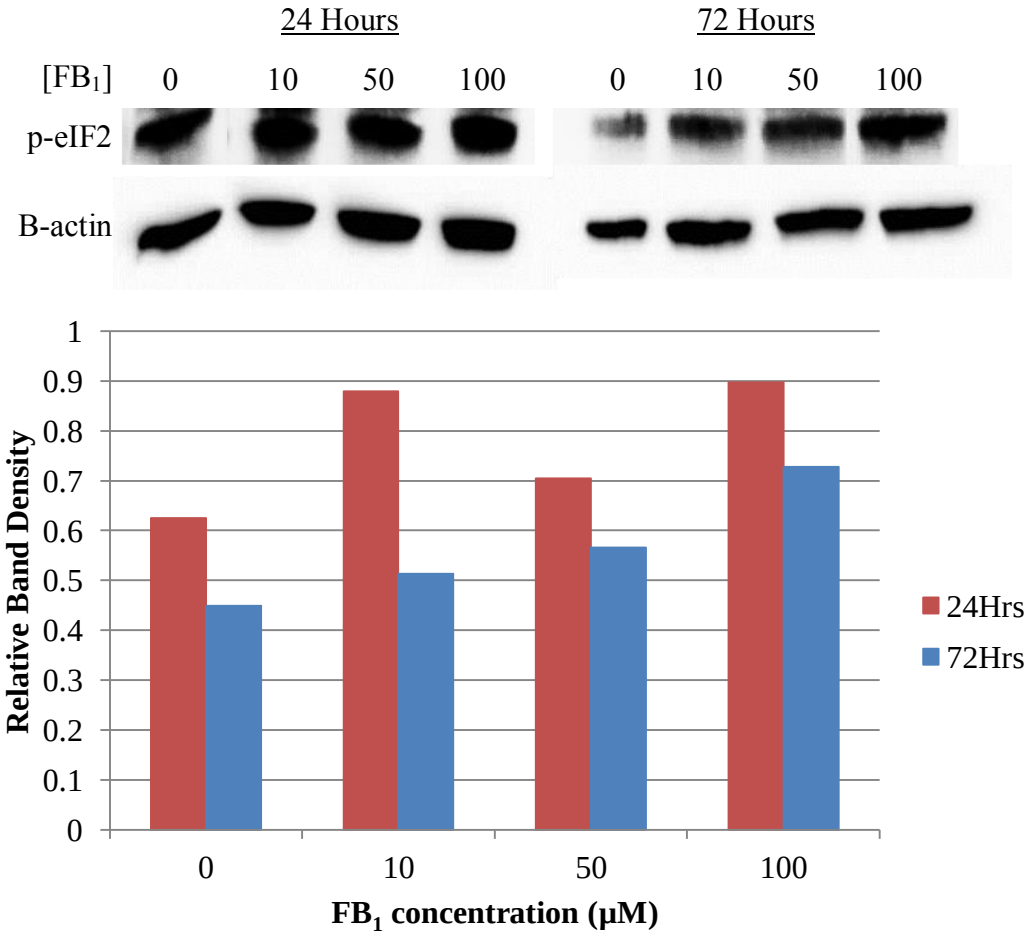

Figure 4.9: The protein expression of p-eIF2 in HepG2 cells after treatment with concentrations 0µM, 10µM, 50µM and 100µM of FB_1 after 24hours (red bars) and 72hours (blue bars). Results were normalised against β-actin. The mean relative band densities are represented by the bars. Representative of two separate experiments.

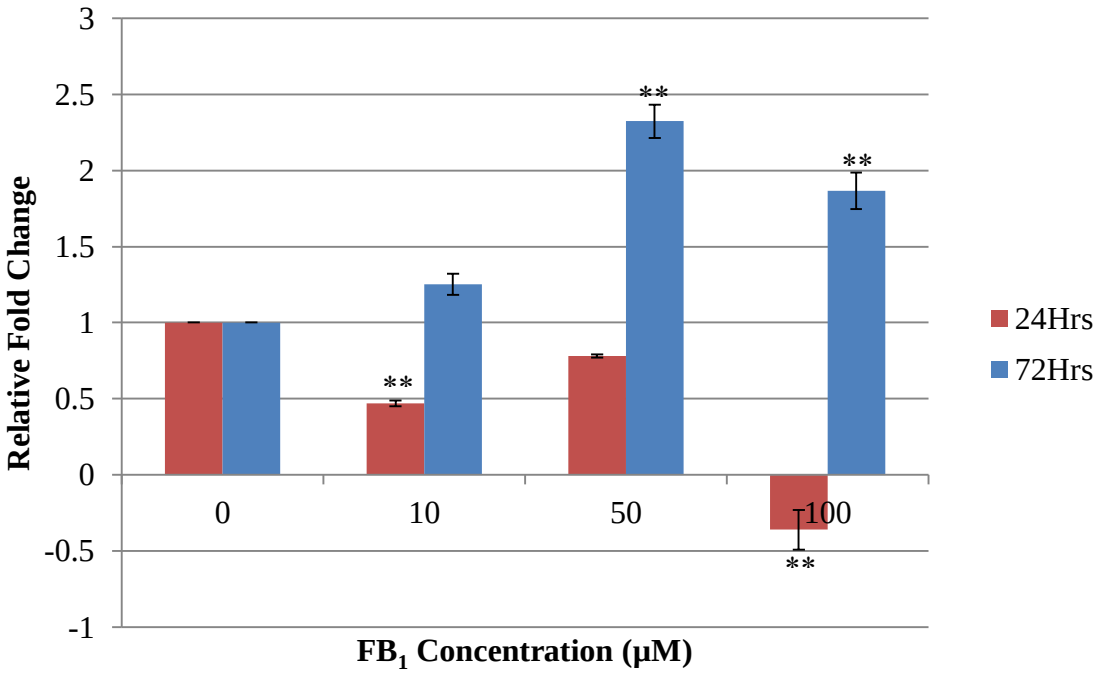

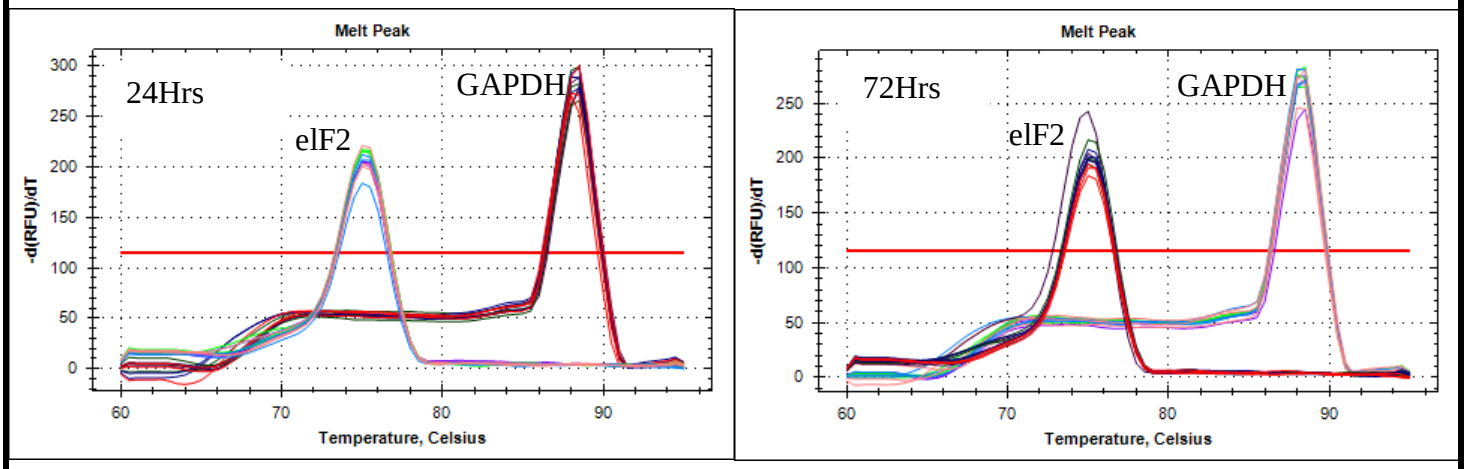

Figure 4.10: The expression of eIF2 mRNA in HepG2 cells after treatment with 0µM, 10µM, 50µM and 100µM FB_1 for 24hours (red bars) and 72hours (blue bars) (Above). Mean ± standard error. Statistical significance: ** shows $p<0.001$ and *** shows $p<0.0001$. The melt curves for eIF2α and GAPDH amplicons show specificity of the primers and no artefacts were present (Below). Representative of three separate experiments.

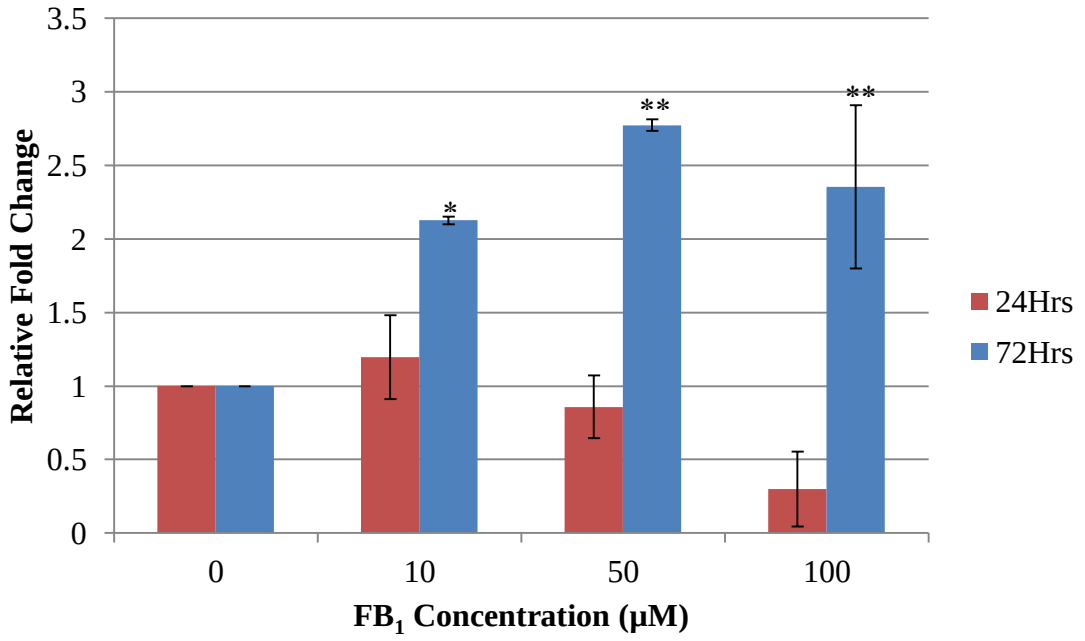

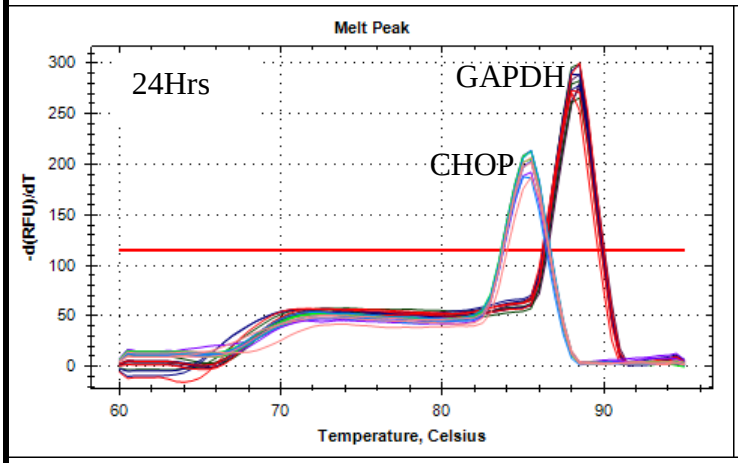

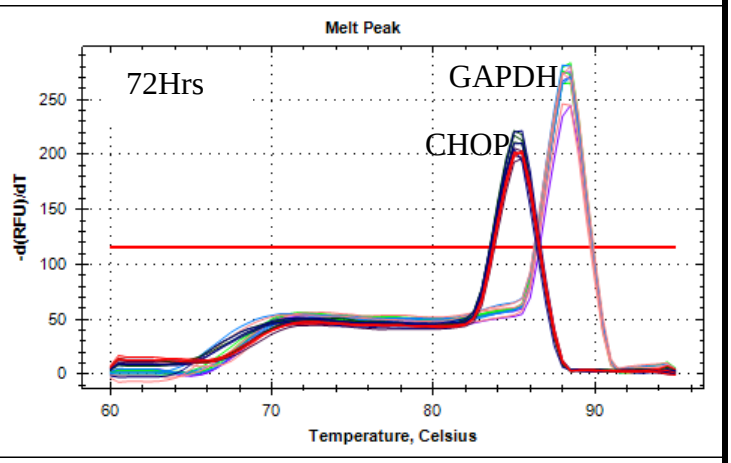

Figure 4.11: The expression of CHOP mRNA in HepG2 cells after treatment with 0µM, 10µM, 50µM and 100µM FB_1 for 24hours (red bars) and 72hours (blue bars) (Above). Mean ± standard error. Statistical significance * shows $p<0.05$ and **shows $p<0.001$. The melt curves for CHOP and GAPDH amplicons show specificity of the primers and no artefacts were present (Below). Representative of three separate experiments.

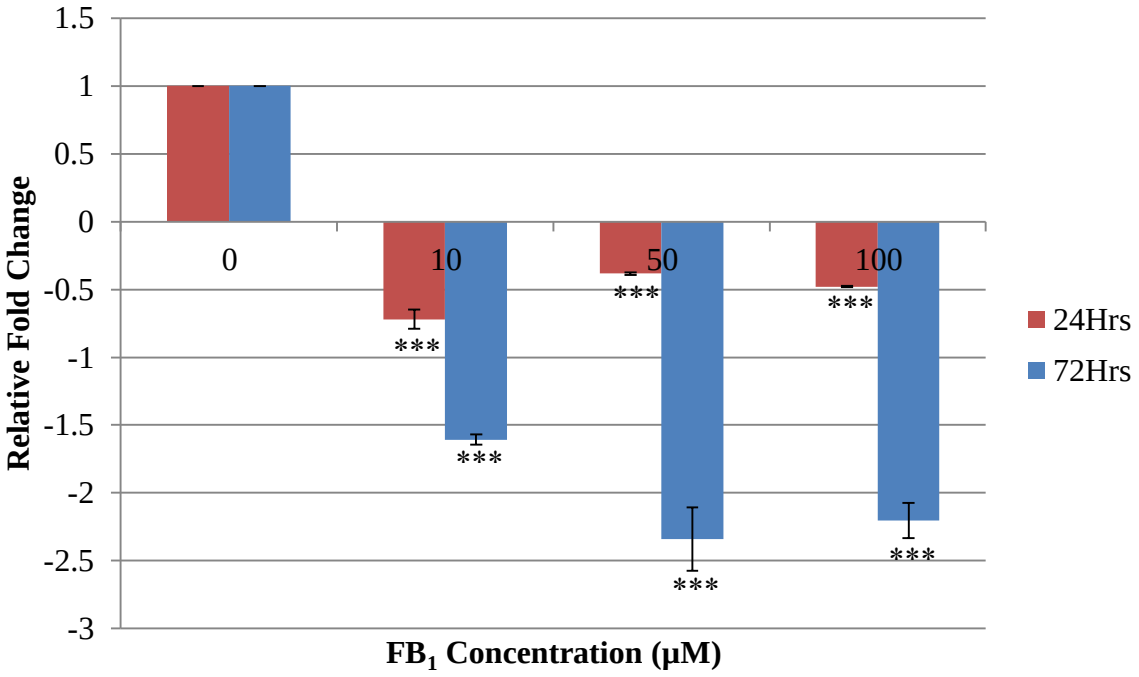

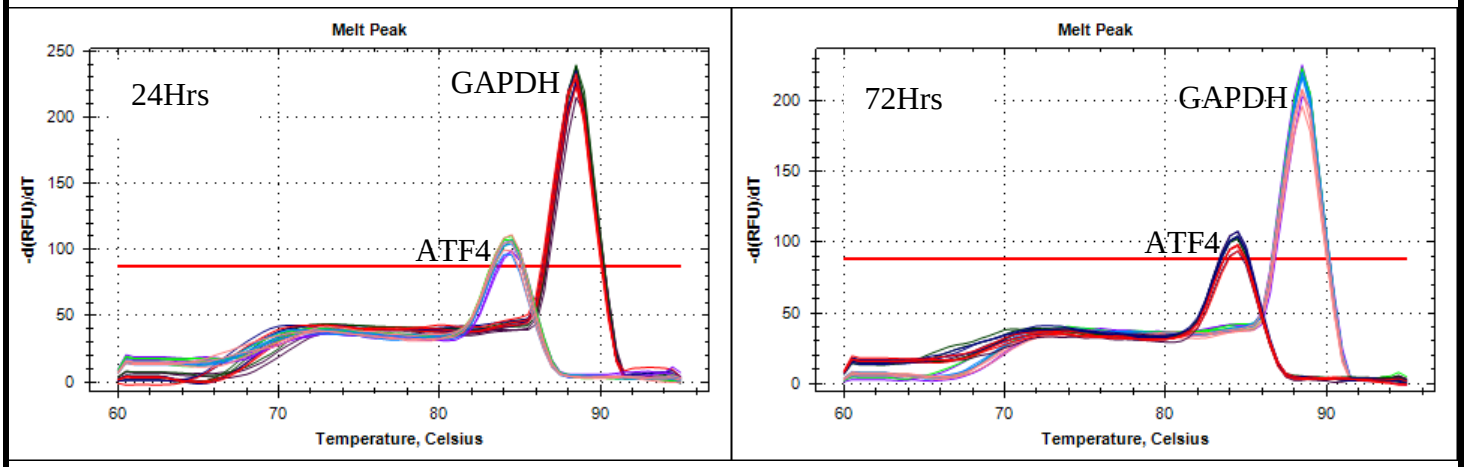

Figure 4.12: The expression of ATF4 mRNA in HepG2 cells after treatment with 0µM, 10µM, 50µM and 100µM FB_1 for 24hours (red bars) and 72hours (blue bars) (Above). Mean ± standard error. Statistical significance: *** shows $p<0.0001$. The melt curves for ATF4 and GAPDH amplicons show specificity of the primers and no artefacts were present (Below). Representative of three separate experiments.

4.3.2 Nuclear factor kappa B phosphorylation and Tissue transglutaminase induction as a result of Endoplasmic Reticulum stress.

The TG2 and NFkB activity were investigated after subcellular fractionation of HepG2 cells treated with FB_1. After 24hours there was decrease in phosphorylation of nuclear NFkB at 10µM and 100µM FB_1 whilst at 50µM FB_1 there was an increase in phosphorylation of nuclear NFkB. The corresponding cytoplasmic NFkB showed a decrease in phosphorylation at 10µM and 50µM FB_1 with an increase observed at 100µM FB_1 with a corresponding decrease in cytoplasmic p-NFkB. However after 72hours there was an increase in the basal level of phosphorylation of NFkB as well as increased phosphorylation observed in the nuclear NFkB with a corresponding decrease in cytosolic p-NFkB (Figure 4.13). The expression of nuclear TG2 increased after 24hours with a corresponding increase in cytosolic TG2 expression (Figure 4.14). The nuclear TG2 mRNA expression was significantly reduced ($p<0.05$) after 24hours (Figure 4.15). However, after 72hours of FB_1 treatment there was an increase in nuclear TG2 observed and a slight decrease in the corresponding cytosolic TG2 expression (Figure 4.14). The expression of nuclear TG2 mRNA was significantly increased at 10µM FB_1 ($p<0.05$), whilst significantly reduced at 50µM FB_1 ($p<0.05$) and showed an increase in expression at 100µM FB_1 treatment although it was not significant (Figure 4.15). A potential downstream effector of TG2 apoptosis, Sp1 showed a significant decrease in mRNA expression after 24hours at 50µM ($p<0.05$) and 100µM FB_1 ($p<0.05$) (this is not true for 10µM FB_1). A significant increase in Sp1 expression after 72hours at 10µM FB_1 ($p<0.05$) was observed (this is not true for 50µM and 100µM FB_1, as a decrease in expression is noted) (Figure 4.16).

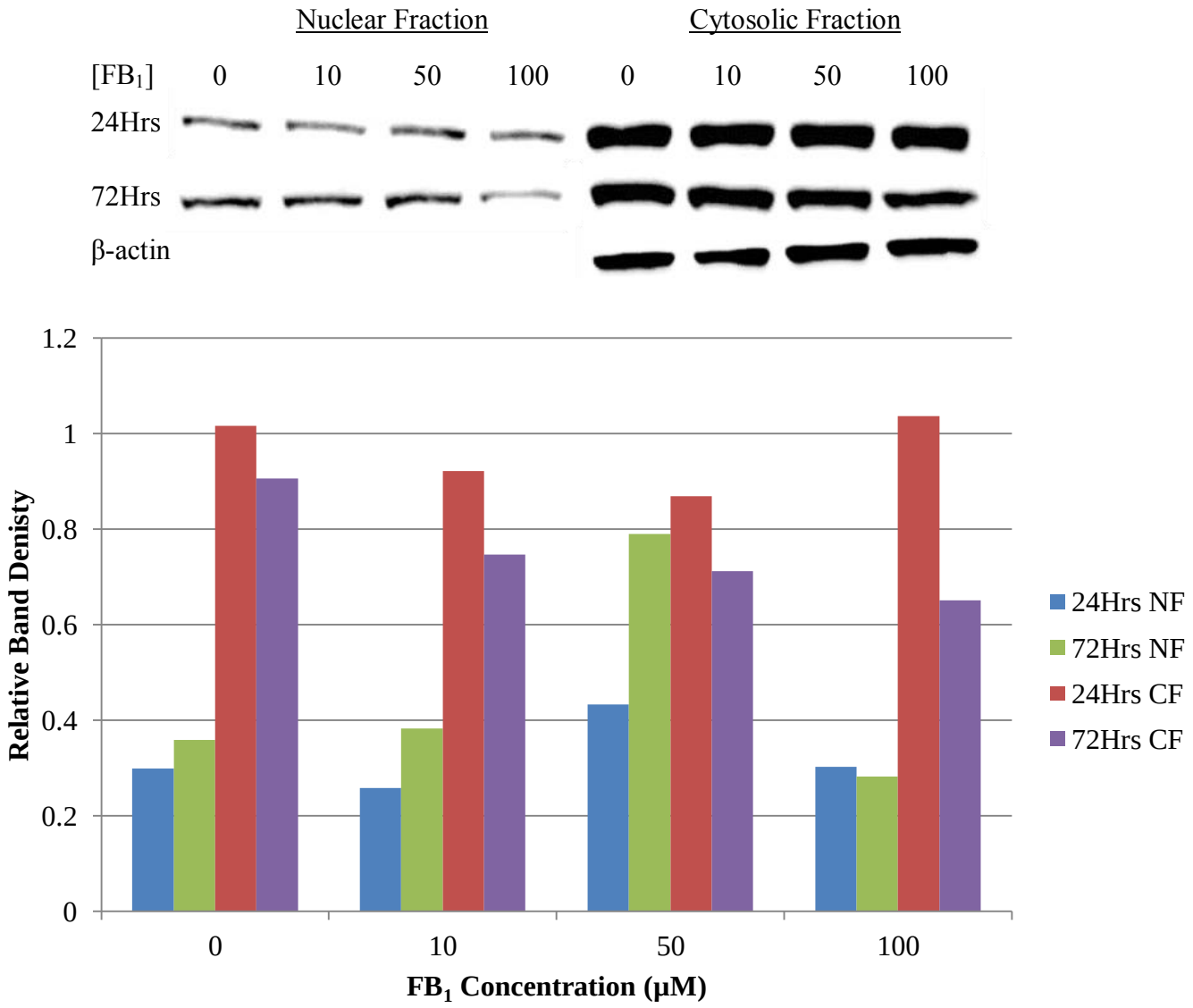

Figure 4.13: The protein expression of p-NFkB in the nuclear and cytosolic fraction of HepG2 cells treated with 0µM, 10µM, 50µM and 100µM FB_1 after 24hours and 72hours. Results were normalised against β-actin. The bars represent the mean relative band densities. Representative of two separate experiments.

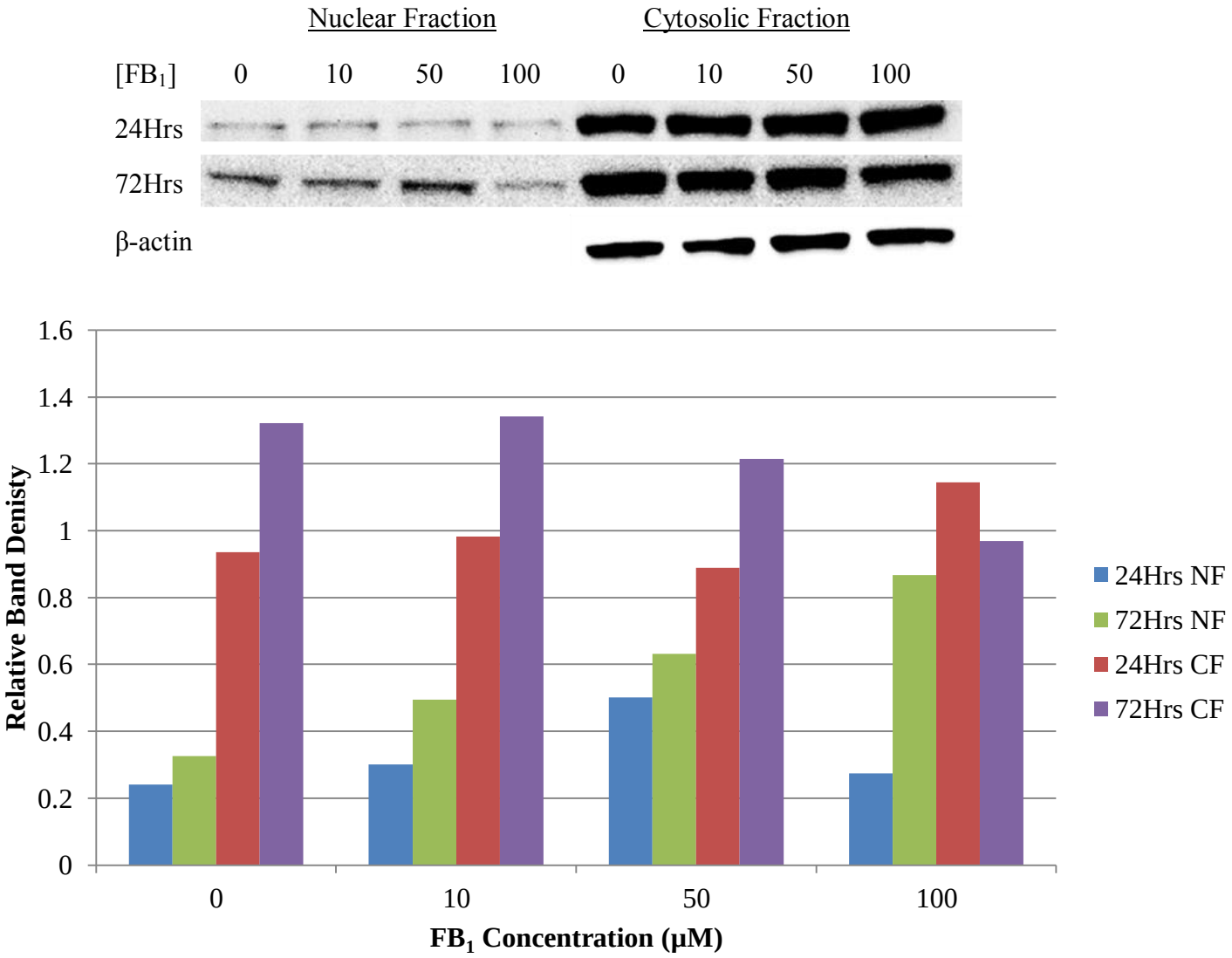

Figure 4.14: The protein expression of TG2 in the nuclear and cytosolic fraction of HepG2 cells treated with 0µM, 10µM, 50µM and 100µM FB_1 after 24hours and 72hours. Results were normalised against β-actin. The bars represent the mean relative band densities. Representative of two separate experiments.

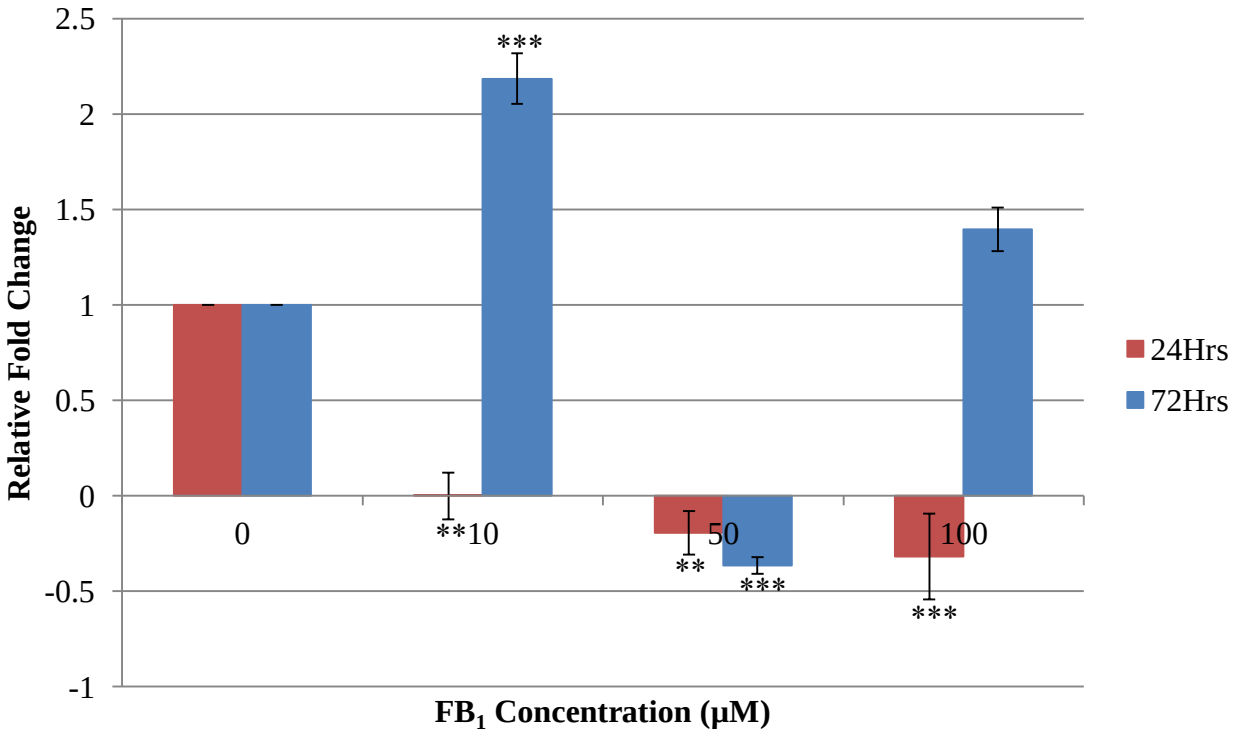

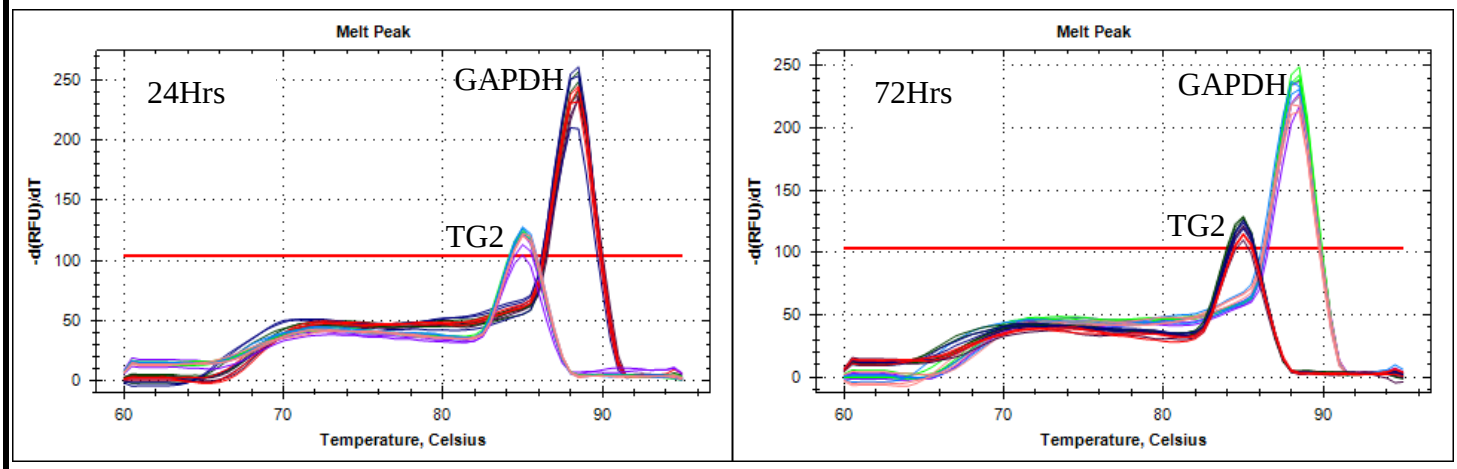

Figure 4.15: The expression of TG2 mRNA in HepG2 cells after treatment with 0µM, 10µM, 50µM and 100µM FB_1 for 24hours (red bars) and 72hours (blue bars) (Above). Mean ± standard error. Statistical significance ** shows $p<0.001$ and ***shows $p<0.0001$. The melt curves for TG2 and GAPDH amplicons show specificity of the primers and no artefacts were present (Below). Representative of three separate experiments.

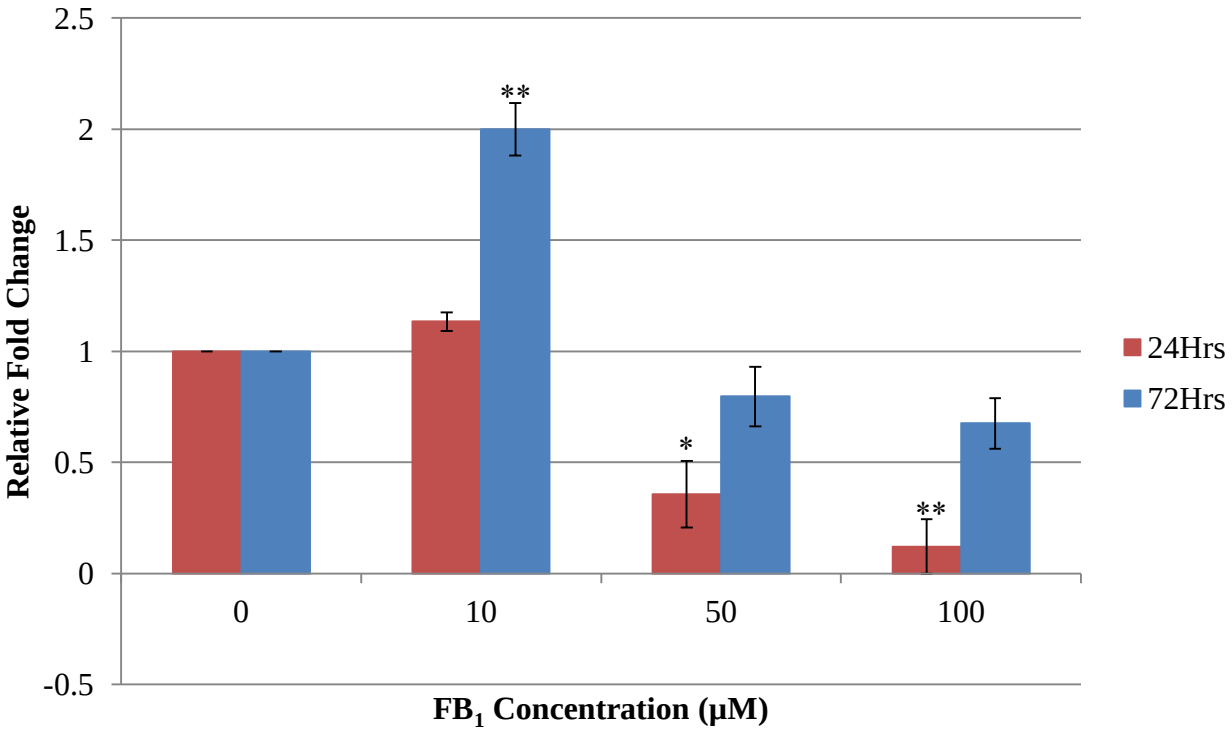

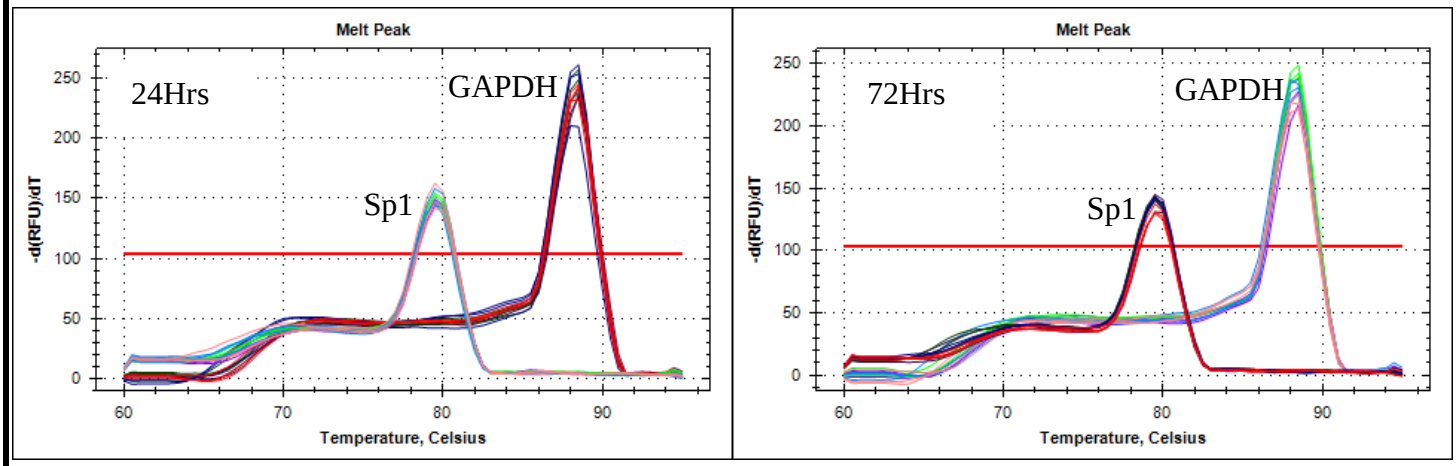

Figure 4.16: The expression of Sp1 mRNA in HepG2 cells after treatment with 0µM, 10µM, 50µM and 100µM FB_1 for 24hours (red bars) and 72hours (blue bars) (Above). Mean ± standard error. Statistical significance * shows $p<0.05$ and **shows $p<0.001$. The melt curves for Sp1 and GAPDH amplicons show specificity of the primers and no artefacts were present (Below). Representative of three separate experiments.

4.4 Apoptotic effect of Fumonisin B_1

The apoptotic effect of FB_1 was investigated after 72hour treatment of HepG2 cells with varying concentrations of FB_1. Caspase's are initiators and effectors of the apoptotic pathway and were investigated using luminometry. Caspases 3 and 8 (Figure 4.17 and 18) activities were significantly reduced at 100µM FB_1 ($p<0.05$) and 50µM FB_1 ($p<0.05$) (caspase 8 only). A decrease in caspase 9 activity was observed although not significant (Figure 4.19). There was a significant reduction in ATP levels after 100µM FB_1 ($p<0.05$) treatment (Figure 4.20). The Annexin-V-FITC and JC-1 MitoScreen experiments were done to determine the percentage of apoptotic, live cells and depolarised mitochondria present after 72hours of FB_1 treatment. The results showed that there was a significant increase in apoptotic cells when HepG2 cells were treated with 10µM FB_1 ($p<0.05$) (Figure 4.21) with a corresponding significant decrease ($p<0.05$) in the amount of healthy cells (Figure 4.22). There is also an increase in the percentage of depolarised mitochondria with the 10µM FB_1 ($p<0.05$) treatment (Figure 4.23). However, when HepG2 cells are treated with 50µM of FB_1 there is a decrease in the percentage of apoptotic cells (Figure 4.21) with a corresponding significant increase ($p<0.05$) in healthy cells (Figure 4.22) and a significant decrease in depolarised mitochondria ($p<0.05$) (Figure 4.23).

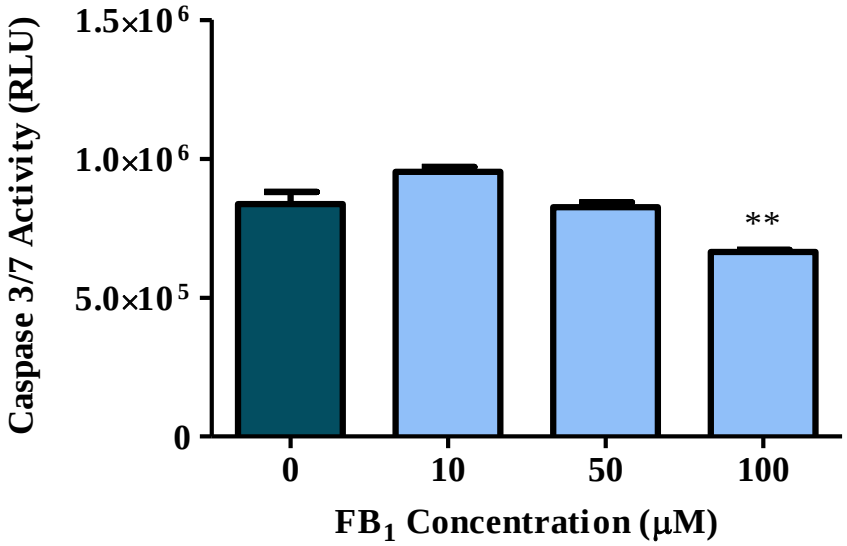

Figure 4.17: Caspase 3/7 activity in HepG2 cells treated with 0μM, 10μM, 50μM and 100μM FB_1 for 72hours. Mean ± Standard error. Statistical significance: ** shows $p<0.001$. Representative of three separate experiments.

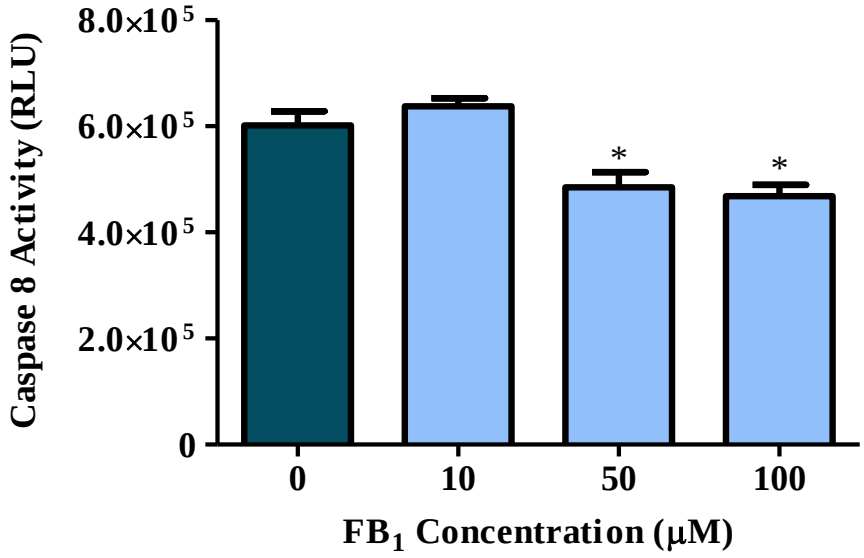

Figure 4.18: Caspase 8 activity in HepG2 cells treated with 0μM, 10μM, 50μM and 100μM FB_1 for 72hours. Mean ± Standard error. Statistical significance: * shows $p<0.05$. Representative of three separate experiments.

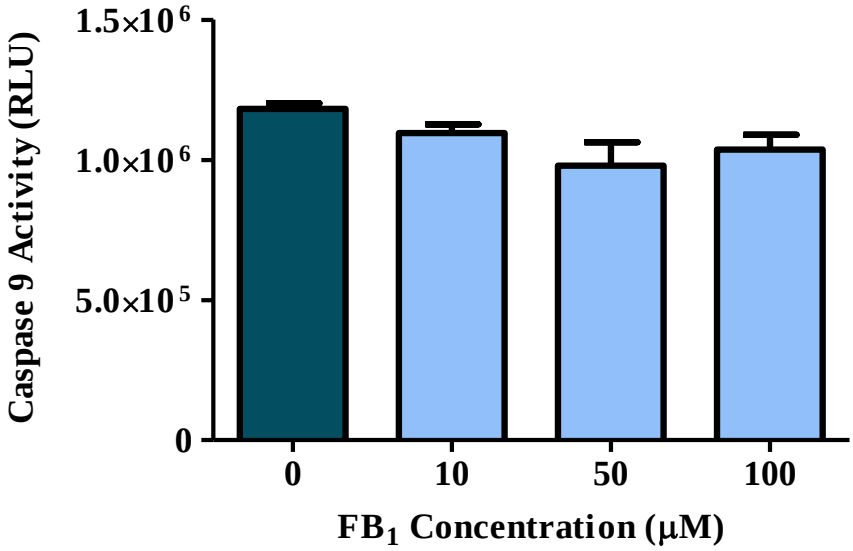

Figure 4.19: Caspase 9 activity in HepG2 cells treated with 0μM, 10μM, 50μM and 100μM FB_1 for 72hours. Mean ± Standard error. Representative of three separate experiments.

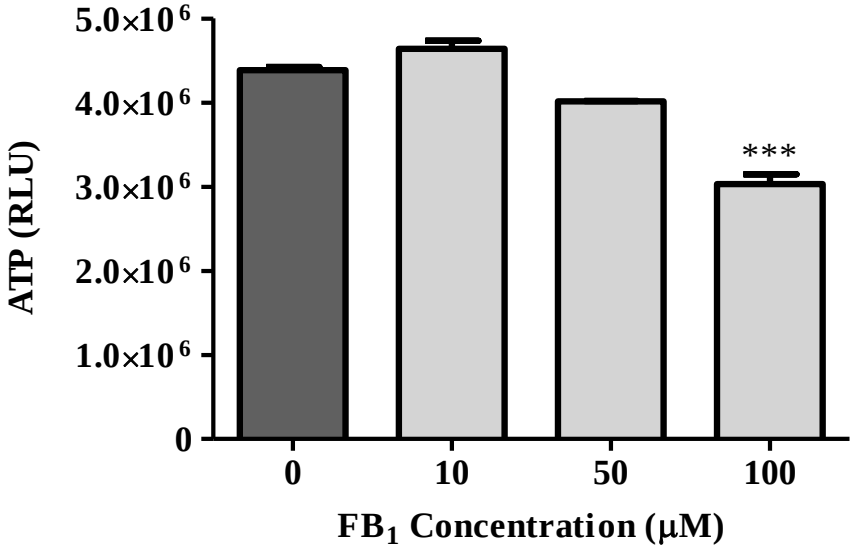

Figure 4.20: The ATP levels in HepG2 cells treated with 0μM, 10μM, 50μM and 100μM FB_1 for 72hours. Mean ± Standard error. Statistical significance: *** shows $p<0.0001$. Representative of three separate experiments.

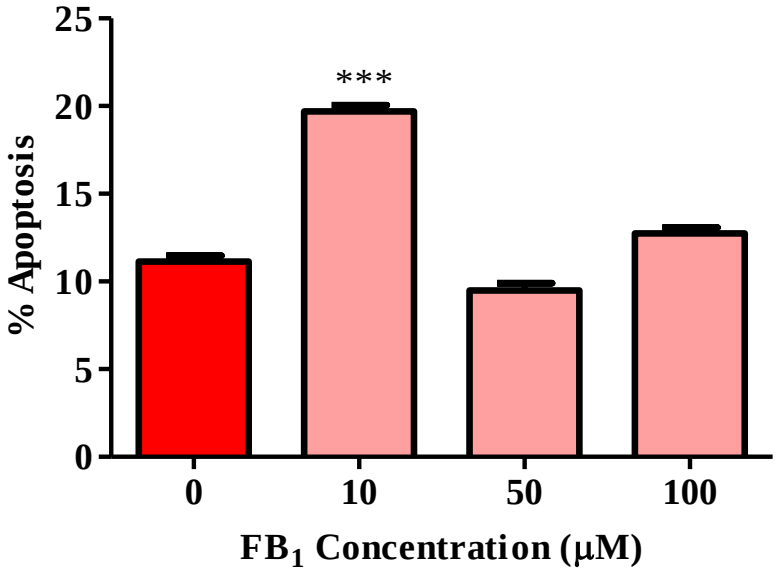

Figure 4.21: The percentage of Annexin positive or apoptotic cells in HepG2 cells treated with 0µM, 10µM, 50µM and 100µM FB_1 for 72hours. Mean ± Standard error. Statistical significance: *** shows p<0.0001. Representative of three separate experiments.

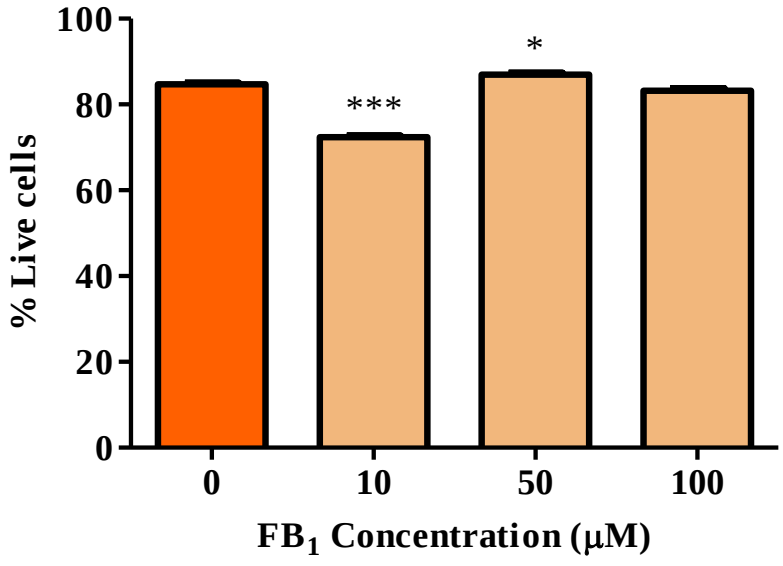

Figure 4.22: The percentage of healthy/live cells in HepG2 cells treated with 0µM, 10µM, 50µM and 100µM FB_1 for 72hours. Mean ± Standard error. Statistical significance: * shows p<0.05; *** shows p<0.0001. Representative of three separate experiments.

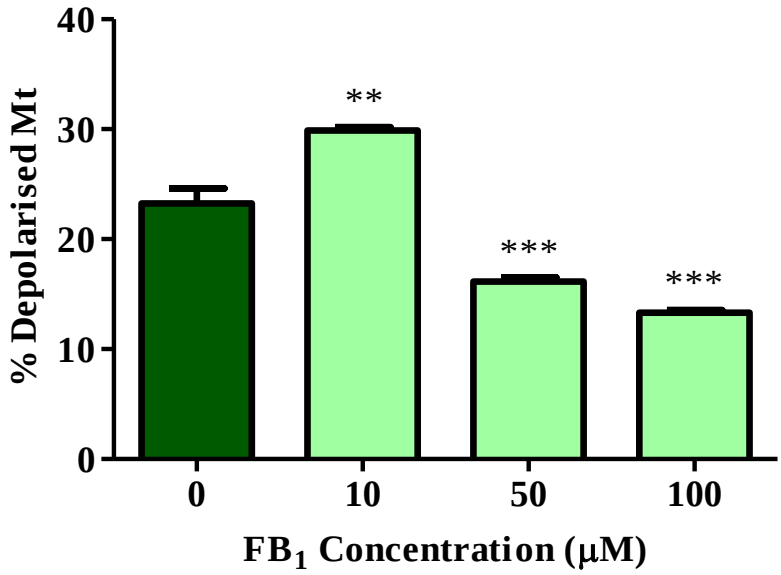

Figure 4.23: The percentage of depolarised mitochondria in HepG2 cells treated with 0μM, 10μM, 50μM and 100μM FB_1 for 72hours. Mean ± Standard error. Statistical significance: ** shows $p<0.001$ and *** shows $p<0.0001$. Representative of three separate experiments.

CHAPTER FIVE

5 DISCUSSION

Fumonisin B_1 toxicity is well characterised to be a result of ceramide synthase inhibition which interrupts sphingolipid biosynthesis (Grenier et al. 2012) leading to the disruption of the cell and its plasma membrane; which is a possible cause of cell stress leading to ER stress. This study investigated the possible role of TG2 induction by FB_1 and the effect FB_1 toxicity has on the ER stress pathway in HepG2 cells. A novel association between FB_1 and TG2 was observed (Figure 4.1, 4.2, 4.3 and 4.5) in the HepG2 liver cells where FB_1 induced TG2 expression and activity, with FB_1 acting as a potential crosslinking substrate for this enzyme. Further, the ability of FB_1 to induce ER stress was investigated using western blotting and qPCR (Figure 4.8-4.12); with TG2 and NFkB involvement being investigated by western blotting and qPCR (Figure 4.13-4.16). Apoptotic markers were determined using luminometry (caspase assays) (Figure 4.17-4.20), and flow cytometry [Annexin-V-FITC (Figure 4.21 and 4.22) and the JC-1 MitoScreen assays (Figure 4.23)].

The ubiquitous enzyme TG2 catalyses the post-translational modifications of proteins through a transamidation reaction which results from the acyl transfer between a γ-carboxyamide glutamine residue (acyl donor) and a lysine Ɛ-amino residue of a primary amine (acyl acceptor) which forms a proteinase-resistant covalent N-γ-glutamyl-Ɛ-lysyl-isopeptide bond (crosslink) (Martin et al. 2012); with the crosslinked protein product being a higher molecular mass (Park et al. 2010). The TG2 activity assay demonstrated a novel interaction between FB_1 and the calcium-dependent catalytic activity of TG2 (Figure 4.1, 4.2, 4.3 and 4.5), where TG2 appears to catalytically incorporate FB_1 into fibronectin-crosslinked high molecular polymers. This observation exposed FB_1 as a possible substrate for TG2 activity (Figure 4.1, 4.2 and 4.3). Fibronectin was used as it is a well

characterised extracellular matrix protein that TG2 binds and crosslinks with high affinity (Griffin et al. 2002). A covalent association between fibronectin (acyl donor) and FB_1 (acyl acceptor) was observed because through SDS-PAGE experimentation the bond was not broken and the resulting crosslinked-fibronectin had a higher molecular weight (Park et al. 2010). The results showed that TG2 activity is dependent on calcium (Figure 4.1B and 4.2B), FB_1 concentration and time (Figure 4.2B and 4.3B). High calcium conditions are essential as calcium activates TG2 through the conformational change which exposes its active site allowing the reaction to occur (Park et al. 2010). Dependence on FB_1 and time was seen as increasing the availability of the substrate and the time for the reaction to occur increased FB_1 incorporation into fibronectin. This association was further validated using immunofluorescent microscopy (Figure 4.5 and 4.6) which showed TG2 up-regulation by FB_1 (Figure 4.5D and 4.6D) and co-localisation of FB_1 and TG2 (Figure 4.5F and 4.6F) where FB_1 may be catalytically incorporated intracellularly when treated with 50µM FB_1. As FB_1 toxicity has been characterised to disrupt membrane-sphingolipid metabolism (Heidtmann-Bemvenuti et al. 2011), the activity of TG2 to incorporate FB_1 into the plasma membrane (Figure 4.5F and 4.6F) may have a possible novel role of TG2 in FB_1-associated stress response signalling pathways (Giussani et al. 2006).

The inhibition of ceramide synthase due to FB_1 toxicity leads to decreased ceramide formation and a decrease in complex sphingolipids, which are essential components of the plasma membrane (Heidtmann-Bemvenuti et al. 2011). Fumonisin B_1 caused cytoskeletal damage and disrupted cell membranes in HepG2 cells (Figure 4.7). The activation of TG2 (Figure 4.3) is a calcium-dependent occurrence where calcium levels need to be above 700-800nM which occurs only in supraphysiological conditions i.e. when the cell is damaged (Kuo et al. 2011). The ER acts as a major reservoir of intracellular calcium and therefore plays a critical role in calcium homeostasis (Hetz 2012; Hotamisligil 2010). Therefore due to high levels of calcium required for TG2 activation

it can be suggested that the ER function is disrupted leading to the activation of the ER stress pathway.

The ER stress pathway or UPR is activated when protein folding becomes compromised (Rutkowski & Kaufman 2004). The PERK arm of the UPR is activated upon BiP dissociation as a result of increased UP (Hotamisligil 2010; Pagliassotti 2012). Upon PERK activation, it phosphorylates serine 51 on eIF2α which leads to protein synthesis attenuation (Lasfargues et al. 2013). The phosphorylation of e-IF2α stimulates the translation of ATF4 mRNA (Lasfargues et al. 2013) which controls selective pro-survival genes (Hetz 2012). A transcription factor CHOP is upregulated by ATF4 and is involved in ER stress-induced apoptosis (Lasfargues et al. 2013). The 24hour FB_1 treatment showed an increase in total PERK at 10μM (Figure 4.8), an increase in p-eIF2α (Figure 4.9) with a corresponding significant decrease in eIF2α mRNA expression at 10μM FB_1 ($p<0.05$) (Figure 4.10) and an increase in CHOP (Figure 4.11) mRNA expression although not significant. After 72hours however total PERK was decreased (Figure 4.8) and there was a reduction in the basal level of p-eIF2α although still activated (Figure 4.9) with a significant increase in eIF2α mRNA expression at 50μM ($p<0.05$) and 100μM FB_1 ($p<0.05$) (Figure 4.10). At 50μM ($p<0.05$) and 100μM FB_1 ($p<0.05$) CHOP mRNA expression was also significantly induced (Figure 4.11). These results are in agreement with a study by Aflaki et al. (2012) on macrophages. This shows that FB_1 induced ER stress via the PERK pathway with increased ER stress being observed after 72hours due to the significant increase in CHOP after 72hours. However unlike Aflaki et al. (2012), this study in HepG2 cells showed a significant decrease in ATF4 mRNA expression ($p<0.05$) both at 24 and 72hours (Figure 4.12). This could suggest that the PERK-eIF2α pathway was activated but p-eIF2α levels were too low to impair the initiation at the second μORF of ATF4 gene (Lasfargues et al. 2013) therefore preventing its transcription. The genes induced downstream of ATF4 transcription are important for the cell to recover from various stresses

(Rutkowski & Kaufman 2004); according to Aflaki et al. (2012) FB_1 reduced but failed to abolish the ER stress in macrophages. This could potentially explain the reduction in ATF4 observed in this liver model as pro-survival downstream genes of ATF4 would not be transcribed therefore preventing recovery of ER stress in HepG2 cells. However this requires further investigation due to the difference in cell lines; although the liver is an immune organ and FB_1 has shown to be immunotoxic *in vitro* (Stockmann-Juvala et al. 2008), the effects on hepatocarcinoma cells would differ. As ATF4 is a known inducer of CHOP (Rutkowski & Kaufman 2004) and ATF4 showed a significant decrease ($p<0.05$) in mRNA expression (Figure 4.12) but CHOP showed a significant increase ($p<0.05$) in mRNA expression (Figure 4.11), further studies are required to identify other transcription factors that could induce CHOP. ATF6 is thought to also induce CHOP, so its induction could be a result of the other arms of the UPR (Rutkowski & Kaufman 2004).

It has been reported that ER stress activates NFkB (Tam et al. 2012). Nuclear factor kappa B activation has been linked to PERK-mediated eIF2α phosphorylation; where the attenuation of translation leads to a rapid decrease in IkBα due to its relatively short-half life and the inhibition of translation (Tam et al. 2012). Fumonisin B_1 treatment showed a decrease in both nuclear NFkB and cytosolic NFkB after 24hours at 10µM FB_1 (Figure 4.13). However, after 72hours there was an increase in the basal level of NFkB as well as an increase in nuclear NFkB with a corresponding decrease in cytosolic NFkB at 10µM and 50µM FB_1 (Figure 4.13), evidence for PERK activation of NFkB and nuclear translocation. Nuclear factor kappa B is a transcriptional inducer of TG2 where NFkB binds the TGM2 promoter gene directly and induces TG2 transcription (Ientile et al. 2007). Fumonisin B_1 treatment showed an increase in nTG2 expression with a corresponding decrease in cytosolic TG2 (Figure 4.14) and a significant decrease in nTG2 mRNA expression ($p<0.05$) (Figure 4.15) which correlated with a decrease in nNFkB at 50µM FB_1 (Figure 4.13). After 72hours however, there is an increase in nTG2 (Figure 4.14) with a corresponding significant increase in

nTG2 mRNA expression at 10µM FB_1($p<0.05$) (Figure 4.15) and with a slight decrease in cytosolic TG2 at 100µM FB_1 (Figure 4.14), evidence for NFkB induction of nTG2 via PERK ER stress pathway. Kuo et al. (2012) showed a potential mechanism for TG2-induced apoptosis as a result of free fatty acid treatment (Figure 5.1). This mechanism involved the activation of PERK-ER stress pathway which induced NFkB activation which then stimulated nTG2 transcription and activation leading to apoptosis through its crosslinking of Sp1, a general transcription factor responsible for the expression of c-Met an important growth factor (Kuo et al. 2011). Fumonisin B_1-treated HepG2 cells (72hours) showed an activation of both the PERK ER stress pathway and NFkB (Figure 4.13) and a subsequent induction of nTG2 (Figure 4.14 and 4.15). Also there was a significant increase in Sp1 mRNA at 10µM FB_1 ($p<0.05$) (Figure 4.16) which suggests that Sp1 crosslinking could be a potential inducer of FB_1-induced apoptosis. However, after 24hours there was a significant reduction in Sp1 mRNA expression ($p<0.05$) (Figure 4.16) suggesting that FB_1-induced apoptosis occurs only after 72hours.

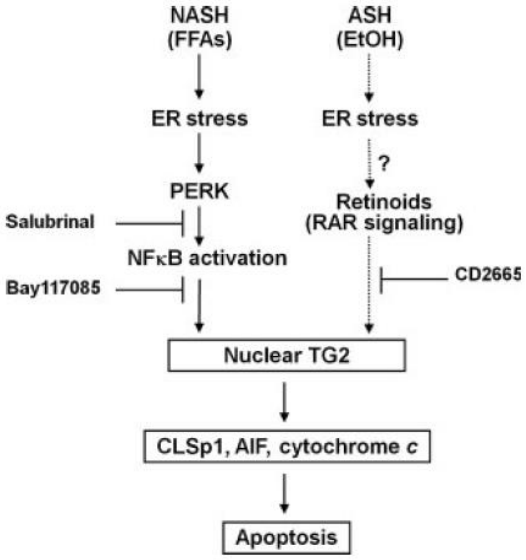

Figure 5.1: Schematic diagram illustrating nuclear TG2 induction via the ER stress-mediated PERK and NFkB activation which leads to hepatic apoptosis; as a result of free fatty acid treatment of liver cells (Kuo et al. 2012).

TG2 has been characterised as an end-stage apoptotic factor where it functions as a crosslinking-catalytic enzyme that stabilises apoptotic cells prior to phagocytosis (Elli et al. 2009; Fesus & Szondy 2005; Park et al. 2010). Various studies have associated TG2 activation and induction with apoptosis (Fesus & Szondy 2005; Griffin et al. 2002). The inhibition of ceramide synthase by FB_1 causes an increase in pro-apoptotic factors: sphingosine and sphinganine (Grenier et al. 2012; He et al. 2005; Voss et al. 2007). Therefore the apoptotic induction due to FB_1 treatment of HepG2 cells was investigated. Apoptotic markers were only investigated using the 72hour treatment period because it was observed that CHOP (Figure 4.11), a transcription factor that is involved in ER stress-mediated apoptosis (Rutkowski & Kaufman 2004) and Sp1 (Figure 4.16) mRNA expression were only significantly increased after 72hours ($p<0.05$). Apoptosis occurs via two pathways: the extrinsic/cytoplasmic and intrinsic/mitochondrial pathway. The extrinsic pathway involves Fas (member of TNF family) death receptor-induced activation of initiator caspase 8 which activates downstream effector caspase 3. The intrinsic pathway involves mitochondrial induction by Bcl-2 family of proteins (example Bax) to release cytochrome *c* which binds Apaf-1 resulting in initiator caspase 9 activation and forms an apoptosome which activates caspase 3 (Ghobrial et al. 2009). Caspases 3/7 (Figure 4.17) and 8 (Figure 4.18) showed a significant decrease in activity at 100µM FB_1 ($p<0.05$) and a decrease in caspase 9 (Figure 4.19) activity although not significant. A biochemical feature of early stages of apoptosis is the externalisation of PS and depolarised mitochondria. After 72hours of 10µM FB_1 treatment a significant increase ($p<0.05$) in PS externalisation (Figure 4.21), a significant decrease ($p<0.05$) in healthy/live cells (Figure 4.22) and a significant increase ($p<0.05$) in depolarised mitochondria (Figure 4.23) were observed. There was also a significant increase in Sp1 mRNA expression ($p<0.05$) in HepG2 cells (Figure 4.16). These results show that at a low chronic dose of FB_1, apoptosis could be induced via the mitochondrial pathway due to a depolarised mitochondrial membrane, however further markers of this pathway need to be investigated. However, at 50µM FB_1 treatment there is a decrease in PS externalisation (Figure 4.21), a significant increase ($p<0.05$) in live cells (Figure 4.22) and a significant decrease

($p<0.05$) in depolarised mitochondria (Figure 4.23). This high chronic dose of FB_1 is unable to induce apoptosis but may cause ER stress to persist as observed by elevated ER stress markers previously discussed. The increase in apoptosis as seen by the externalisation of PS shows apoptosis is induced; however due to decreased effector caspase 3/7 activity apoptosis is not completed. This could possibly be due to increased inhibitors of apoptosis such as inhibitor of apoptosis protein 3, however this requires further investigation.

A summary of the proposed FB_1 mechanism of toxicity via the induction of TG2 and the PERK ER stress pathway is illustrated in Figure 5.2 below:

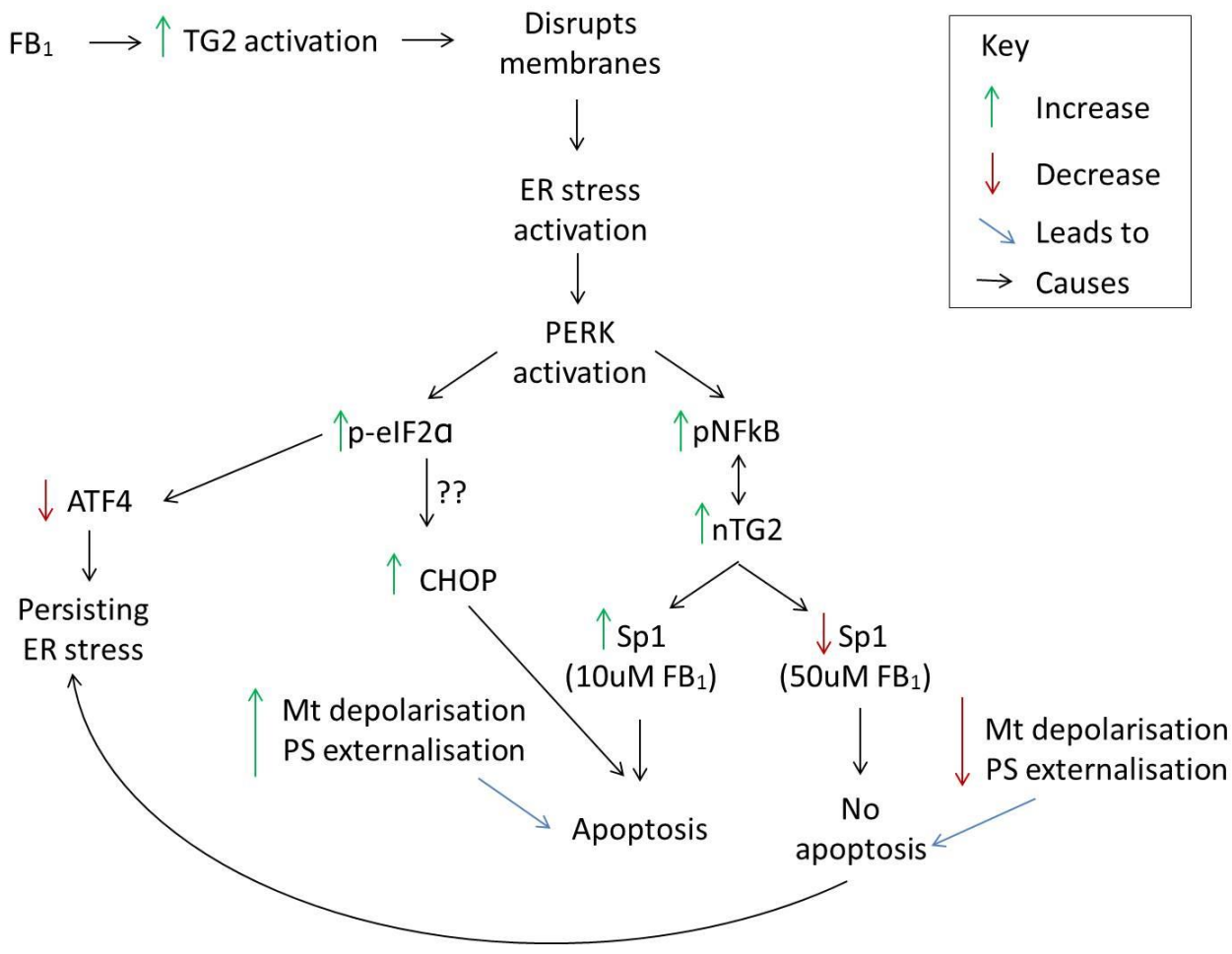

Figure 5.2: Schematic diagram of FB_1 mechanism of toxicity in HepG2 cells.

CHAPTER SIX

6 CONCLUSION

A novel interaction between FB_1 and TG2 was revealed in this study; confirming FB_1 as a high affinity substrate for TG2-crosslinked fibronectin. It was demonstrated that FB_1-induced ER-stress via the PERK pathway. Endoplasmic reticulum stress persisted in HepG2 cells with no apoptosis or cell recovery occurring at high chronic doses of FB_1 whilst ER stress-induced apoptosis at low chronic doses of FB_1 in HepG2 cells. These results confirm for the first time that increased TG2 activity and expression occurs in HepG2 cells after FB_1 treatment which supported the hypothesis. The TG2 expression and activation are preliminary data as n=2, therefore require further investigation. The study also confirms the activation of the ER stress pathway as a result of FB_1 treatment which supports the second hypothesis.

This study only researched the PERK arm of the UPR. Future studies could therefore investigate the effect of FB_1 on the IRE1 and ATF6 arms of the UPR; which could identify possible inducers of CHOP. The specific apoptotic pathway induced by low chronic FB_1 treatment in HepG2 cells could also be researched by investigating other apoptotic markers within the mitochondrial and extrinsic pathways.

REFERENCES

Aflaki, E. et al., 2012. C16 ceramide is crucial for triacylglycerol-induced apoptosis in macrophages. *Cell death and Disease*, 3(3), p.e280.

Arya, M. et al., 2005. Basic principles of real-time quantitative PCR. *Future Drugs Ltd*, 5(2), pp.209–219.

Ballestar, E., Abad, C. & Franco, L., 1996. Core histones are glutaminyl substrates for tissue transglutaminase. *Journal of Biological Chemistry*, 271, pp.18817–18824.

Banga, J.., 1998. SDS-Polyacrylamide gel electrophoresis (SDS-PAGE). *Encyclopedia of Immunology, Volume 4*, pp.2143–2144.

BDBiosciences, 2013. BD Accuri C6 flow cytometer. *Product Catalog*. Available at: http://www.bdbiosciences.com/instruments/accuri/features/index.jsp [Accessed November 21, 2013].

BDbiosciences, 2013a. BD FACSCalibur flow cytometer. *Product Catalog*. Available at: http://www.bdbiosciences.com/instruments/facscalibur/features/ [Accessed November 21, 2013].

BDbiosciences, 2013b. *Flow Cytometry Mitochondrial Membrane Potential Detection Kit Instruction Manual*,

Bertolotti, A. et al., 2000. Dynamic interaction of BiP and ER stress transducers in the unfolded-protein response. *Nature Cell Biology*, 2, pp.326–332.

Biolegend, 2013. Alexa Fluor® 488 anti-human CD95 (FAS) Antibody. *Product Catalog*, p.1. Available at: http://www.biolegend.com/alexa-fluor-488-anti-human-cd95-fas-antibody-3365.html [Accessed November 21, 2013].

Bridge, P.D., 1998. *Applications of PCR in Mycology*, CABI.

Campbell, N.A., Reece, J.B. & Simon, E.J., 2007. Essential Biology. In San Francisco: Pearson Benjamin Cummings, p. 63.

CellSignaling, 2013. PROTOCOLS & APPLICATIONS GUIDE. , pp.1–27. Available at: http://worldwide.promega.com/resources/product-guides-and-selectors/protocols-and-applications-guide/cell-signaling/.

Chacko, S.M. et al., 2010. Hypoxic preconditioning induces the expression of prosurvival and proangiogenic markers in mesenchymal stem cells. *American Journal Of Physiology - Cell Physiology*, 299, pp.C1562–C1570.

DiDonato, J. et al., 1996. Mapping of the inducible IkappaB phosphorylation sites that signal its ubiquitination and degradation. *Molecular and Cellular Biology*, 16(4), pp.1295–1304.

Domijan, A. & Abramov, A.Y., 2011. Fumonisin B 1 inhibits mitochondrial respiration and deregulates calcium homeostasis — Implication to mechanism of cell toxicity. *The International Journal of Biochemistry and Cell Biology*, 43(6), pp.897–904.

Elli, L. et al., 2009. Transglutaminases in inflammation and fibrosis of the gastrointestinal tract and the liver. *Digestive and Liver Disease*, 41(8), pp.541–550.

Fawcett, T.W. et al., 1999. Complexes containing activating transcription factor (ATF)/cAMP-responsive-element-binding protein (CREB) interact with the CCAAT/enhancer-binding protein (C/EBP)-ATF composite site to regulate Gadd153 expression during the stress response. *Biochemical Journal*, 339, pp.135–141.

Fesus, L. & Piacentini, M., 2002. Transglutaminase 2 : an enigmatic enzyme with diverse functions. *Trends in Biochemical Sciences*, 27(10), pp.534–539.

Fesus, L. & Szondy, Z., 2005. Transglutaminase 2 in the balance of cell death and survival. *Federation of European Biochemical Societies*, 579, pp.3297–3302.

Fesus, L., Thomazy, V. & Falus, A., 1987. Induction and activation of tissue transglutaminase during programmed cell death. *Federation of European Biochemical Societies Letters*, 224(1), pp.104–108.

Fincham, J.E. et al., 1992. Atherogenic effects in a non-human primate of Fusarium moniliforme cultures added to a carbohydrate diet. *Atherosclerosis*, 94, pp.13–25.

Gelderblom, W.C. et al., 1991. Toxicity and carcinogenicity of the Fusarium moniliforme metabolite, fumonisin B1, in rats. *Carcinogenesis*, 12(7), pp.1247–1251.

Gelderblom, W.C.A. et al., 1988. Fumonisins-Novel Mycotoxins with Cancer-Promoting Activity Produced by Fusarium moniliforme. *Applied and Environmental Microbiology*, 54(7), pp.1806–1811.

Gelineau-van Waes, J. et al., 2005. Maternal fumonisin exposure and risk for neural tube defects: Mechanisms in an in vivo mouse model. *Birth Defects Research Part A: Clinical and Molecular Teratology*, 73(7), pp.487–497.

Gentile, V., Davies, P.J.A. & Baldini, A., 1994. The Human Tissue Transglutaminase Gene Maps on Chromosome 20q12 by in Situ Fluorescence Hybridization. *Genomics*, 20(2), pp.295–297.

Ghobrial, I.M., Witzig, T.E. & Adjei, A.A., 2009. Targeting Apoptosis Pathways in Cancer Therapy. *CA: A Cancer Journal for Clinicians*, 55(3), pp.178–194.

Giussani, P. et al., 2006. Sphingosine-1-phosphate phosphohydrolase regulates endoplasmic reticulum-to-golgi trafficking of ceramide. *Molecular and Cellular Biology*, 26(13), pp.5055–5069.

Grenier, B. et al., 2012. The low intestinal and hepatic toxicity of hydrolyzed fumonisin B (1) correlates with its inability to alter the metabolism of sphingolipids. *Biochemical Pharmacology*, 83, pp.1465–1473.

Griessler, D.K., 2008. Fumonisins - Mycotoxins of increasing importance! *International Food Safety and Quality Network*. Available at:

http://www.ifsqn.com/articles_detail.php?newsdesk_id=535&t=Fumonisins+-+Mycotoxins+of+increasing+importance! [Accessed November 20, 2013].

Griffin, M., Casadio, R. & Bergamini, C.M., 2002. Transglutaminases: nature's biological glues. *Biochem J*, 368(Pt 2), pp.377–396.

Harisha S, 2007. Cell Count by Hemocytometer. *Biotechnology Procedures and Experiments Handbook*, p.1. Available at: http://www.globalspec.com/reference/54403/203279/exercise-6-cell-count-by-hemocytometer-or-measuring-volume [Accessed November 21, 2013].

Harrison, L.F. et al., 1990. Pulmonary edema and hydrothorax in swine produced by fumonisin B1, a toxic metabolite of Fusarium moniliforme. *Journal of Veterinary Diagnostic Investigation*, 2, pp.217–221.

He, Q., Kim, J. & Sharma, R.P., 2005. Fumonisin b1 hepatotoxicity in mice is attenuated by depletion of Kupffer cells by gadolinium chloride. *Toxicology*, 207, pp.137–147.

Heidtmann-Bemvenuti, R. et al., 2011. Biochemistry and metabolism of mycotoxins: A review. *African Journal of Food Science*, 5(16), pp.861–869.

Hetz, C., 2012. The unfolded protein response: controlling cell fate decisions under ER stress and beyond. *Nature Reviews Molecular Cell Biology*, 13(2), pp.89–102.

Hotamisligil, G.S., 2010. Endoplasmic reticulum stress and the inflammatory basis of metabolic disease. *Cell*, 140(6), pp.900–917.

Hussein, H.S. & Brasel, J.M., 2001. Toxicity, metabolism, and impact of mycotoxins on humans and animals. *Toxicology*, 167, pp.101–134.

IARC, 1993. Some Naturally Ocurring Substances: Food Items and Constituents, Heterocyclic Aromatic Amines and Mycotoxins. In *IARC Monographs on the Evaluation of Carcinogenic Risks to Humans*, vol 56., Lyon: IARCPress, pp. 445–466.

Ientile, R., Caccamo, D. & Griffin, M., 2007. Tissue transglutaminase and the stress response. *Amino Acids*, 33(2), pp.385–394.

IPCS, 2001. *Safety evaluation of certain mycotoxins in food. WHO food additives series*, vol. 47., Geneva: WHO, pp. 1011-1020.

Jones, R. a et al., 1997. Reduced expression of tissue transglutaminase in a human endothelial cell line leads to changes in cell spreading, cell adhesion and reduced polymerisation of fibronectin. *Journal of cell science*, 110, pp.2461–72.

Kaufman, R.J., 2004. Regulation of mRNA translation by protein folding in the endoplasmic reticulum. *Trends in Biochemical Sciences*, 29(3), pp.152–158.

Kellerman, T. et al., 1990. Leukoencephalomalacia in two horses induced by oral dosing of fumonisin B1. *The Onderstepoort Journal of Veterinary Research*, 57(4), pp.269–275.

Knight, C.R.L., Reesb, R.C. & Griffina, M., 1991. Apoptosis: a potential role for cytosolic transglutaminase and its importance in tumour progression. *Biochimica et Biophysica Acta (BBA) - Molecular Basis of Disease*, 1096(4), pp.312–318.

Kuo, T. et al., 2012. Free Fatty Acids Induce Transglutaminase 2-Dependent Apoptosis in Hepatocytes Via ER Stress-Stimulated PERK Pathways. *Journal of Cellular Physiology*, 227(3), pp.1130–1137.

Kuo, T., Tatsukawa, H. & Kojima, S., 2011. New insights into the functions and localization of nuclear transglutaminase 2. *Federation of European Biochemical Societies Journal*, 278, pp.4756–4767.

Kurien, B.T. & Scofield, R.H., 2006. Western blotting. *Methods*, 38, pp.283–293.

Lai, T. et al., 1998. Regulation of human tissue transglutaminase function by magnesium-nucleotide complexes. Identification of distinct binding sites for Mg-GTP and Mg-ATP. *Journal of Biological Chemistry*, 273, pp.1776–1781.

Lasfargues, C. et al., 2013. Changes in Translational Control after Pro-Apoptotic Stress. *International Journal of Molecular Sciences*, 14(1), pp.177–190.

Lee, J. et al., 2004. Transglutaminase 2 Induces Nuclear Factor-κB Activation via a Novel Pathway in BV-2 Microglia. *Journal of Biological Chemistry*, 279, pp.53725–53735.

Lesort, M. et al., 2000. Tissue transglutaminase: a possible role in neurodegenerative diseases. *Progress in neurobiology*, 61(5), pp.439–63.

Li, Y. et al., 2005. Free cholesterol-loaded macrophages are an abundant source of tumor necrosis factor-alpha and interleukin-6: model of NF-kappaB- and MAP kinase-dependent inflammation in advanced atherosclerosis. *Journal of Biological Chemistry*, 280, pp.21763–21772.

Lichtman, J.W. & Conchello, J.-A., 2005. Fluorescence microscopy. *Nature Methods*, 2(12), pp.910–919.

Liu, S., Cerione, R.A. & Clardy, J., 2002. Structural basis for the guanine nucleotide-binding activity of tissue transglutaminase and its regulation of transamidation activity. *Proceedings of the National Academy of Sciences of the United States of America*, 99(5), pp.2743–2747.

Livak, K.J. & Schmittgen, T.D., 2001. Analysis of Relative Gene Expression Data Using Real-Time Quantitative PCR and the 2-ΔΔCt Method. *Methods*, 25, pp.402–408.

Malhotra, J.D. & Kaufman, R.J., 2007. The endoplasmic reticulum and the unfolded protein response. *Seminars in Cell & Developmental Biology*, 18(6), pp.716–731.

Mallmann, C.A. et al., 2001. Fumonisin B1 levels in cereals and feeds from Southern Brazil. *Arquivos do Instituto Biológico*, 68, pp.41–45.

Marasas, W.F. et al., 1988. Fusarium moniliforme contamination of maize in oesophageal cancer areas in Transkei. *South African Medical Journal = Suid-Afrikaanse tydskrif vir geneeskunde*, 74(3), pp.110–4.

Martin, A. et al., 2012. Pathophysiological Roles of Transglutaminase-Catalyzed Reactions in the Pathogenesis of Human Diseases. *Inflammation & Allergy-Drug Targets*, 11(4), pp.278–284.

Mehta, K., 2005. Mammalian Transglutaminases: A Family Portrait J. . Bertino, ed. *Progress in Experimental Tumor Research*, 38, pp.1–18.

Melan, M.A., 1999. Overview of Cell Fixatives and Cell Membrane Permeants. In L. C. Javois, ed. *Immunocytochemical: Methods and Protocols*. Totowa, NJ: Humana Press Incorporated, pp. 45–55.

Merrill, A.H.J. et al., 2001. Sphingolipid Metabolism: Roles in Signal Transduction and Disruption by Fumonisins. *Environmental Health Perspectives*, 109(supp. 2), pp.283–289.

Mirza, A. et al., 1997. A role for tissue transglutaminase in hepatic injury and fibrogenesis, and its regulation by NF-kappaB. *American Journal of Physiology - Gastrointestinal and Liver Physiology*, 272, pp.G281–G288.

Nour, A.M.A. et al., 2007. Folate receptor and human reduced folate carrier expression in HepG2 cell line exposed to fumonisin B1 and folate deficiency. *Carcinogenesis*, 28(11), pp.2291–2297.

Pagano, M., 1999. Application of electrophoresis and related methods , such as western blotting and zymography to the study of some proteins and enzymes. *Analytica Chimica Acta*, 383, pp.119–125.

Pagliassotti, M.J., 2012. Endoplasmic reticulum stress in nonalcoholic fatty liver disease. *Annual Review of Nutrition*, 32, pp.17–33.

Park, D., Choi, S.S. & Ha, K.S., 2010. Transglutaminase 2: a multi-functional protein in multiple subcellular compartments. *Amino Acids*, 39(3), pp.619–631.

Park, J.W. et al., 2005. Fungal mycoflora and mycotoxins in Korean polished rice destined for humans. *International Journal of Food Microbiology*, 103, pp.305–314.

Peng, X. et al., 1999. Interaction of tissue transglutaminase with nuclear transport protein importin-alpha3. *Federation of European Biochemical Societies Letters*, 446, pp.35–39.

Pinkas, D. et al., 2007. Transglutaminase 2 undergoes a large conformational change upon activation. *PLoS Biology*, 5, p.e327.

Piredda, L. et al., 1997. Piredda, L. et al. (1997) Lack of "tissue" transglutaminase protein cross-linking leads to leakage of macromolecules from dying cells: relationship to development of autoimmunity in MRLlpr/lpr mice. *Cell Death and Differentiation*, 4, pp.463–472.

Rahman, M., 2006. *Introduction to Flow Cytometry*, AbD seroTEC A division of MorphoSystems.

Ramos-Vara, J.A., 2005. Technical aspects of immunohistochemistry. *Veterinary Pathology*, 42(4), pp.405–426.

Riley, R.. et al., 2001. Sphingolipid perturbations as mechanisms for fumonisin carcinogenesis. *Environmental Health Perspective*, 109(suppl. 2), pp.3001–308.

Ron, D., 2002. Translational control in the endoplasmic reticulum stress response. *Journal of Clinical Investigation*, 110(10), pp.1383–1388.

Rutkowski, D.T. & Kaufman, R.J., 2004. A trip to the ER: coping with stress. *Trends in cell biology*, 14(1), pp.20–28.

Saito, A. et al., 2011. Endoplasmic reticulum stress response mediated by the PERK-eIF2 {alpha}-ATF4 pathway is involved in osteoblast differentiation induced by BMP2. *Science Signaling*, 286(6), p.4809.

Sapan, C. V, Lundblad, R.L. & Price, N.C., 1999. Colorimetric protein assay techniques. *Biotechnology and Applied Biochemistry*, 29, pp.99–108.

ScienceGateway.org, 2013. Cell count using hemocytometer. *Cell Biology Protocols*, p.1. Available at: http://www.sciencegateway.org/protocols/cellbio/cell/ccuh.htm [Accessed November 21, 2013].

Shen, J. et al., 2002. ER Stress Regulation of ATF6 Localization by Dissociation of BiP/GRP78 Binding and Unmasking of Golgi Localization Signals. *Developmental Cell*, 3(1), pp.99–111.

Simms, D., Cizdziel, P.E. & Chomczynski, P., 1993. Trizol: A New Reagent for Optimal Single-Step Isolation of RNA. *Focus*, 15(4), pp.99–102.

Smale, M., Byerlee, D. & Jayne, T., 2013. Maize revolutions in sub-Saharan Africa. In *An African Green Revolution*. Part 2. Netherlands: Springer, pp. 165–195.

Soriano, J.M., Gonza, L. & Catala, A.I., 2005. Progress in Lipid Research Mechanism of action of sphingolipids and their metabolites in the toxicity of fumonisin B1. *Progress in Lipid Research*, 44, pp.345–356.

Stockmann-Juvala, H., Alenius, H. & Savolainen, K., 2008. Effects of fumonisin B1 on the expression of cytokines and chemokines in human dendritic cells. *Food and Chemical Toxicology*, 46, pp.1444–1451.

Tam, A.B. et al., 2012. ER Stress Activates NF-κB by Integrating Functions of Basal IKK Activity, IRE1 and PERK. *PloS one*, 7(10), p.e45078.

Voss, K.A., Smith, G.W. & Haschek, W.M., 2007. Fumonisins: Toxicokinetics - mechanism of action and toxicity. *Animal Feed Science and Technology*, 137, pp.299–325.

Wang, E. et al., 1991. Inhibition of sphingolipid biosynthesis by fumonisins, mycotoxins produced by Fusarium moniliforme. *Journal of Biological Chemistry*, 266, pp.14486–14490.

Yan, W. et al., 2002. Control of PERK eIF2a kinase activity by the endoplasmic reticulum stress-induced molecular chaperone P58IPK. *Proceedings of the National Academy of Sciences of the United States of America*, 99(25), pp.15920–15925.

APPENDIX A

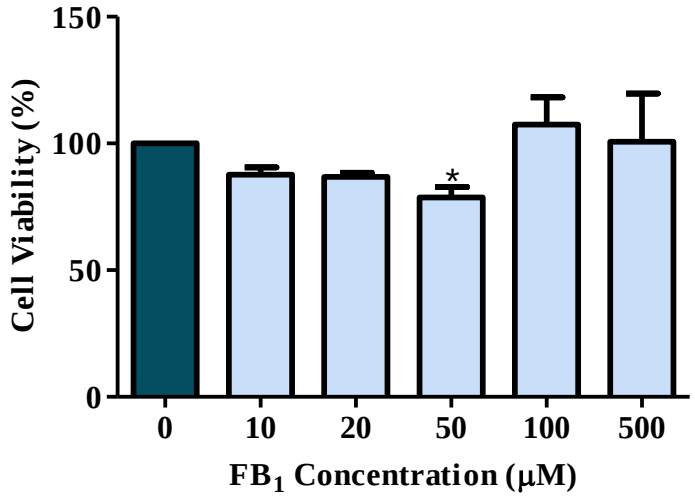

Figure A1: MethylThiazol Tetrazolium cell viability assay. A significant reduction in cell metabolism after 50µM FB_1 treatment was observed. The assay was performed on HepG2 cells treated with FB_1 at varying concentrations over 24hours, wavelength measured at 570nm with a reference of 690nm. Representative of two separate experiments. Statistical significance * shows $p<0.05$.

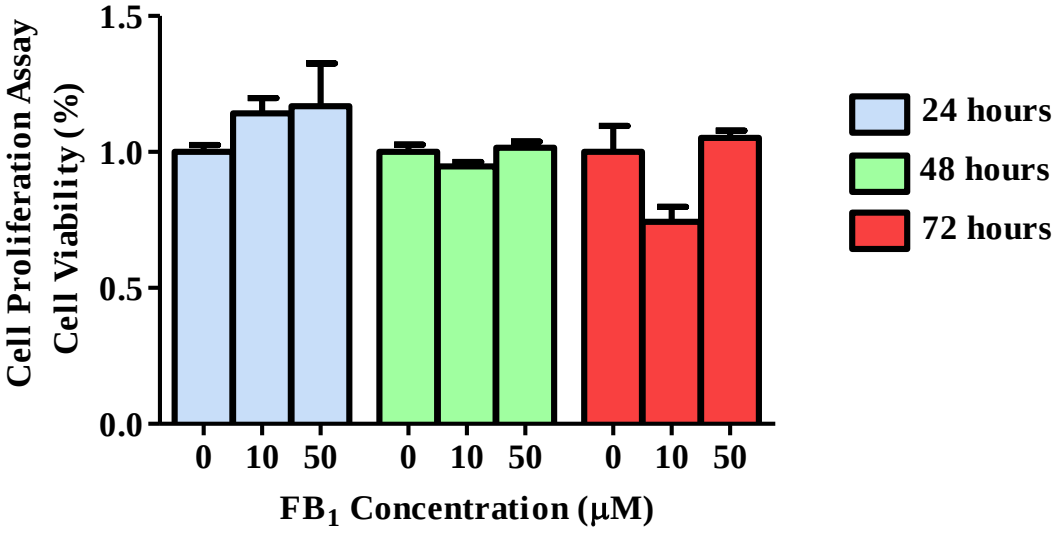

Figure A2: CellTiter 96® AQueous One Solution Cell Proliferation assay. A reduction in cell viability occurred after 72hours when HepG2 cells where treated with 10µM FB_1. The assay was performed on HepG2 cells treated with varying concentrations of FB_1 for 24, 48 and 72 hours measured at wavelength 490nm and reference wavelength 690nm after 1hour incubation at 37°C. the data presented is the percentage of cell viability and the associated standard deviations. Representative of three separate experiments.

APPENDIX B

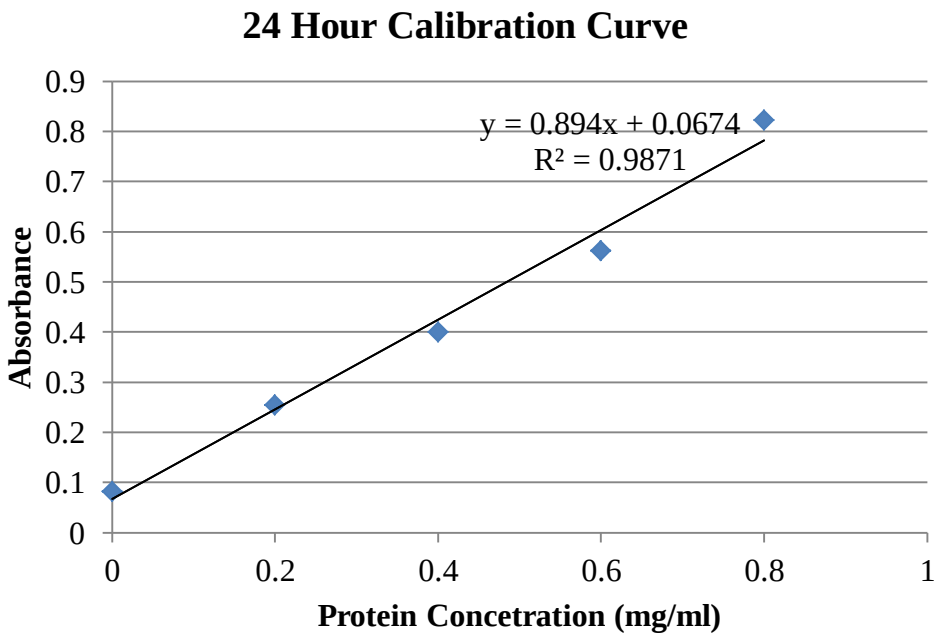

Figure B1: Bicinchoninic acid assay calibration curve used to determine the protein concentration of homogenised HepG2 cells treated with 0, 10, 50 and 100µM FB_1 for 24hours from known concentrations of bovine serum albumin.

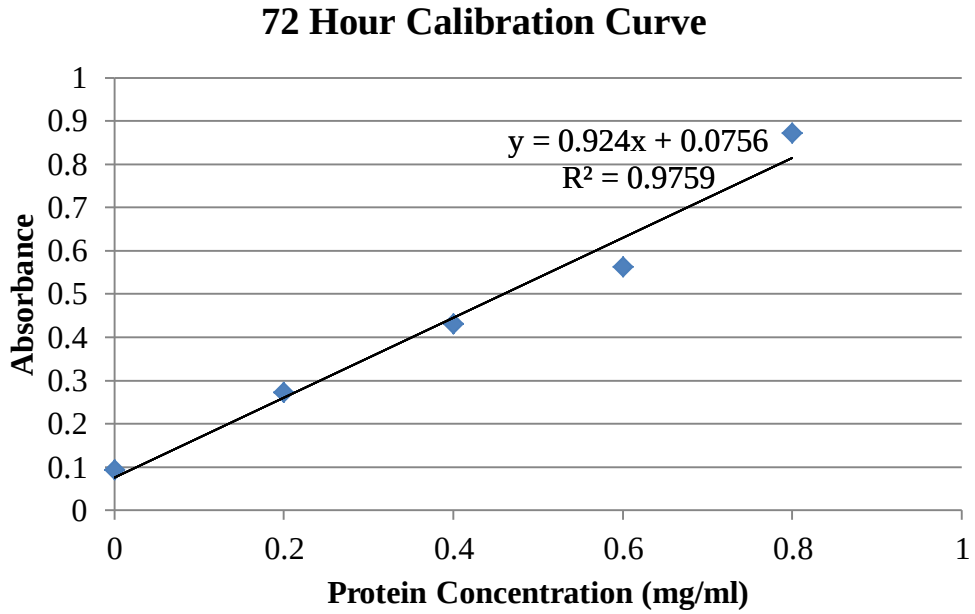

Figure B2: Bicinchoninic acid assay calibration curve used to determine the protein concentration of homogenised HepG2 cells treated with 0, 10, 50 and 100µM FB_1 for 72hours from known concentrations of bovine serum albumin.

Table B1: Standardisation of protein to 1mg/ml using the calibration curves for sodium dodecyl sulfide- polyacrylamide gel electrophoresis.

	FB_1 concentration (µM)	Average Absorbance	Protein Concentration (mg/ml)	C2 (mg/ml)	V2 (ml)	V1 (ml)	Lysis buffer (ml) to make 1mg/ml
24 Hours	0	1.707	1.83	1	0.4	0.219	0.181
	10	1.674	1.80	1	0.4	0.222	0.178
	50	1.626	1.74	1	0.4	0.230	0.170
	100	1.641	1.76	1	0.4	0.227	0.173
72 Hours	0	1.629	1.68	1	0.4	0.238	0.162
	10	1.495	1.54	1	0.4	0.260	0.140
	50	1.471	1.51	1	0.4	0.265	0.135
	100	1.267	1.29	1	0.4	0.310	0.090

APPENDIX C

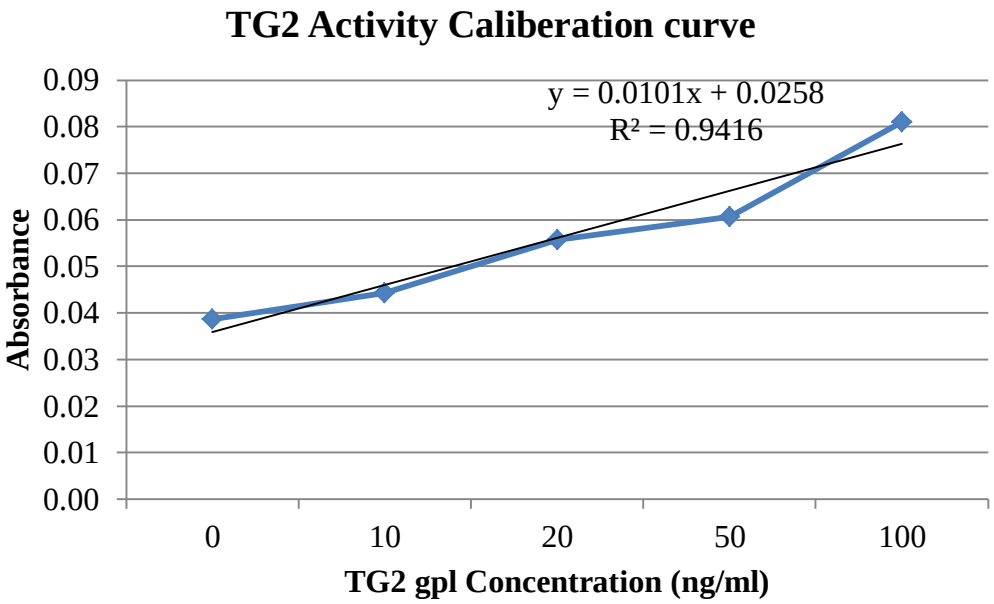

Figure C1: Biotin-cadaverine incorporation into fibronectin – Tissue transglutaminase (TG2) calibration curve represented by the absorbance of varying TG2 *gpl* concentrations (0, 10, 20, 50, 100 and 1000mg/ml).

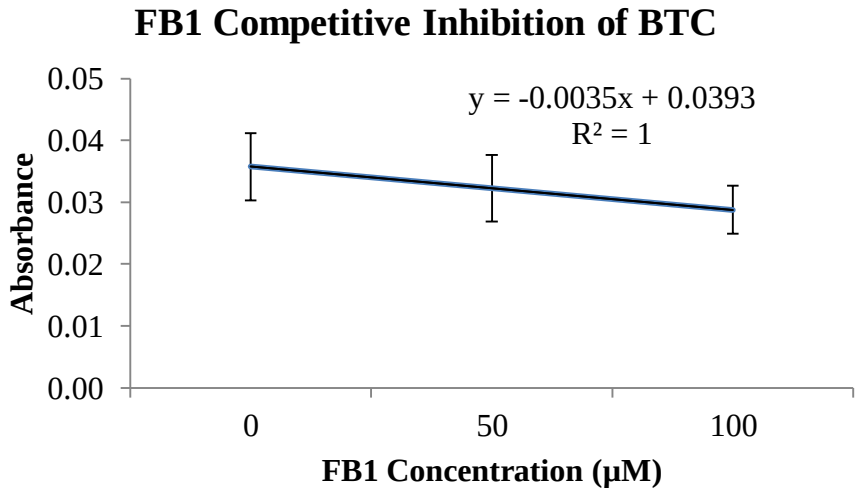

Figure C2: Biotin-cadaverine incorporation into fibronectin with competitive inhibition by FB_1. The line graph shows the absorbance values representative of TG2 activity when 100ng/ml *gpl* TG2 is exposed to FB_1 concentrations of 0µM, 50µM and 100µM in the presence of calcium.

APPENDIX D

Table D1: The Ct, ΔCt and ΔΔCt values for eIF2 mRNA expression and three housekeeping genes: GAPDH, 18s and actin.

	eIF2	GAPDH	ΔCt	ΔΔCt	18s	ΔCt	ΔΔCt	Actin	ΔCt	ΔΔCt
24 hours										
control	26.507	19.757	6.750	1.000	19.750	6.757	1.000	22.790	3.717	1.000
10	26.873	19.537	7.337	0.587	19.603	7.270	0.513	22.677	4.197	0.480
50	26.643	18.933	7.710	0.960	19.153	7.490	0.733	22.090	4.553	0.837
100	25.723	19.140	6.583	-0.167	19.220	6.503	-0.253	22.860	2.863	-0.853
72 hours										
control	24.273	19.870	4.403	1.000	19.893	4.380	1.000	22.983	1.290	1.000
10	24.913	19.257	5.657	1.253	19.270	5.643	1.263	22.187	2.727	1.437
50	25.070	18.343	6.727	2.323	19.193	5.877	1.497	22.243	2.827	1.537
100	25.893	19.333	6.560	2.157	20.193	5.700	1.320	23.080	2.813	1.523

Table D2: The Ct, ΔCt and ΔΔCt values for CHOP mRNA expression and three housekeeping genes: GAPDH, 18s and actin.

	CHOP	GAPDH	ΔCt	ΔΔCt	18s	ΔCt	ΔΔCt	Actin	ΔCt	ΔΔCt
24 hours										
control	29.153	19.757	9.397	1.000	19.610	9.543	1.000	22.660	6.493	1.000
10	29.823	19.537	10.287	0.890	19.503	10.320	0.777	22.577	7.247	0.753
50	28.953	18.933	10.020	0.623	19.103	9.850	0.307	22.190	6.763	0.270
100	28.343	19.140	9.203	-0.193	19.310	9.033	-0.510	22.600	5.743	-0.750
72 hours										
control	22.000	19.870	2.130	1.000	19.963	2.037	1.000	22.490	-0.490	1.000
10	22.953	19.257	3.697	1.567	19.263	3.690	1.653	22.360	0.593	1.083
50	23.247	18.343	4.903	2.773	19.207	4.040	2.003	22.060	1.187	1.677
100	24.473	19.333	5.140	3.010	20.223	4.250	2.213	22.867	1.607	2.097

Table D3: The Ct, ΔCt and ΔΔCt values for ATF4 mRNA expression and three housekeeping genes: GAPDH, 18s and actin.

	ATF4	GAPDH	ΔCt	ΔΔCt	18s	ΔCt	ΔΔCt	Actin	ΔCt	ΔΔCt
24 hours										
control	21.673	16.190	5.483	1.000	19.233	2.440	1.000	22.287	-0.613	1.000
10	21.017	16.253	4.763	-0.720	19.250	1.767	-0.673	22.180	-1.163	-0.550
50	21.003	16.123	4.880	-0.603	19.143	1.860	-0.580	22.123	-1.120	-0.507
100	21.917	17.127	4.790	-0.693	20.133	1.783	-0.657	23.057	-1.140	-0.527
72 hours										
control	24.973	17.063	7.910	1.000	20.047	4.927	1.000	23.053	1.920	1.000
10	22.487	16.183	6.303	-1.607	19.170	3.109	3.109	22.223	0.056	0.056
50	21.283	15.713	5.570	-2.340	19.143	2.131	2.131	21.847	-0.572	-0.572
100	22.530	16.823	5.707	-2.203	19.840	2.687	2.687	22.877	-0.350	-0.350

Table D4: The Ct, ΔCt and ΔΔCt values for TG2 mRNA expression and three housekeeping genes: GAPDH, 18s and actin.

	TG2	GAPDH	ΔCt	ΔΔCt	18s	ΔCt	ΔΔCt	Actin	ΔCt	ΔΔCt
24 hours										
control	29.725	18.856	10.870	1.000	19.153	10.572	1.000	22.363	7.362	1.000
10	28.835	17.964	10.870	0.001	19.163	9.671	-0.901	22.173	6.661	-0.701
50	28.406	17.730	10.677	-0.193	19.067	9.340	-1.233	22.347	6.060	-1.303
100	29.026	18.474	10.552	-0.318	19.830	9.196	-1.376	22.987	6.039	-1.323
72 hours										
control	28.291	19.241	9.050	1.000	19.677	8.614	1.000	22.077	6.214	1.000
10	28.119	17.096	11.022	1.972	18.087	10.032	1.418	21.120	6.999	0.784
50	26.488	17.372	9.116	0.066	18.790	7.698	-0.917	21.613	4.874	-1.340
100	28.735	18.572	10.164	1.114	19.117	9.619	1.004	22.617	6.119	-0.096

Table D5: The Ct, ΔCt and ΔΔCt values for Sp1 mRNA expression and three housekeeping genes: GAPDH, 18s and actin.

	Sp1	GAPDH	ΔCt	ΔΔCt	18s	ΔCt	ΔΔCt	Actin	ΔCt	ΔΔCt
24 hours										
control	25.703	18.856	6.847	1.000	19.863	5.839	1.000	22.920	2.783	1.000
10	25.689	17.964	7.725	0.878	19.087	6.603	0.763	22.250	3.439	0.657
50	24.829	17.730	7.099	0.253	19.093	5.736	-0.104	22.147	2.682	-0.100
100	25.442	18.474	6.968	0.121	19.820	5.622	-0.217	22.890	2.552	-0.230
72 hours										
control	26.296	19.241	7.055	1.000	20.233	6.063	1.000	23.417	2.879	1.000
10	25.836	17.096	8.740	1.685	18.697	7.140	1.077	21.883	3.953	1.074
50	25.040	17.372	7.668	0.613	19.007	6.033	-0.030	22.097	2.943	0.064
100	26.302	18.572	7.731	0.676	19.823	6.479	0.416	23.027	3.276	0.396

APPENDIX E

Table E1: The percent of apoptosis after HeepG2 cells were treated with 5µMCampthothecin; a positive control for apoptosis.

Treatment	% Apoptosis	Mean	Standard Deviation
Campthothecin	28.2	28.2	
Control	10.7	10.8	0.141
Control	10.9		

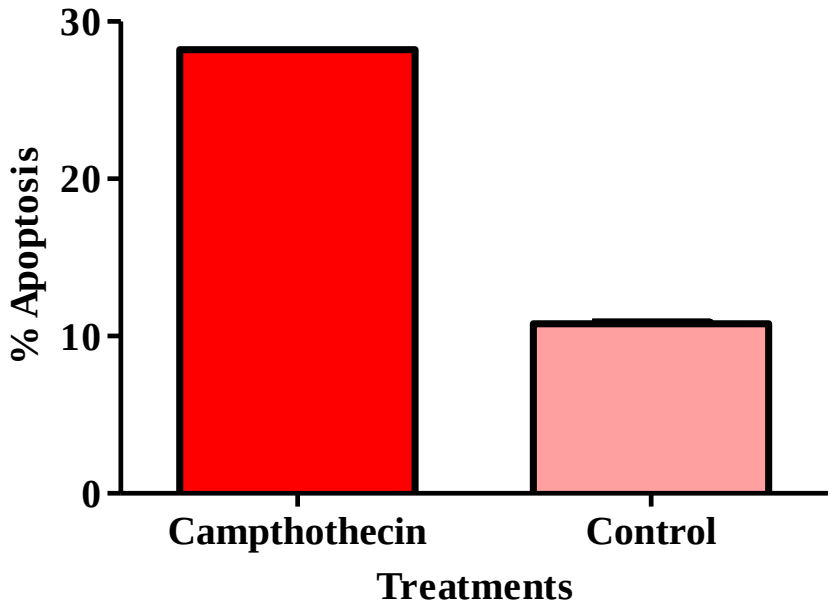

Figure E1: The percentage of apoptosis after HepG2 cells were treated with 5µM Campthothecin; a positive control for apoptosis.

Table E2: Percentage of depolarised mitochondria after HepG2 cells were treated with 5µM Campthothecin; a positive control for apoptosis.

Treatment	Polarised	Depolarised	Mean	Standard Deviation
Campthothecin	64.9	35.1	35.1	
Control	76.76	23.24	23.42	0.255
Control	76.4	23.6		

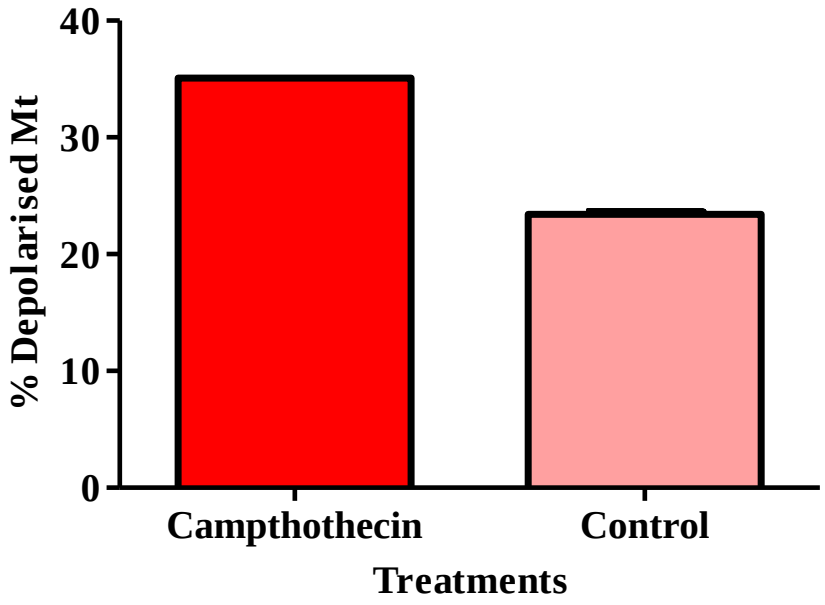

Figure E2: The percentage of depolarized mitochondria after HepG2 cells were treated with 5µM Campthothecin; a positive control for apoptosis.